Landslide Volume Estimation Using Reconstructed Failure Surfaces

JIANNAN HAN

March, 2018

SUPERVISORS:
Dr. C.J. (Cees) Van Westen
Prof. Dr. N. (Norman) Kerle
Dr. O.C. (Olga) Mavrouli

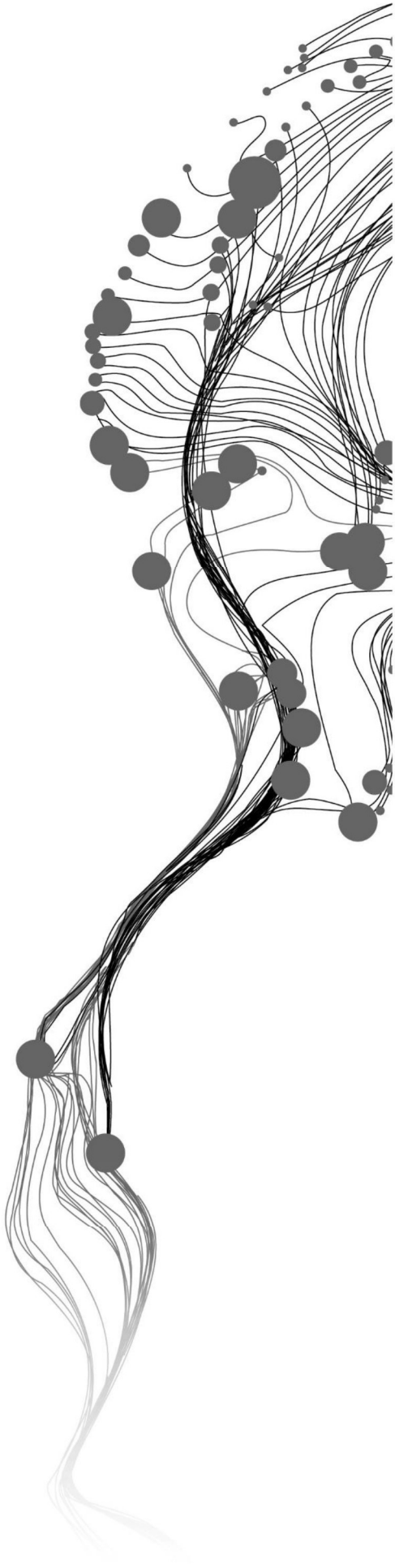

Landslide Volume Estimation Using Reconstructed Failure Surfaces

JIANNAN HAN
Enschede, The Netherlands, March, 2018

Thesis submitted to the Faculty of Geo-Information Science and Earth Observation of the University of Twente in partial fulfilment of the requirements for the degree of Master of Science in Geo-information Science and Earth Observation.
Specialization: Applied Earth Sciences

SUPERVISORS:
Dr. C.J. (Cees) van Westen
Prof. Dr. N. (Norman) Kerle
Dr. O.C. (Olga) Mavrouli

THESIS ASSESSMENT BOARD:
prof. Dr. V.G. (Victor) Jetten
dr. A.C. (Harry) Seijmonsbergen

ABSTRACT

Landslide is one of the most dangerous disasters threatening our properties and lives.

To better understand the mechanism and the impact of landslides, accurate landslide volume estimation is gaining concern, since it plays a very important role in the relevant research.

However, the existing methods of landslide volume estimation show problems in their results due to the subsurface information of landslides is usually unknown.

While, reconstructing the rupture surface base on the exposed scarps could be a way to solve it, since it forms the exposed part of the rupture surface.

Therefore, this research aims to develope a geometric approach for landslide volume estimation using the DEM of the topographic surface after the landslide event, limited field survey data and to reconstruct the surface of rupture and analyze its applicability for different types of landslides. The scarp information and limited data about the depths to rupture surface were incorporated to a paraboloid fitting to generate the most possible rupture surface. The volumes of landslides were calculated by the difference between the reconstructed rupture surface and the pre- or post- event DEM.

The proposed method was tested in nine analogue landslides and one real landslide, in both cases, compared with other methods, the proposed method shows an advantage in accurate landslide volume estimation.

Keyword: Landslide, rupture surface, analogue experiment, volume estimation

ACKNOWLEDGEMENTS

First and foremost, I would like to express my sincere gratitude to my parents. Thank you for everything that you gave to me. Without your unconditional support, everything is impossible.

I would also like to thank my three supervisors, Cees Van Westen, Norman Kerle and Olga Mavrouli. I am grateful to them for their insightful and valuable suggestions. I feel very proud to conduct my study under your supervision. Especially for Cees Van Westen, you inspired me a lot during the whole period of my MSc research. This thesis can never be completed without your help.

A special mention and thanks to my friend Jiong Wang, I learned a lot from you, not only from the technical skills but also from many excellent personal qualities of you.

Many thanks to Chengxiao Tang and everybody who helped me during the field work as well, it was a great time working with you.

I also owe many thanks to Jianqiang Zhang, from whom I got many useful advices about the research and career.

Sincere appreciation also goes to every classmate and staff in ESA department, especially Nanette Kingma, who encouraged me a lot during my time in Enschede, and Bart Korl who readily replies to any question I had about ITC. I cherish every moment I spent with you.

Last but not the least, I would like to express my great gratitude and love to my girlfriend Wanqing Lin who always trusts and stands by me no matter what happens. Your company means a lot to me and is worth than a thousand encouraging and comforting words.

TABLE OF CONTENTS

1. INTRODUCTION

1.1. Background

Landslides, as one of the most dangerous natural disasters in the world, are commonly defined as the failure and movement of rock, soil, or artificial material under the impact of gravity (Clague, 2013). They constitute an important threat to the built and natural environment. Indicatively, it has been reported by CRED (2017) that every year the fatalities involve thousands of people and that monetary loss is of the other of some tens of billions of dollars (CRED, 2017). With increasing population pressures leading to the development of the constructions in the landslide-prone areas, those losses tend to increase in the future.

The volume of landslides is a subject that is quite important in the landslide-related research. To evaluate the destructive effects of landslides, landslide volume needs to be considered due to the importance of the mobilized volume for determining the destructive potential of an event and its influence on the run-out of it (Dade & Huppert, 1998) as well as secondary disasters like landslide dams and floods (Bosa & Petti, 2011; Fan et al., 2012; Murty, 2003; Samia et al., 2017). Accurate landslide volume figures can decrease the uncertainties existing in hazard and risk analysis. Besides, landslide volume is a frequently considered parameter in terms of engineering measures design for landslide control projects such as retaining walls, anchor cables, anti-slide piles. Hence, the research of landslide volume could help people improve the understanding of landslide events and assist the hazard and risk reduction.

Among all volumetric analysis, how to measure landslide volume is gaining importance since it plays a crucial role in two aspects mainly: (1) Providing input for the magnitude (size) and intensity (energy, velocity) of the landslide events (Scheidegger, 1973). (2) Reducing uncertainties related to the construction of hazard scenarios. Lots of research use the landslide volume as an input or an index for validation. For example, Lo et al. (2011) used landslide volume as one of the important arguments to evaluate the success of landslide numerical modelling. Those research are only meaningful with reliable volume figures. (3) Providing input for the quantitative risk assessment. From the perspective of landslide risk assessment, landslide volumes can be used as indicators of the magnitude of the landslide events (Brardinoni & Church, 2004; Catani et al., 2016; Dai & Lee, 2001). Therefore, volume estimation is of great importance in facilitating the risk and hazard assessment of landslide disasters (van Westen et al., 2008). In some cases, it was also applied to evaluate the secondary disasters such as landslide tsunamis (Murty, 2003; Samia et al., 2017). All those works put an emphasis on the calculation of the landslide volume.

1.2. Problem statement

While determining landslide volume is still a challenging task due to the lack of the subsurface information. The most traditional way of landslide volume measurement is based on some oversimplified geometric factors (length, width, depth) with some certain assumptions of the landslide shape (Cruden & Varnes, 1996). In general, landslide volume is obtained by multiplying the area of the landslide with the average depth. Due to the fact that the subsurface information is often inaccessible or incomplete, the volume figures obtained by this process are quite general and should be regarded with caution.

Thanks to the advancement of remote sensing technologies such the use of the unmanned aerial vehicle (UAV) digital photogrammetry, nowadays, Digital Elevation Model (DEM) of high resolution can be obtained at different periods allowing people to monitor the topographic changes on a slope. For landslide volumetric analysis, multi-temporal DEMs (pre and after failure) are critical inputs. If reliable pre and after failure DEMs are available, the topographic changes needed for the landslide volume calculation can be assessed. But in reality, as the time of occurrence of a landslide is not usually know, the quality of pre-event DEM is arguable (Kerle, 2002). In that case, the effect of DEM low accuracy for volume measurement could be large. Grohmann (Grohmann et al., 2011; Grohmann & Sawakuchi, 2013) resampled a high-resolution LIDAR-derived DEM into low-resolution DEMs and compared the results with each other. It shows that, when the DEM resolution is getting worse, the results start varying around the accurate figure with positive or negative deviations from a certain resolution. It indicates that DEMs' quality is important for the volume measurement. However, in practice, it is hard to guarantee especially for pre-event DEMs. Also, the topographic change detected by multiple DEMs can easily generate errors due to the fact that the difference is quite sensitive to misregistration (Van Niel et al., 2008). All these uncertainties increase the difficulty and inaccuracy of the results.

In some cases, even with reliable and well co-registered multi-DEMs, there is still an underestimation of volume in the result. Most landslide volume estimations are calculated as the difference between pre- and post- event topography. It is suitable for landslides in which the mobilized mass was fully moved out of the surface of rupture, but in reality, many landslides still retain a portion of materials within the original zones. So, it could cause an underestimation when applying this to the volume estimation for cases like deep-seated landslides. Besides, for landslides located in some special sites, such as river bank, the mobilized materials falling into the river channels will be eroded away by water, then the eroded part will not be identified in the post-failure topography and will not be counted in the accumulation zone by the topographic difference.

To overcome these difficulties, information of the shape of the rupture surface is needed. As in most cases, detailed data for this are not available, reconstructing the most likely surface of rupture based on the geometry of the exposed scarps, could be an alternative. The geometry of the exposed scarp, forming part of the rupture surface can partly reflect the trend of how the surface of rupture continues under the sliding mass. Therefore, adjusting a shape based on the exposed part of the rupture surface could provide subsurface information necessary for the calculation of the landslide volume. However, there is no systematic analysis discussing the applicability of the reconstructed sliding surfaces found in literature.

Therefore, to address these significant existing research gaps, this research is aiming to develop a landslide volume estimation method based on the reconstructed rupture surface by scarp information with limited data about the depth of the rupture surface, and analyze the uncertainties in the result. The result would be useful for the accurate measurement of the landslide volume. It could also be useful for the calibration of physically-based models because it is expected to provide a relatively more accurate result of the landslide volume. A relevant study of the applicability of using physically-based models to calculate landslide volume will be further discussed in Ma's MSc thesis.

Since the rupture surface is usually beneath the landslide body, so it is not visible from the remote sensing techniques, and it is therefore difficult to obtain the elevation models. It would cause difficulty in method validation due to the lack of the actual volume. The analogue experiment, which has been proved as a useful method in landslide research, could be to solve this (Awal et al., 2007; Bozzano et al., 2013; Eckersley, 1991; Lourenço et al., 2006; Manzella & Labiouse, 2009; Okura et al., 2002; Olivares & Damiano, 2007; Parsons

et al., 2001; Wang & Sassa, 2001). In this study, analogue experiments were designed in which the sliding material can be dug out, and the actual rupture surfaces can be fully exposed for remote sensing monitoring.

1.3. Objectives and research questions

1.3.1. General objective

The main objective of this research is to develop a geometric approach for landslide volume estimation using the DEM of the topographic surface after the landslide event, limited field survey data and to reconstruct the surface of rupture and analyze its applicability for different types of landslides.

1.3.2. Specific objectives

1. To reconstruct the rupture surface of landslides by fitting geometric shapes through the scarps around landslides and limited field survey data

   Research question:

   - What are the best fitted geometric shapes of the surfaces of rupture for different landslide types?

2. To test the applicability of applying the fitted surface to calculate the landslide volume in a controlled environment, based on small-scale experiments

   Research question:

   - What are the volumes calculated by the fitted surface of ruptures?

3. To evaluate the volume figures calculated from the surface of ruptures in controlled environment

   Research question:

   - How are the calculated figures compared with the volume figures calculated by the previous methods?

4. To apply the proposed method in a real landslide

   Research question:

   - What are the volumes calculated by the proposed method?
   - How do the results compare with those from the previous method?

5. To systematically compare the applicability of the proposed method and other methods?

   - What are the pros and cons of each method?

1.4. Research design

To be able to evaluate the quality of the landslide volume measurement method, the analysis of this research was carried out based on several experiments on sand piles in which it is possible to generate high resolution pre-and post-event DEMs and to dig out the failure materials out of the deposition zones. Three types of landslide were simulated during the experiments: deep-seated landslides by water infiltration, shallow landslides by toe excavation, and shallow landslides by vibration. Each landslide topography was measured

3 times, before failure, after failure, and after cleaning the deposition zone. The DEMs were generated photogrammetrically using a drone, DJI Phantom 3, and the real-time kinematic (RTK) global positioning system (GPS). Using these laboratory-scale landslides, it is allowed to get the fully exposed surface of ruptures and accurate volume after digging. The basic research process is shown in Figure 1. The set-up and data processing were illustrated in detail in chapter 3.

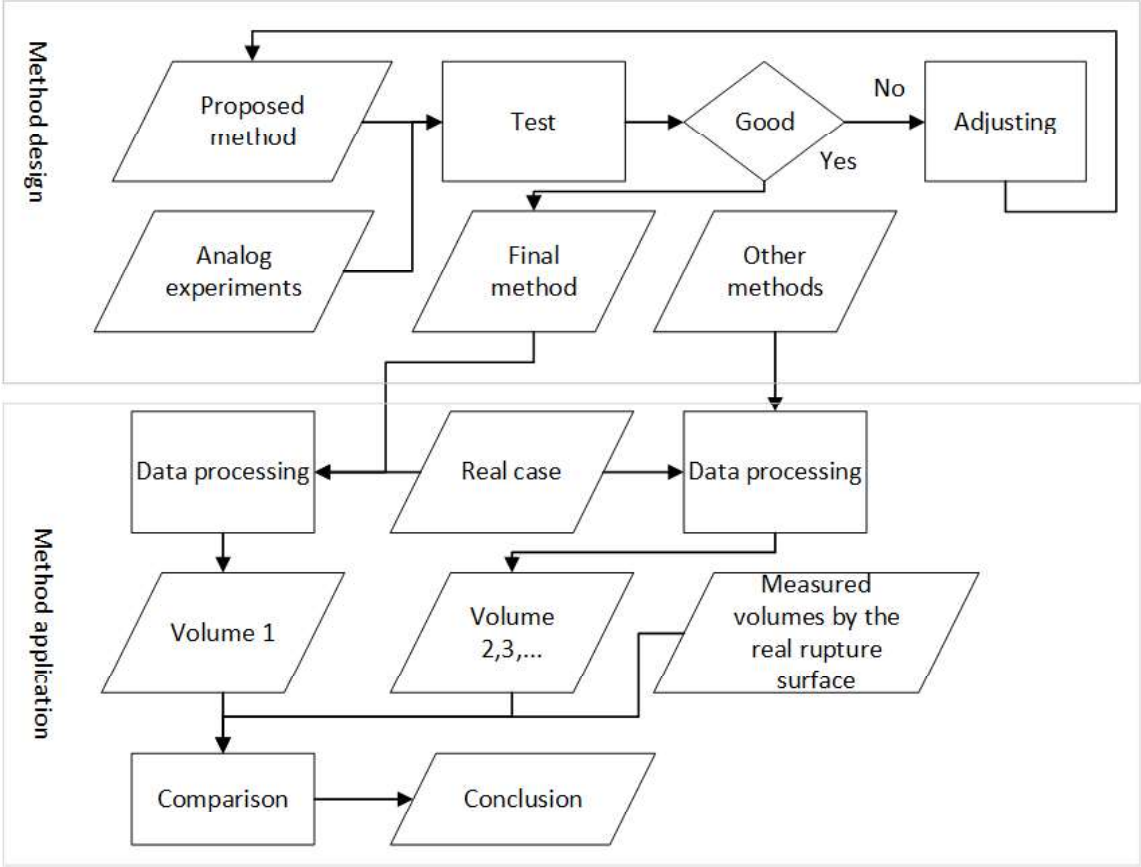

Figure 1: Research framework

1.5. Thesis outline

This thesis is structured into 6 chapters. The outline is shown below:

Chapter 1: Introduction

This chapter presents the justification, a literature review, the objectives and research questions of this research.

Chapter 2: Literature review

This chapter presents the state-of-the-art methods of landslide volume estimation and illustrates their limitations. Also, related studies of reconstructing the landslide surface of rupture and the technologies in terms of DEM generation are discussed.

Chapter 3: Methodology

This chapter illustrates in detail the experiments designed for testing the proposed method and describes the data acquisition and processing of the experiments. And it demonstrates the processes of reconstructing the surface of ruptures, volumes calculated by different methods, and error analysis.

Chapter 4: Results of the experiment landslides

This chapter shows the results of the reconstructed surface of rupture and the consequent volume figures of the experiment landslides. Also, different volume figures derived from multiple methods are compared here.

Chapter 5: Application to the case study of Vajont

This chapter shows an example of how to apply this proposed method to an actual case: the Vajont landslide in Italy.

Chapter 6: Discussion

This chapter discusses the analysis results and the performance and limitations of the proposed method as compared to other methods and ends with outlining the scope for future research directions.

2. LITERATURE REVIEW

In this chapter, several landslide volume estimation methods are reviewed, as well as previous studies related to the reconstruction of the surface of rupture including the geometric characteristics in section 2.1 and section 2.2. The landslide classification and the terminology used in this thesis are illustrated in section 2.3. Laboratory-scale landslide research is introduced in section 2.4. Photogrammetry used in data processing is reviewed in section 2.5.

2.1. Landslide volume estimation methods

The methods that have been proposed for landslide volume estimation are mainly from four types with different focuses: field survey, physically-based modelling, empirical modelling, multi-temporal DEM analysis, and geometrical estimation.

The general review table is shown in Table 1.

Table 1: The review of landslide volume estimation methods

Estimation methods	Main Limitations	References
Field survey	Data amount; Interpretation; costs	(Le Roux et al., 2011; Lugaizi, 2008; Samyn et al., 2012)
Physically-based modelling	Not site-specific	(Marchesini et al., 2009; Mergili, 2012; Reid et al., 2010)
Empirical modelling	Region-dependent	(Guzzetti et al., 2009a; Larsen et al., 2010)
Multi-temporal DEMs	Underestimation	(R. F. Chen et al., 2006; Z. Chen et al., 2014)
Geometrical estimation	Over simplified	(Adegbe et al., 2014; Cruden & Varnes, 1996; Dewitte & Demoulin, 2005; Dewitte et al., 2008)

Field surveys for the measurement of subsurface terrain were implemented in some cases (Le Roux et al., 2011; Lugaizi, 2008; Samyn et al., 2012). Geophysical measurements like seismic refraction profiles and borehole data are used for the reconstruction of the surface of rupture at a site investigation level. According to a review by Jongmans and Garambois (2007), the most widely-used geophysical methods and their application examples are listed in Table 2. These measurements could provide the depth of the rupture surface for a profile or some points, from which, with interpolation, the subsurface terrain could be inferred. By subtracting the elevation of the surface of rupture from the post-landslide DEM, the landslide volume could be extracted. This method may provide a relatively precise landslide volume. Nevertheless, an accurate reconstruction of the surface of rupture usually requires a large amount of survey data. Lugaizi (2008) showed an example of how a huge amount of the data are needed to measure a single landslide. So, these approaches are always limited in reality due to the lack of data. Besides, geophysical data like seismic reflection sometimes are also difficult to interpret correctly which would increase the uncertainty in the

results. And these processes are also time-consuming and labor-intensive, while quick responses are always necessary for emergency management.

Table 2: A summary of geophysical methods for landslide depth measurements

Method	References
Seismic reflection	Bichler et al. (2004), Bruno and Marillier (2000), Ferrucci et al. (2000)
Seismic refraction	Glade et al. (2005), Mauritsch et al. (2000) Caris and Van Asch (1991)
Seismic tomography	Jongmans et al. (2000) Méric et al. (2005)
Seismic noise measurements (H/V method)	Lapenna et al. (2005) Méric et al. (2006)
Vertical electrical sounding (VES)	Agnesi (2005) Schmutz et al. (2000) Caris and Van Asch (1991)
Electrical tomography	Batayneh and Al-Diabat (2002) Lebourg et al. (2005) Lapenna et al. (2005) Havenith et al. (2000) Méric et al. (2005) Wisen et al. (2003)
Spontaneous Potential (SP)	Bruno (2000) Lapenna et al. (2005)
Electro-magnetism (EM34 or TEM)	Bruno and Marillier (2000) Méric et al. (2005) Schmutz et al. (2000) Mauritsch et al. (2000) Caris and Van Asch (1991)
Ground penetrating Radar (GPR)	Bichler et al. (2004) Petinelli et al. (1996) Jeannin et al. (2005)
Gravimetry	Del Gaudio et al. (2000)

Physically-based modelling is an approach to approximately simulate failure process by soil and rock mechanics. In this case, the estimation of landslide volume is strictly linked with the mechanism of slope stability (Marchesini et al., 2009). For landslide volume estimation, the key issue is to precisely locate the failure surface. 3D-model software or scripts like Scoops3D, r.rotstab and the script made by Marchesini were developed integrated with the volume-calculation function, and has been used in some cases (Marchesini et al., 2009; Mergili, 2012; Reid et al., 2015). But for many landscapes, it is hard to parameterize the models given the site-specific model features which could reduce the accuracy (Reid et al., 2015). So, they are all designed to predict the possible landslide event and can hardly be used in terms of volume measuring.

The empirical relationship between landslide area and volume is the most used method which depends on historical landslide data from previous studies from literature. The relation is expressed in the form of $V = \alpha A^{\gamma}$, where A is the total disturbed area of the landslide, and V is the volume of mobilized mass. These relationship has been developed in several regional studies with site-specific α and γ values, and varies between different regions (Guzzetti et al., 2009b; Larsen et al., 2010; Tseng et al., 2013), and has been widely

used in volume estimation. But to develop this relationship in a new area requires a lot of data, and applying it based on landslide area, may lead to large differences for individual landslides. Even in the most widely used equations which have been broadly applied, in most cases, the input volume data are only based on simple estimates coming from literature where the volume was estimated by multiplying the landslide area with the mean depth of the sliding surface (Guzzetti et al., 2008). In literature on the generation of the empirical relations, the landslide depth was actually measured for a limited number of landslides. As landslide depth varies spatially, this limitation brings a high degree of uncertainty in landslide depth, and therefore volume estimation. Landslide mapping is another source of uncertainty in generating this relationship, detailed landslide extent is difficult to map correctly especially for those landslides which only have images with coarse resolution (Tanyaş et al., 2017). Tseng et al.(2013) showed an example that the α and γ could have 12% and 2.4% variation when using different mapping results. Due to this variation, in a landslide which has an area of 10^6 km^2, the volume difference can reach to 33.3%. It indicates that this relationship is also quite sensitive to the landslide mapping. Since the input data are mostly derived from literature, it is not possible to make sure that all of them were using the same mapping strategy. These significantly existing uncertainties in the input data can influence the reliability of the empirical relationship because it is only meaningful with reliable data sources. Basically, the quality of the input volume and area data was not taken into account in their regression analysis. Based on the research by Kerle (2002), the simple field estimation sometimes shows a difference in an order of magnitude compared with the precisely measured result.

Due to the development of remote sensing techniques, DEMs are easier to acquire now. It facilitated landslide volume calculation by using the elevation difference between a pre-landslide and a post-landslide DEM. As long as these are precise and with good co-registration, the accumulated and removed material could be generated by subtraction of the two DEMs (Chen et al., 2014). Based on this logic, a Height Difference Model (HDM) is created. But in HDM, the result is quite sensitive to the accuracy of the input DEMs. The uncertainties come from co-registration, interpolation algorithm, mesh grid distance and datum, geographical reference ellipsoid and projection system, and these factors could generate random and systematic errors. To minimize the errors, the Advanced Height Difference Model (AHDM) was proposed which select several subareas in multi-temporal DEMs with no changes in elevation around the landslide body, then correlated average height in different subareas so as to adjust DEMs to perform in the same baseline (Chen et al., 2006). The results showed that it is a feasible method in the multi-temporal DEMs co-registration for the landslide volume determinations. The Mass Balance Model (MBM) is another method for volume estimation that incorporates mass balance principle to AHDM to reduce the systematic errors (Chen et al., 2014). In Chen et al.'s study, they made an assumption that, in landslides, usually the volume of the mobilized material may have changed after the failure due to the change in density, but since the composition of the material stay the same as the initiation, the mass of the material should remain unchanged. According to this mass balance principle, the pre- and post- DEM height data would be adjusted until the calculated volumes meet the change in density. However, the assumption of MBM is questionable in many cases like the landslides were triggered by rail fall infiltration, the mass of the mobilized material in these cases should be changed after the failure.

But it is worth noting that the landslide volumes calculated by these multi-temporal DEMs are not the volume of the whole mobilized mass since the subsurface information was missing. They are actually the accumulated or depletion materials identified by DEM difference. Ignoring this point will cause a significant underestimation of the real landslide volume as it is shown in Figure 2. As these volumes are not the actual volume of the mobilized material, from here onward, "accumulation volume" and "depletion volume" are used respectively in this study to indicate the volumes of the part (1) and part (2) in Figure 2.

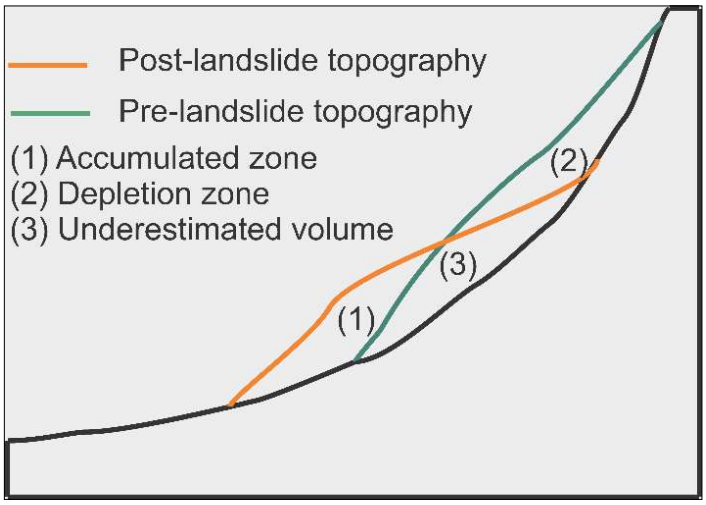

Figure 2: A schematic illustrating how the underestimate would be once mistaking the DEMs difference as the landslide volume.

From the perspective of slip surface geometry, only limited research efforts have been made. The landslide geometry was usually assumed as a hemiellipsoid and the volume was calculated by the hemiellipsoid volume formula $V = \frac{\pi}{6} D_r W_r L_r$, where Dr, Wr, Lr are respectively the depth, width, length of the rupture surface (Adegbe et al., 2014; Cruden & Varnes, 1996; Dewitte & Demoulin, 2005; Dewitte et al., 2008). But it does not take into account the specific form of the failure surface and the specific geomorphology of single landslide types into account, and it is an oversimplified formula.

2.2. Rupture surface reconstruction

As mentioned in the previous chapter, reconstructing the surface of rupture from the exposed scarp around the landslide could be a possible way to overcome the drawbacks of these estimation methods. Previous research proposed to use certain shapes to simulate it. Zhanpeng at al. (2013) used a terrestrial laser scanner to extract the landslide volume in the Wenchuan area by assuming a planar subsurface topography. However, this is a rather specific case, in which the landslide was totally separated from the initial zone. So, it is not generally applicable in a wider context. Nikolaeva et al. (2014) assumed a partly ellipsoid surface truncated by two parallel planes representing the rupture surface beneath the sliding material and the superficial topography, and then estimated the volume of a landslide that occurred in the central western part of Georgia. However, since they did not use the actual terrain surface in the volume calculation, the detailed actual topography was not considered, and it was therefore more a simplification than an actual measurement. Also, in both cases, due to the lack of subsurface information, these two works did not validate the calculated volume figures with reliable well-measured volume figures. Also, in both cases, the type of landslide was not considered in the analysis. When it comes to physical modelling, which is also based on certain assumptions of the surface of rupture, similar problems still exist. For example, Scoops3D uses a sphere to approximate the potential surface of rupture (Reid et al., 2015), while r.rotstab uses a truncated circle or ellipsoid (Mergili, 2012). Likewise, both methods do not differentiate between specific landslide types and have not explained the reason why the certain shape was chosen. Landslides with different failure mechanism can have various geometrical shapes. So, to reconstruct the surface of rupture, it is necessary to evaluate the capability of using a certain geometric shape to fit the actual surface of rupture for different landslide types at the first step. And in some cases, due to field surveys, data of the surface of

rupture are available, and although they are not enough to reveal the whole surface of rupture, they are still interesting to analyze the performance if this information was combined in the reconstructing results.

The principal aim of this research is to develop a method to calculate the volume of the landslide from the reconstructed DEM using the scarp information and limited field survey data to overcome the weakness of previous research.

2.3. Landslide geometry

2.3.1. Nomenclature and classification

To fit the surface of ruptures by certain geometric shapes, differentiating various landslide types is necessary at the very beginning because each of them could appear with distinctive geometric characteristics. Therefore, the existing landslide nomenclatures and classification were reviewed with their relation to the shape of the failure surface.

The most widely used landslide nomenclature was firstly devised by Varnes in 1978 and then became popular after several times editing (Cruden & Varnes, 1996; IAEG, 1990; Varnes, 1978). In the system proposed by Varnes, landslides are divided by their movement types and the landslide materials. The classification is as shown in Table 3.

Table 3: Three types of landslides according to USGS (2004), with the expected shape of the rupture surface in italics

Type of movement		**Type of material**		
		Bedrock	**Engineering soils**	
			Predominantly coarse	**Predominantly fine**
Falls		Rock fall *(any shape)*	Debris fall *(initiation zone could be ellipsoid, sphere, paraboloid or planar)*	Earth fall *(initiation zone could be ellipsoid, sphere, paraboloid or planar)*
Topples		Rock topple *(Not relevant)*	Debris topple *(Not relevant)*	Earth topple *(Not relevant)*
Slides	Rotational	Rock slump *(sphere, paraboloid or ellipsoid)*	Debris slump *(sphere, paraboloid or ellipsoid)*	Earth slump *(sphere, paraboloid or ellipsoid)*
	Translational	Rock slide *(Plane, paraboloid or truncated ellipsoid)*	Debris slide *(Plane, paraboloid or truncated ellipsoid)*	Earth slide *(Plane, paraboloid or truncated ellipsoid)*
Lateral spreads		Rock spread *(any shape)*	Lateral spread *(any shape)*	Earth spread *(any shape)*
Flows		Rock flow *(initiation zone could be ellipsoid, sphere, paraboloid or planar)*	Debris flow *(initiation zone could be ellipsoid, sphere, paraboloid or planar)*	Earth flow *(initiation zone could be ellipsoid, sphere, paraboloid or planar)*
Complex: combination of two or more principle types of movement				

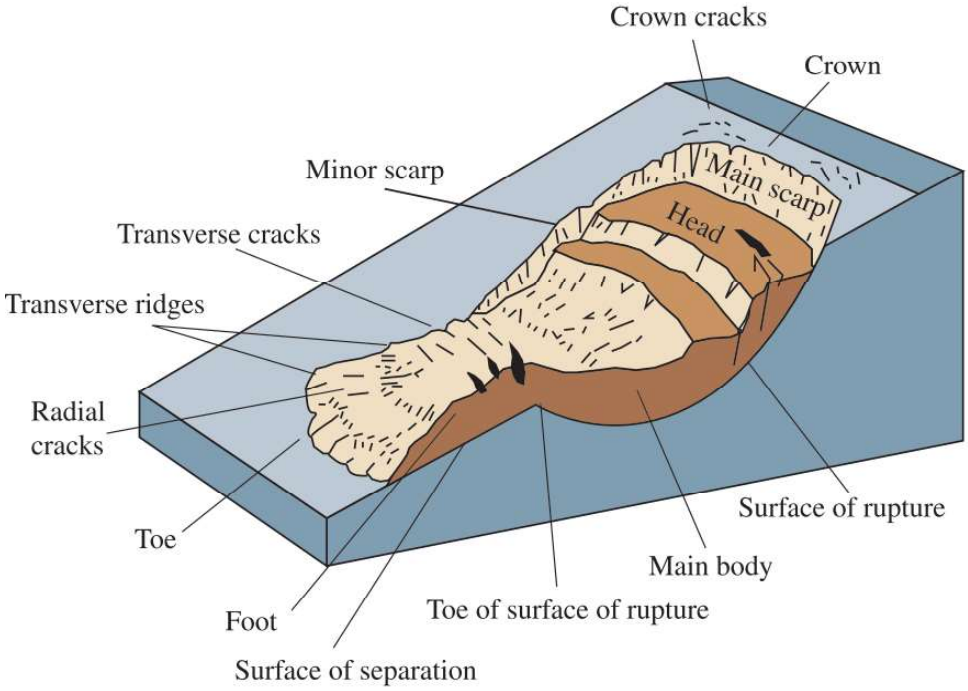

Figure 3: The schematic of landslide components drawn by USGS (2004), in which the scarps are the exposed part of the rupture surface.

While in practice, researchers' focuses are various. So, it is also common to have different nomenclatures in specific cases. For instance, Dai et al. (2011) categorized the landslides triggered by the Wenchuan earthquakes into four types: shallow landslides, rock falls, deep-seated landslides, rock avalanches, while in the same study area, Tang et al. (2016) classified those landslides into falls, slides, flow. Due to the difference between the multiple emphases of research purposes, Hungr et.al. (2014) proposed that the landslide term assignments should follow and reflect the researcher's particular focus.

In this research, since the landslide geometry is directly linked to the analysis, we proposed to group the landslides into two types: deep-seated landslides and shallow landslides. This can be corresponding to the categories rotational types and translational types in Varnes' system but emphasize more on the morphological features. And meanwhile, this research only focused on landslides with the partially exposed surfaces of ruptures namely scarps, because once the surface of rupture has been fully exposed, the volume figure can be simply calculated by multi-DEMs subtracting.

For avoiding the ambiguity in terms of landslides components, the terminology proposed by IAEG (1990) was adopted in this thesis. Figure 3 shows a schematic presenting each component and their term.

2.4. Laboratory analysis of landslides

To acquire landslide data in which sliding material could be removed out of the initial zone, and the rupture surface could be clearly observed, laboratory-scaled landslides were designed in this study. Laboratory-scaled landslides are experiments which are taken for simulating landslides in controlled environments. For landslide research, these experiments in controlled environments sometimes are also called analogue experiments or analogue modellings and were often taken place with certain set-ups to reveal the processes of landslide happenings.

In the field of landslides, analogue experiments have been widely applied due to their advantages in idealizing the landslide processes and addressing the key variables of interest from the complex environment (Awal et al., 2007; Bozzano et al., 2013; Eckersley, 1991; Lourenço et al., 2006; Manzella & Labiouse, 2009; Okura et al., 2002; Olivares & Damiano, 2007; Parsons et al., 2001; Wang & Sassa, 2001). These laboratory-scaled landslide scales vary from 83 m3 to less than 0.2 m3. Analogue experiments have provided a bundle of well-measured data to validate the effectiveness of their proposed methods in a reproducible way (Iverson, 1997). Ventisette et al. (2015) presented an example that showed how to use an analogue experiment to reoccur the landslide processes, in which they used quartz sands to simulate the Vaiont landslide. Emery et al. (2014) also made an attempt in a sandbox to test the geometrical similarities between the simulated landslide rupture surface and the actual rupture surface. It proved that analogue experiments are an effective tool in landslide analysis.

In the light of this, in this research, several experiments were set up in sand piles to test the proposed method in a controlled environment where we can measure the volumes of mass movement and test the proposed method.

It is worth noting that landslide sizes in nature range from thousands of meters to only tens of centimeters (Figure 4). The laboratory-scale landslides are just to mimic nature. Considering the scale effect that the physical-mechanical property of the landslide material can be disproportionately different for experiments and real cases, and the complex of the natural condition which is hard to strictly set up, it needs to be cautious when applying the conclusions drawn by them into real examples (Iverson, 2015).

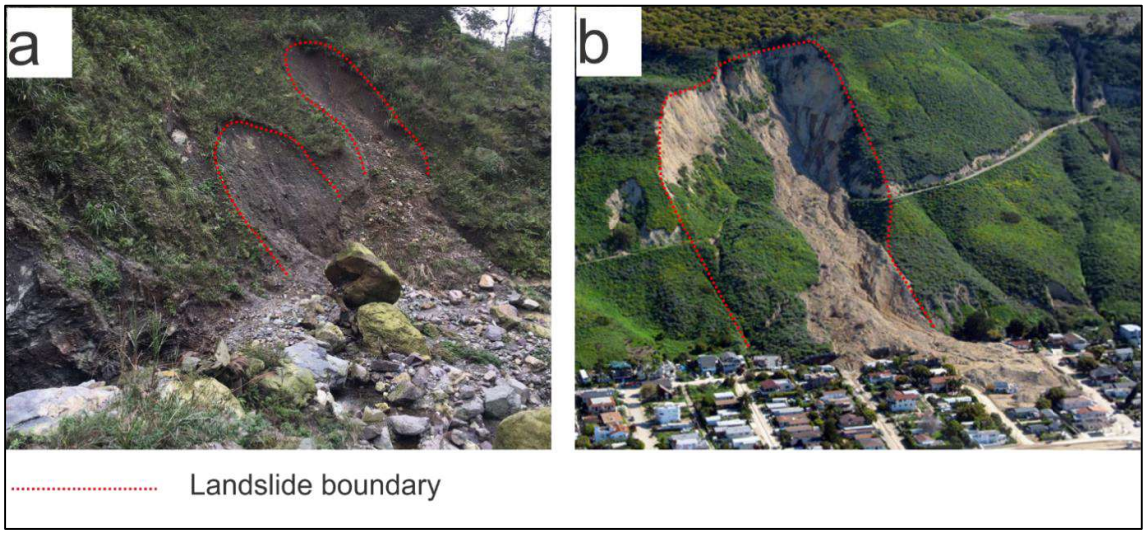

Figure 4: Landslide examples, in which photo (a) is the small-scale landslide in a river channel sized about 2 cubic meters (photograph by Han), (b) is the big scale landslide La Conchita landslide sized about 1.3 million cubic meters (photograph by Reid)

2.5. Photogrammetry

Photogrammetry is the technique of making the measurement of the surface models by measurements on several photographs with overlapped sections. It has become the most useful tool for extracting DEMs which are of great importance in topography monitoring. Traditionally, creating DEMs costs highly due to land surveying (Uysal et al., 2015). In time, thanks to the development of photogrammetry, DEM generation can be conducted in a more cost-efficient way.

With photogrammetry, especially Structure from Motion (SfM) which has been incorporated in several commercial software like Pix4D, Smart3DCapture, PhotoScan, DEMs can be generated by photos automatically by non-photogrammetric specialists. The processes were summarized by Küng et al. (2012). Basically, it can be divided into 5 phases: (1) The points matching (2) The bundle block adjustment by those matching points with their approximate position information (3) The calculation of the 3D coordinates for those points (4) The interpolation for the 3D model (5) The image projection for generating the orthomosaic.

With the photogrammetry techniques, satellite-derived DEMs have been widely applied in landslide monitoring. High resolution DEMs acquired from many sources such as Quickbird, IKONOS, CARTOSAT-1 are able to provide enough accuracy for landslide monitoring (van Westen et al., 2008). Also, in recent years, with the increasing availability of the UAV-based images, UAV (sometimes was also called by drone) is becoming another important platform for landslide monitoring. Niethammer et al. (2012) made use of a low-cost (1000 euros in total) quad-rotor and a consumer-grade camera (Praktica Luxmedia 8213) to generate the DEM of the Super-Sauze landslide which has an area of 850m×250m. The result shows a vertical root mean squared error (RMSE) of 0.3m and an average horizontal offset of 0.5m in contrast with a LIDAR-DEM.

However, the photogrammetry can be hindered by the lack of contrast, or the change in light incidence (Konecny, 2014). And in natural landslides, the vegetation is another issue which should be considered, as it may cover the area before landslides happen and could remain on the landslide bodies (e.g., in case of slow-moving landslides) which could cause an overestimation in volume figures because the actual terrain surfaces were not properly addressed by photogrammetry. So, for landslide volume estimation in areas with lush vegetation, this part should be corrected since it forms parts of the photogrammetric surface. Martha et al. (2010) showed an example of how to remove the vegetation height from the pre-failure surface model, in which an ununiform vegetation height surface based on visual interpretation on stereo images were subtracted from an automatically generated digital surface model (DSM). These limitations of the photogrammetry should be considered in the data quality.

In the experiments performed in this research, drone-photogrammetry was used for generating DEMs of the laboratory-scaled landslide topography, since its advantages in covering an area which allows us to generate the DEMs of several landslides at one flight.

2.6. Summary

According to the review, the inaccuracy in landslide volume measurement stems from the existing methods and photogrammetry both. For the existing methods, relatively limited work has been carried out on the possible solution: rupture surface reconstruction from the scarp information and limited data about the rupture surface.

3. METHODOLOGY

The proposed method based on rupture surface reconstruction in this study was designed and tested firstly in the analogue experiments with photogrammetrically-derived DEMs and then was applied in a real case.

In the analogue experiments, three types of landslides were simulated on piles with homogeneous sands. The results were used to test and validate the proposed method.

Nine landslides in total were simulated and measured: one deep-seated landslide was triggered by water infiltration, four shallow landslides were triggered by toe excavation, and four shallow landslides were triggered by vibration. For each landslide, DEMs were generated from point clouds using the photometrical methods available in the Pix4d software, from photos taken by the camera FC300C carried by a small unmanned aerial vehicle DJI Phantom 3.

This chapter was divided into 4 sections: experimental set-up, data acquisition, and processing, rupture surface reconstruction, and volume calculation. In the experimental set-up, the experiments were described in this chapter including the material composition, sizes of landslides, and triggering methods. The section data acquisition and processing illustrated the processes to acquire the terrain models of the landslide topography. In the section on the rupture surface reconstruction, the proposed method to simulate the rupture surface was presented. The section on the volume calculation presented the method to combine the landslide terrain models and the reconstructed rupture surface.

3.1. Experimental set-up

Table 4: The lengths, widths, depths of the experimental landslides

	Deep-seated	Shallow landslides by toe excavation				Shallow landslides by vibration			
		1	2	3	4	1	2	3	4
L_r: length(cm)	83	144	120	215	165	256	78	90	113
W_r: width(cm)	82	98	75	114	85	198	50	70	80
D_r: depth(cm)	25	14	15	15	20	35	18	13	21
D_r/L_r	0.30	0.10	0.13	0.07	0.12	0.14	0.23	0.14	0.19

The experiments were conducted on sand piles, located in a sand mining area of the landslides and debrisflows of the Hongchun catchment in Yingxiu, Sichuan, China. The experiments were organized in such a way that the sliding material could be removed from the deposition zones, and the rupture surfaces could be fully exposed. When the mobilized material slides from its initial location, the geotechnical properties will be changed, because the failure will disturb the original material structure, and the sliding material tends to be looser than the undetached material. This difference in properties can be felt by hand clearly in these cases. To guarantee the minimal disturbance in the digging-out of the rupture surface, we first used shovels to dig out the main sliding mass. When approaching the rupture surface, we changed to brooms and hands to carefully remove the remaining loose sand. Based on this, the rupture surface was carefully exposed, and the drone was used to make detailed photographs, which were later also used for making a DEM of the rupture surface. When comparing it with the pre-topography, the volume can be

measured from the topographic difference. The terrain models were made by drone-based photogrammetry, using Pix4D. As a result, the lengths (L_r), widths (W_r), depths (D_r) and their depth-to-length ratios of these landslides were measured and shown in Table 4.

3.1.1. Deep-seated landslides triggered by water infiltration

To trigger a "deep-seated" landslide by water infiltration, a waterproof sheet was put in the sand to intercept the water infiltration. A terrace was made at the top, and water was poured on it. Surface run-off which could cause problems in the volume calculation was avoided in this experiment, as it would carry some material away from the landslide. To avoid it, the pouring was conducted slowly to makes sure that all the water infiltrated in the slope. While pouring more water in the upper slope, some cracks appeared at the top, then immediately, a landslide with a deep-seated rupture surface collapsed. The evolution of this process is shown in Figure 5.

Figure 5: The experiment record of the deep-seated landslide. Figure (a) is the landscape before the failure, where (b) and (c) are after the failure and after digging the sliding material.

3.1.2. Shallow landslides triggered by toe excavation

To simulate shallow landslides by toe excavation, we created four slopes with gradients of 45°, 45°, 38°, 34°, and then we used shovels to undercut the toes of these slopes until slope failure. The post-landslide situation is shown in Figure 6.

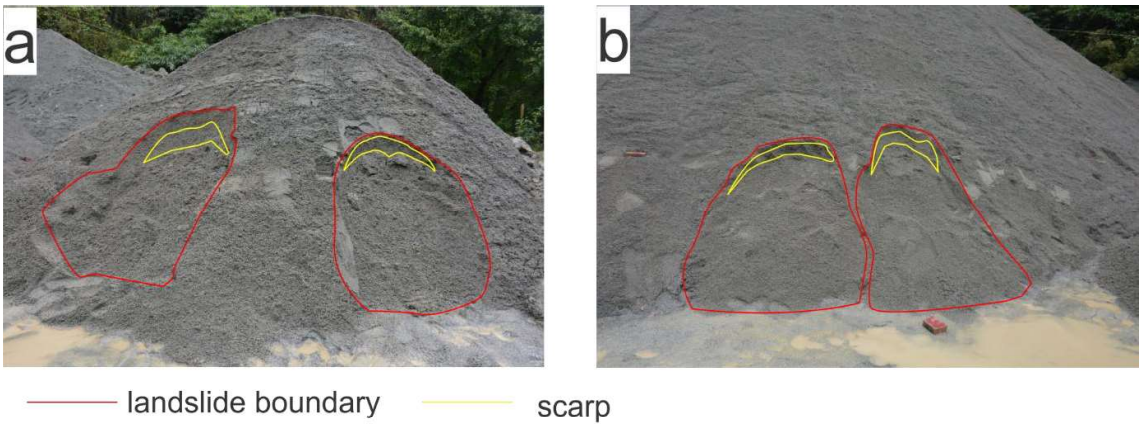

Figure 6: The post-landslide photos of shallow landslides triggered by toe excavation.

3.1.3. Shallow landslides triggered by vibration

To simulate shallow landslide by vibration, four slopes with gradients of 45°, 57°,71°, and 74°, were created, and then we used shovels to vibrate the terrain around these slopes until the slope failure took place. As a result, in the three relatively steeper slopes, the detached sand only collapsed from the top of the slopes, and then totally traveled away from the initial zones, in other words, none of the sliding material was retained within the rupture surfaces. Two of these landslides were shown in Figure 7.

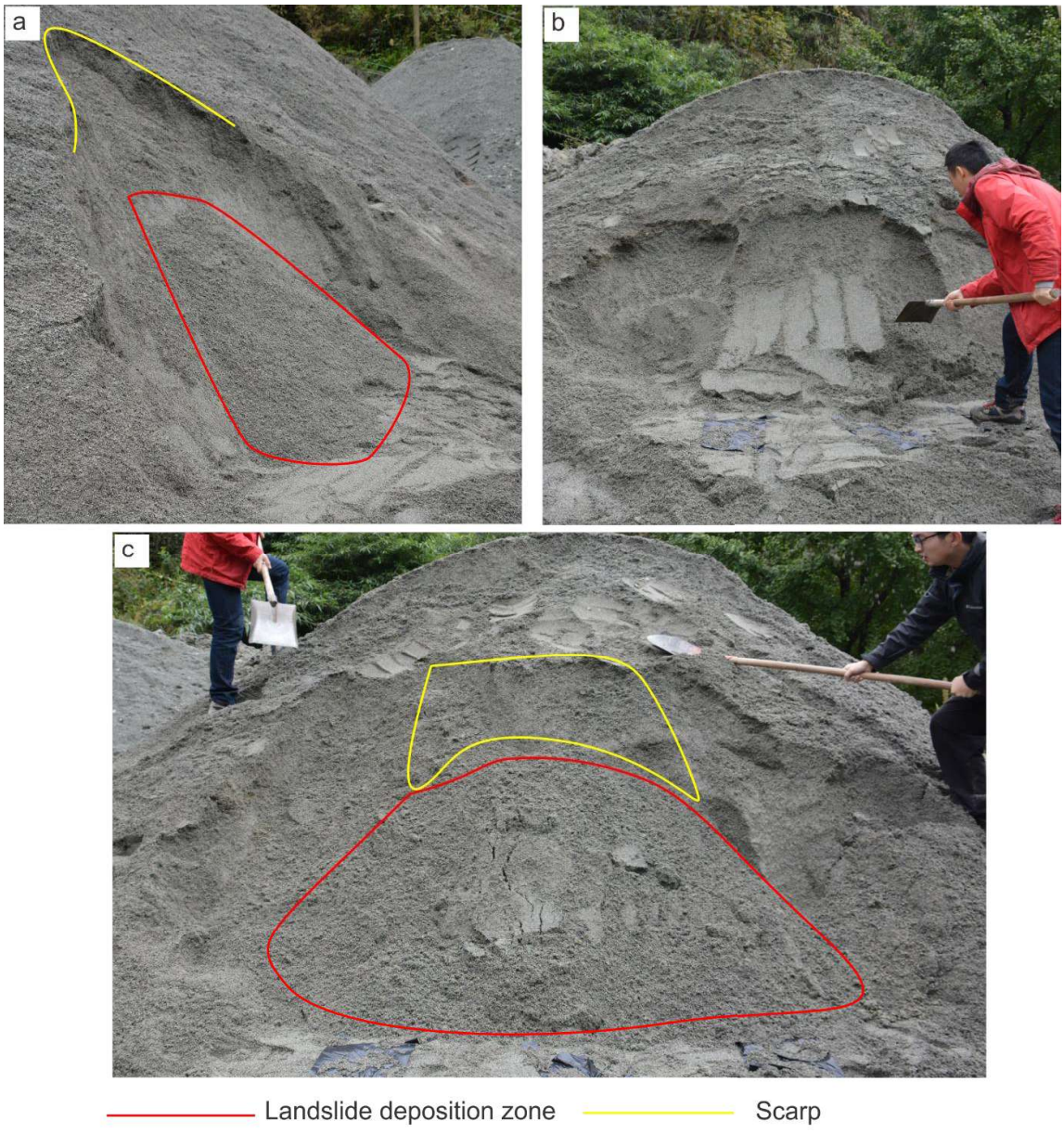

Figure 7: Landslides triggered by vibration. (a) is post-topography of the landslide in which the detached sand totally traveled out of the initial zone. (b) and (c) are the pre- and post- topography of the landslide in which the detached sand still retains a part at the rupture surface.

3.2. Data acquisition and processing

As mentioned before, for each experiment, three drone flights were used to take photographs from the top of the slope in order to capture the topography before-, after- the landslide occurred, and for the rupture surface. Figure 8 shows the entire procedures for making the topographical models.

The aerial photos were taken by a DJI Phantom3, a 4-axis, 4-rotor drone with its camera FC300C_3.6_4000x3000 which has a 20mm fixed focal lens and an imaging sensor of 6.317mm by 4.738 mm, this camera can provide 12 million effective pixels (Figure 9). The camera is located at the bottom of the drone attached to an aerial gimbal which is used to maintain the stability of the camera. The flight route can be controlled by a control board, and the image capturing is controlled by a smartphone application DJI GO, on which also the real-time images are displayed.

In order to generate all topography models in the same baseline, eight control points were positioned around the landslides and their geolocation was measured with the RTK-GPS. Usually, the measured control points would be separated as ground control points (GCP) and checkpoints. GCPs would be used to geo-reference the coordinate of the topography model, and the checkpoints would be considered as a benchmark for the absolute error analysis. However, in this case, since the volume calculation is based on the relative difference between two topographical models, the relative errors between multiple topographical models are more important in the volume calculation, therefore all control points were established as GCPs. Also, in order to minimize the relative errors between a pair of topographical models, manually geo-referencing is still necessary before applying the volume calculation.

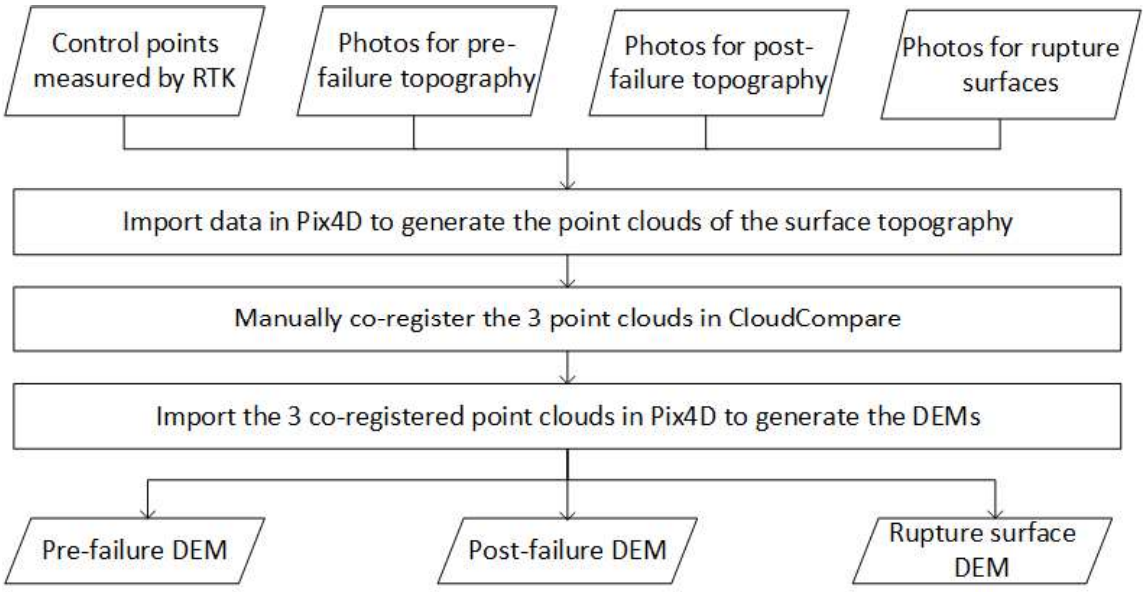

Figure 8: The workflow of generating the topographical models for the experiments

Figure 9: DJI Phantom 3

During the flight, the drone was steered in manual mode flying around the experimental landslides, while the images were captured on the smartphone by another person. In these images, two adjacent images must have an overlapping area. Overall, for each fight, 22 - 55 images in total were collected. An example of the flight path of the drone is presented in Figure 10.

After initial processing and geo-referencing, the point cloud of the topographical model was generated. Similarly, the point clouds for the pre- and post- event topography were generated in the same way. Each point in the point cloud contained the information of its coordinate and RGB values. Then the post-event point cloud was chosen as the reference, the pre-event point cloud and the point cloud of the rupture surface were co-registered to the post-event point cloud in CloudCompare software. The function Align in CloudCompare was used in this process, in the co-registration, several pairs of matching points were selected manually from two point clouds. The co-registration was continuously adjusted until satisfactory results were obtained, in which the aligned point cloud was visually matching with the reference one. It is worth noting that in these cases, it was necessary to apply manual co-registration because the volume calculation of these laboratory-scaled landslides is quite sensitive to the co-registration. Although in a broader context, natural landslides which are much larger, have volumes of hundreds or thousands of cubic meters, and the manual co-registration is not necessary anymore, because the geo-referencing by the RTK-GPS (usually with an error within 2 cm) is already accurate enough for getting accurate volumes (Shuxin et al., 2002).

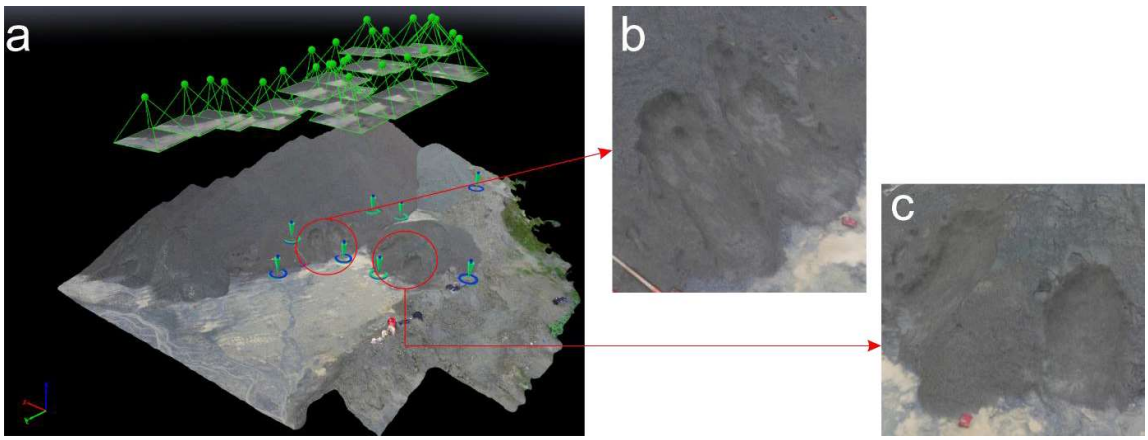

Figure 10: The flight route map. The green dots in figure (a) are the drone's position, and the green boxes are the images' orientation. The blue marks below are the geo-location of the GCPs, and the green marks are the computed geo-location after the geo-referencing. Figure (b) and (c) are the rupture surfaces.

After the co-registration, the point cloud was imported into Pix4d again to generate a DEM. The further volume analysis was based on it.

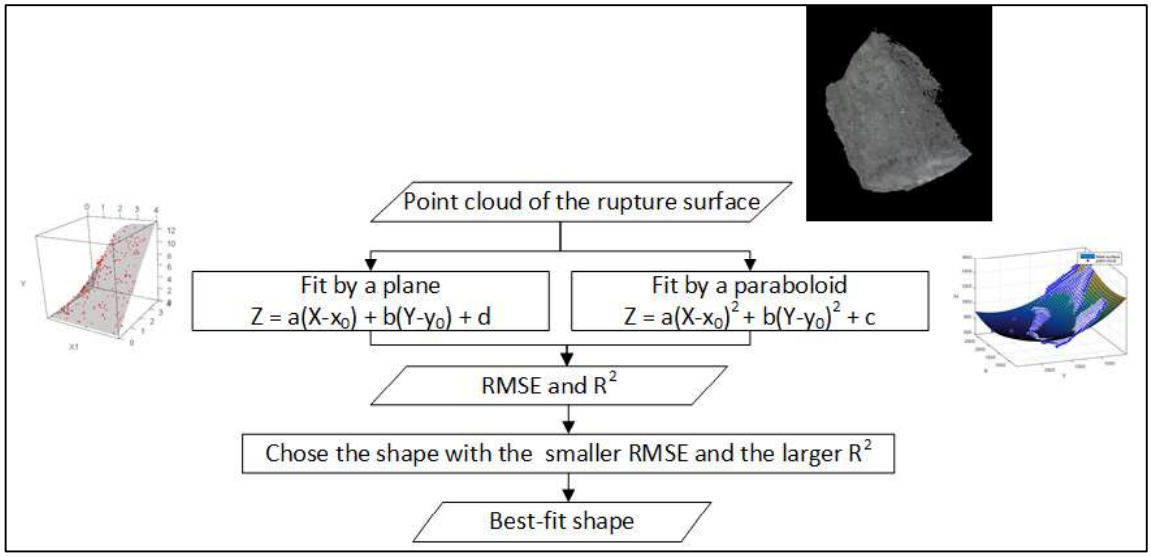

Figure 11: The workflow for choosing the best-fit shape of the rupture surfaces

3.3. Rupture surface reconstruction

As mentioned before, this study is aiming to develop a method in which the rupture surface reconstruction could be based on the exposed scarp and a few points inside of the landslide with known depths to the rupture surface, which could be boreholes, geophysical data or other observations. The purpose of this reconstruction is to infer the depth of the rupture surface where it is not directly visible. Fitting the scarp area and points with known depths into a certain type of geometrical shape could be a feasible way to realize it. However, it is necessary to test the best-fit shape of the rupture surface before applying the method, since the fitted result quite relies on the shape chosen in the fitting method.

From the literature review, quadric surface is the most widely used shape in simulating the rupture surface, nevertheless, it has not been tested. In order to determine the best-fit shape of the rupture surfaces, a workflow was designed (Figure 11). Here the complete rupture surface was selected in fitting instead of the scarp and given points, as this stage focuses on the capability of the shapes. We first clipped the complete rupture surface and then fit it into different shapes. Two types of shapes were selected to compare, the plane and the paraboloid surface. In the 3-dimensional space, the equation of a plane is given by equation [1]

$$Z = a(X - x_0) + b(Y - y_0) + c \qquad [1]$$

In which X, Y, Z are the coordinate of the points in the point cloud, and a, b, d, x_0, y_0, are the constant returned by the fitting, and the equation of paraboloid is

$$Z = a(X - x_0)^2 + b(Y - y_0)^2 + c\,. \qquad [2]$$

In which X, Y, Z are the coordinate of the points in the point cloud, and a, b, d, x_0, y_0, are the constants returned by the the paraboloid fitting.

The root-mean-square error (RMSE) and R-squared (R^2) were used to evaluate the fitting.

RMSE is a widely used measure to evaluate the difference between the input data and the fitted result. The RMSE is computed as

$$\mathrm{RMSE} = \sqrt{\frac{\sum_{i=1}^{n}(\hat{Z}_i - Z_i)^2}{n}} \qquad [3]$$

in which $\hat{z}_i$ is the elevation of the input data, and the z_i is the elevation of the fitted result. It is an absolute value representing the sample standard deviation between the fitted result and the input data.

R^2 is another commonly used measure to evaluate how close the sample data are to the fitted result. The R^2 is computed as

$$R^2 = 1 - \frac{\sum_{i=1}^{n}(\hat{Z}_i - Z_i)^2}{\sum_{i=1}^{n}(\hat{Z}_i - \bar{Z}_i)^2} \qquad [4]$$

In general, R^2 represents how good the fitted equation can explain the input data.

In this workflow, the RMSE and R^2 were used as the indexes for the goodness of fit, since the optimal fitting geometry should generate a relative low RMSE. By comparing the RMSEs of the fitting results with planes and the fitting results with a paraboloid, the best-fit shape would be chosen in the further analysis of the rupture surface reconstruction where the input data are the scarp and the known points.

With the best-fit shape, the proposed method could be determined as shown in Figure 12. A MATLAB script was written that carries out this procedure (See Appendix 1). In the fitting, the weight of the scarp point cloud and the points with known depths of rupture surfaces would be adjusted, otherwise, since the amount of the points in scarp is too large compared with the known depths, the fitting would ignore the known depths. So, in the processing script, the weight of each point with known depth was increased to the weight of the scarp. The final output would be a DEM of the reconstructed rupture surface in GeoTIFF format.

3.4. Volume calculation

In the proposed method, the volumes of the test landslides could be generated by the difference from comparing the reconstructed rupture surface with the pre-event DEM and the post-event DEM. The volume figure from the difference between the reconstruction and the pre-event DEM presents the initial volume of the mobilized mass before the landslide happening, while the figure from the reconstruction and post-event DEM presents the volume after deposition.

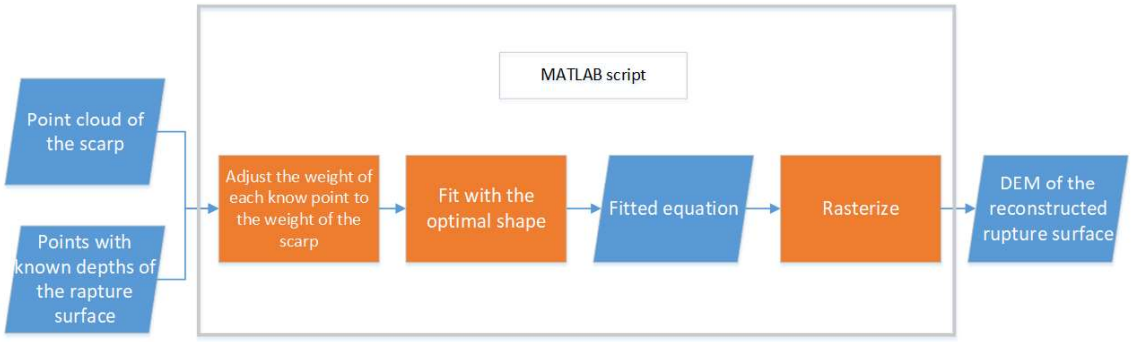

Figure 12: The workflow of the proposed method

Also, as the true rupture surfaces were already measured, comparing it with the post- and pre- topography could give relative more accuracy initial and deposited volumes. They were used as a reference to evaluate the proposed method.

Since the volumes were calculated from DEM differences, the volume figures would be influenced by the systematic difference between DEMs. In order to evaluate the systematic errors, several checkpoints were selected in the unchanged areas around landslides. The DEM values at these places are assumed to remain constant, thus this variation of these elevation values in the pair of DEMs could give indications about the error in the volume calculation. Normally, in multi-temporal DEMs of natural landslides, this error would not influence a lot in the results since the error of geo-referencing by the RTK-GPS is negligible compared with the landslide displacement of multi-temporal DEMs. However, for the laboratory-scaled landslides in this study, it may be an important concern. Thus, the AHDM method mentioned in section 2.1 was incorporated to correct the DEM difference. Here, since the primary geo-referencing was already done by the RTK-GPS and manual adjustment, and it is reasonable to assume that the displacement between DEMs was caused by the up-and-down shift, then the error can be corrected by vertical adjustment. The average value of these checkpoints would be used to correct the volumes. For instance, if the rupture surface intercepts the pre-DEM in a 1 m^2 projection area and the checkpoints show that the rupture surface DEM is relatively lower than the Pre-DEM by 0.01 m on average, the calculated volume would be subtracted by 0.01×1 m^3. Also, according to unbiased estimation method, the standard variation (SD) of the difference values between DEMs can be estimated by the sampling checkpoints as

$$SD = \sqrt{\frac{\sum_{i=1}^{n}(X_i - \bar{X}_i)^2}{n-1}} \qquad [5]$$

where the X_i is the difference value in these checkpoints, and the $\bar{X}$ is the mean. With this standard deviation, in statistics, the most likely range of the adjustment value would be calculated, because the "mean±SD" covers 68.27% in normal distribution in the previous example, it should be 0.01×1±SD×1 m^3. This range was considered as the error range in the volume figure.

For comparison, the volume figures from the empirical area-volume relationship and the post-pre topographical difference were be calculated. The comparison of the results from different methods could contribute a better understanding of these methods.

4. RESULT OF THE EXPERIMENT LANDSLIDES

In this chapter, the results of all experiments were presented. Four sections, data description (section4.1), geometry of experimental landslides (section 4.2), volume calculation (section 4.3) and summary (section 4.4) were included. Section 4.1 described the data procced by Pix4d. Section 4.2 focused on the geometry of the experimental landslides which discussed the depth-to-length ratios and the best-fit shape of experimental landslides. Section 4.3 presented the volume results by the proposed method and compared it with the volume figures by simple pre- and post- DEM difference and area-volume relationships. Here the deep-seated landslide was coded as D, while the four shallow landslides by toe excavation were coded as SE1, SE2, SE3, SE4, and the four shallow landslides by vibration were coded as SV1, SV2, SV3, SV4. For illustration purposes, the focus is given on SV1 in this section, and the results of other landslides were presented in appendix 4 and appendix 5. Section 4.4 summarized and discussed the results of the experiments and the proposed method.

4.1. Data from the drone photogrammetry

As a result, the point clouds, multi-temporal DEMs, orthomosaics of each landslide topography were obtained using Pix4D. Ideally, when using drone-derived topographical models, the generated data would be compared with elevation models made by laser scanning to evaluate their quality. Unfortunately, there are no available laser scanning data in this case. Here we assessed the point cloud density of these topographical models. The density was estimated by counting for each point the number of neighboring points inside a 5 cm-radius sphere. The results of landslide SV1 are shown in Figure 13, and the results of other landslides are shown in Appendix 2. Also, for each topographical point cloud, the average number of the neighboring points of each point of landslide affected areas inside a 5cm radius sphere was computed and shown in Table 5. The pixel sizes of the drone-derived DEMs are also presented in table 5. For some landslides' point clouds and DEMs, the density of points and the cell sizes are very close to each other, since some of them were generated by the same fight. In Figure 5, the point clouds and the raster DEMs made by the same flight were presented in a uniform color.

Table 5: The cell sizes and average point cloud densities and of experimental landslides. The point clouds and the raster DEMs derived from the same flight were presented in the same color. D = Deep-seated landslide, SE = shallow landslides triggered by excavation, SV = Shallow landslides triggered by vibration

Landslide codes	Pre-failure		Post-failure		Rupture surface	
	Neighboring points (n)	Cell size of DEM (cm/pixel)	Neighboring points (n)	Cell size of DEM (cm/pixel)	Neighboring points (n)	Cell size of DEM (cm/pixel)
D	77	0.328	70	0.300	101	0.316
SE1	75	0.486	23	0.540	43	0.401
SE2	110	0.486	26	0.540	49	0.401
SE3	112	0.486	26	0.540	51	0.401
SE4	91	0.486	25	0.540	50	0.401
SV1	131	0.279	171	0.359	50	0.402
SV2	43	0.419	54	0.366	57	0.383
SV3	49	0.419	58	0.366	62	0.383
SV4	42	0.419	61	0.366	52	0.383

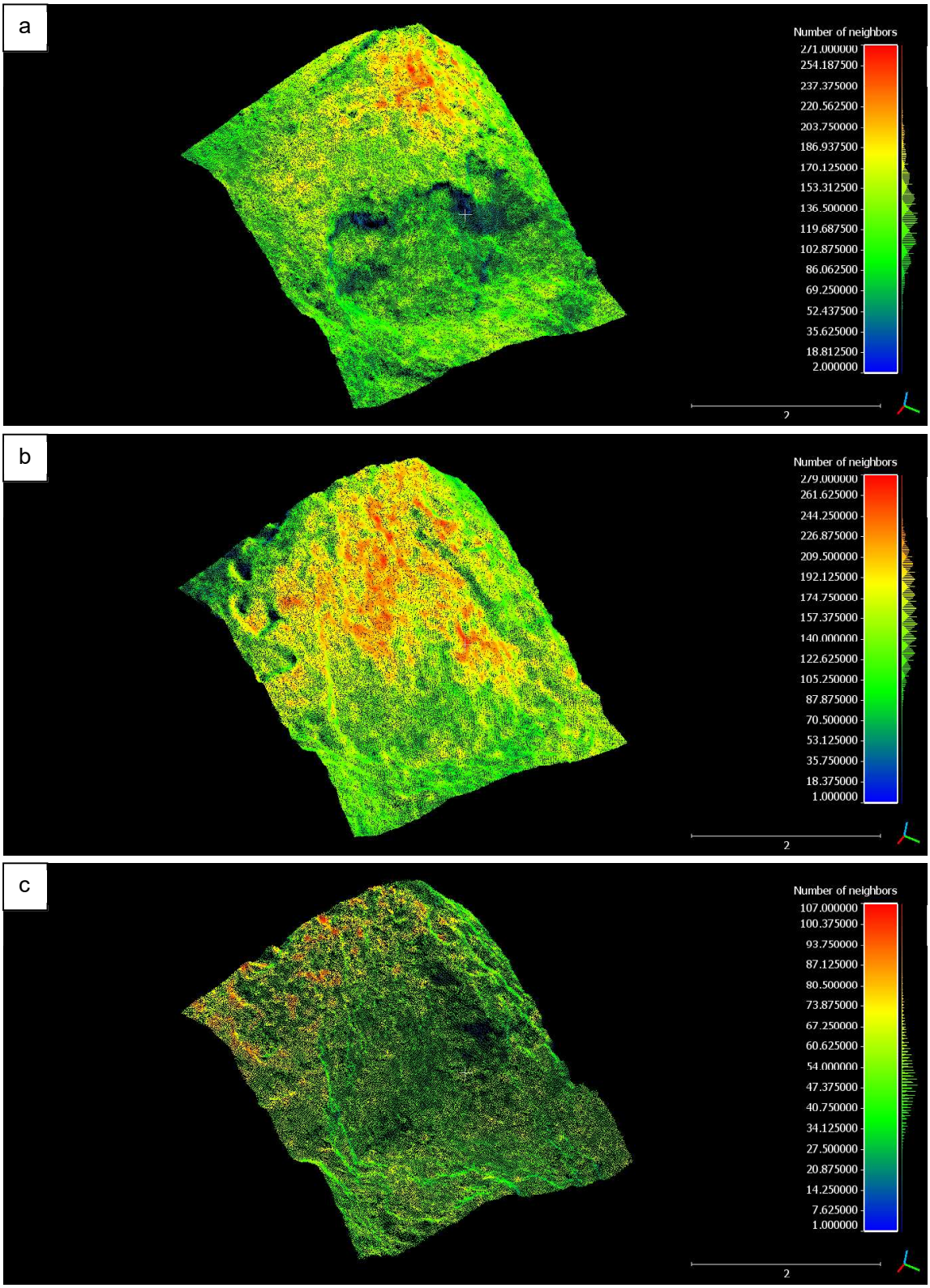

Figure 13: Point cloud density of the experimental shallow landslide SV1 triggered by vibration. The colors on points represent the number of the neighboring points in its 5cm radium sphere. (a) is the point cloud of pre-failure topography, (b) is the point cloud of post-failure topography, (c) is the point cloud of the rupture surface.

The small-scale field test landslides and their lengths, widths, depths, and depth-to-length ratios were shown in Table 4. As mentioned earlier, these experiments are to simulate deep-seated landslides and shallow landslides, however, even though the terms "deep-seated", "shallow" have been extensively used in articles, a quantitative definition is still missing. The judgment of them is still subjective and relies quite on field experience. Here we proposed to use the depth-to-length ration as an indication to evaluate whether a landslide can be classified as deep-seated or shallow. The advantage of this ratio is that it can establish a measure relying on the relative dimensions, by this ratio, the comparison of landslides in different size becomes feasible.

Figure 14 shows the depth-to-length ratio of the experimental landslides and the average values for each landslide types. In these cases, the deep-seated landslide has a depth-to-length ratio of 0.30 which is the highest among all experimental landslides, while the second-high ratio is from the shallow landslides by vibration, with average 0.15. Shallow landslides by toe excavation show the lowest ratio, 0.10. The result shows that the depth-to-length ratios are clearly different among different landslide types. Comparing the ratios of the deep-seated and the shallow landslides, the ratio of the deep-seated landslide, is twice as high as the ratio of the shallow landslides triggered by vibration and is triple the ratio of the excavation triggered shallow landslides. However, in this study, only 1 deep-seated landslide was generated, and more examples are needed before a more general conclusion could be drawn.

For the other experimental landslides, as mentioned in Figure 11, the point clouds of the rupture surfaces were fitted by a plane and a paraboloid. The fitted surfaces of SV1 are presented in Figure 15, and for other landslides, the fitted surfaces are shown in Appendix 3. Their RMSE with the R^2 are illustrated in Table 6. By looking at Table 6, the RMSE of the plane fitting is always larger than the RMSE of the paraboloid fitting. It means that when comparing the elevation value of the actual rupture surface with the fitted result, paraboloid fitting always generates relatively less variance. Also, by checking the R^2 values, for each landslide in the experiments, the paraboloid leads to a larger R^2 which is closer to 1. It means that the paraboloid can explain the geometry of landslides better than the plane. Thus, the paraboloid was chosen for the best-fit of the rupture surface and was incorporated in the proposed method.

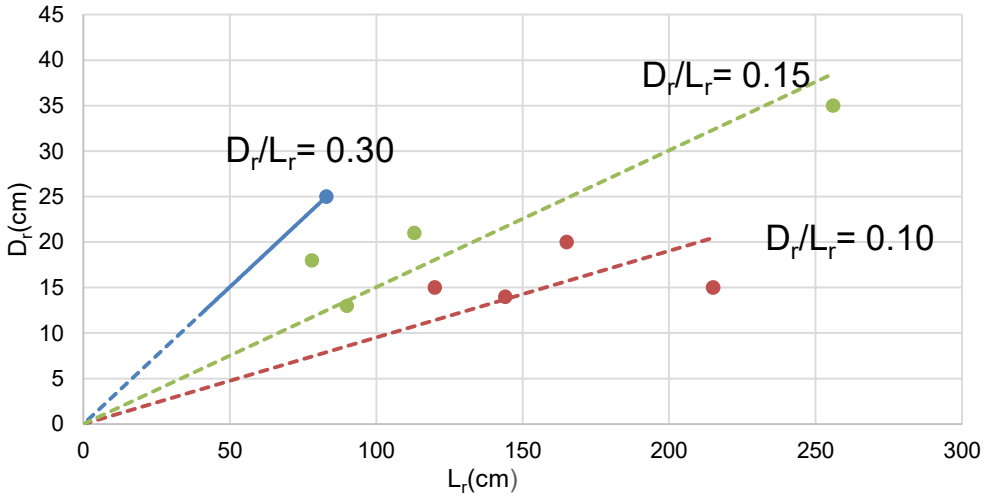

Figure 14: The depth-to-length ratio of the experimental landslides, the blue line represents the ratio of the deep-seated landslide, while the green line and red line represent average ratios of the shallow landslides by vibration and toe excavation.

In landslides SV2, SV3, SV4. The sliding material was totally detached from the rupture surfaces and accumulated at the toes of the initial slopes. Thus, there is no displaced material retaining at the rupture surfaces. In these situations, the increase of the volume in the deposit zone and the decrease of the volume in the accumulation zone can represent the volume of the landslide already (Figure 16). So, the volume can be calculated directly from the DEM difference between post- and pre- DEMs, and then the rupture surface reconstruction is not necessary in these cases (results shown in Appendix 5).

Table 6: The RMSE and R2 of the rupture surface point cloud fitting for the experiments

Landslide codes	RMSE (cm)		R2	
	plane	paraboloid	plane	paraboloid
D	6.3	4.2	0.75	0.89
SE1	6.4	2.9	0.87	0.97
SE2	6.3	2.9	0.90	0.98
SE3	6.5	3.8	0.95	0.98
SE4	6.0	3.8	0.95	0.98
SV1	9.6	6.2	0.96	0.98

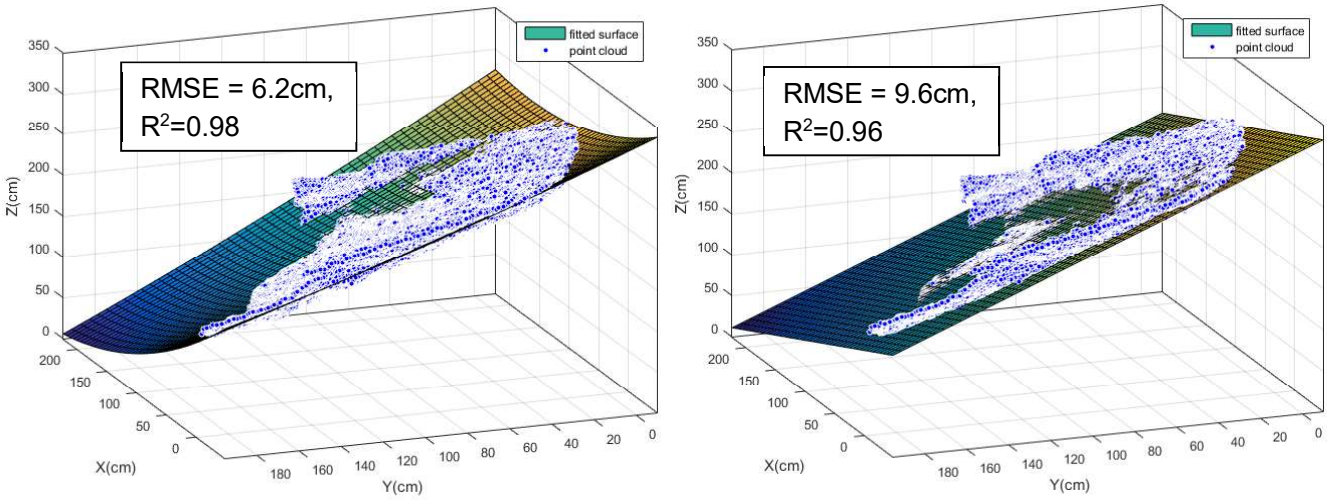

Figure 15: Fitting of the paraboloid and plane from the rupture surface point cloud of the experimental shallow landslide by vibration SV1. The blue points are the initial point cloud of the rupture surface and the surfaces are the fitted plane and paraboloid.

4.3. Volume calculation

In this section, for illustration purposes, landslide SV1 was selected as an example to show the whole processes of the calculation. Other landslide volumes were generated in the same way.

For SV1, the pre-, post, rupture surface DEMs were compared in pairs by subtracting with each other. The net gain and net loss were presented in Figure 17. It is clearly seen that there was still a portion of the displacement material retaining within the rupture surface, and this portion was not addressed at the difference of the post- and pre- subtraction.

For the proposed rupture surface reconstruction, the points in the exposed scarp were clipped from the point cloud of the rupture surface. Also, a point was selected in the middle part of the accumulation zone,

simulating the availability of a borehole (Figure 18). Ideally, based on the proposed method, the scarp is supposed to be clipped from the post- point cloud, but in these small laboratory-scale landslides, the volume analysis could be much sensitive to the systematic elevation difference than in real cases. If the scarp and the borehole were from different sources, the existing systematic difference between the post and the rupture surface point clouds would introduce an uncertainty in the fitting. It may affect significantly the paraboloid fitting. To avoid this potential deviation, clipping them from the rupture surface was applied here instead. The difference of the reconstructed rupture surface between pre-, post- DEM is shown in Figure 19.

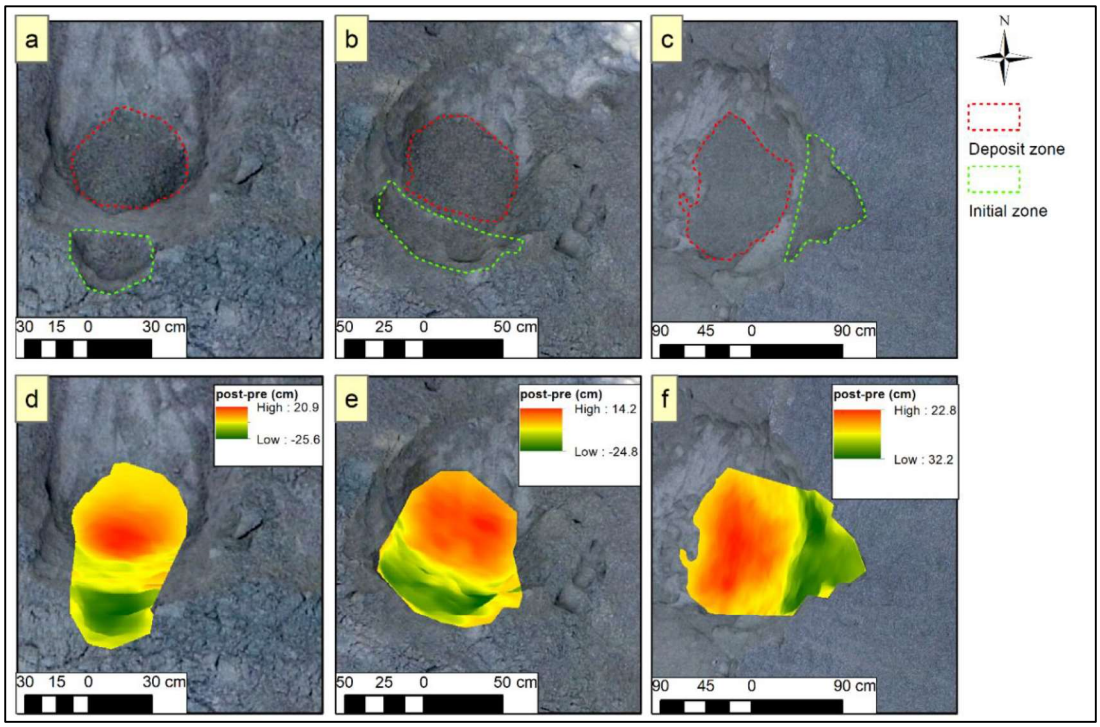

Figure 16: Difference between the pre- and post DEM of the shallow landslides triggered by vibration SV2, SV3, SV4. (a), (b), (c) show the initial zones and the deposition zones of experimental landslides SV2, SV3, SV4 respectively, while (d), (e), (f) show the difference of the elevation values by subtracting the pre-DEMs from the post-DEMs in these areas.

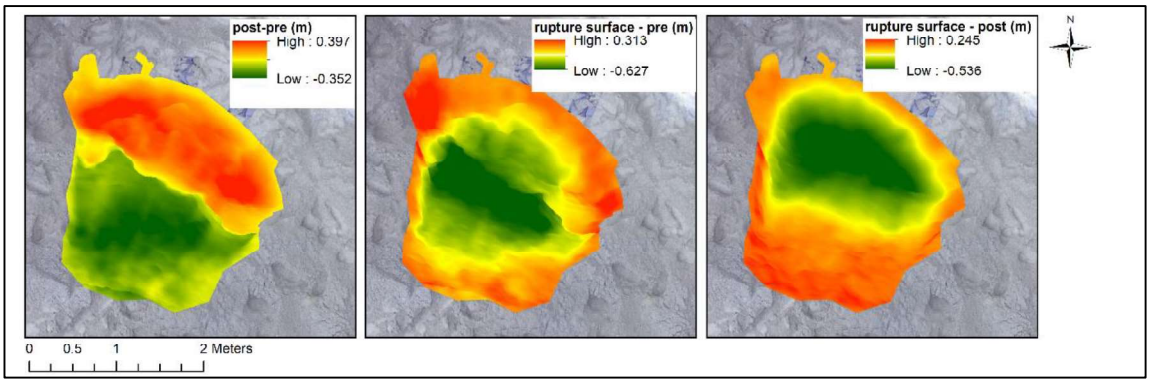

Figure 17: The DEM difference between the post-, pre-, and rupture surface topography of the shallow landslide triggered by vibration SV1

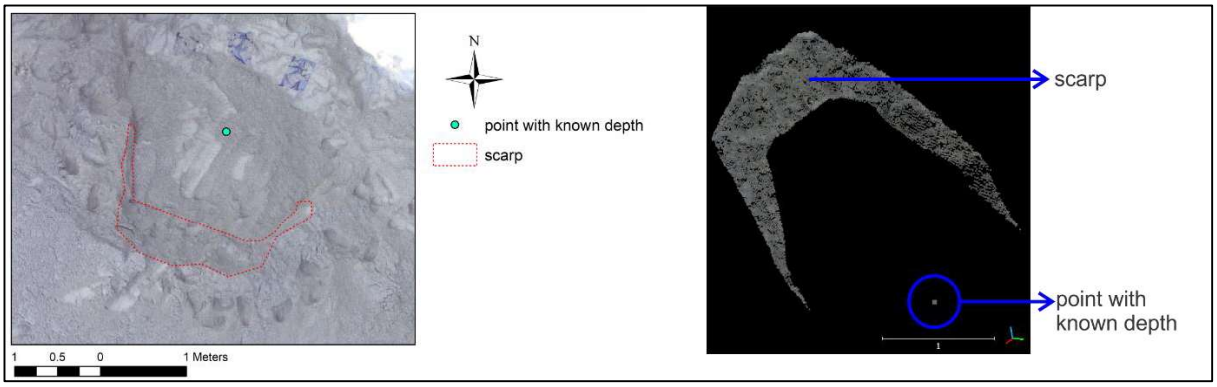

Figure 18: The extraction from the point cloud of the scarp and the point with known depth to rupture surface for fitting the rupture surface of shallow landslide by vibration SV1

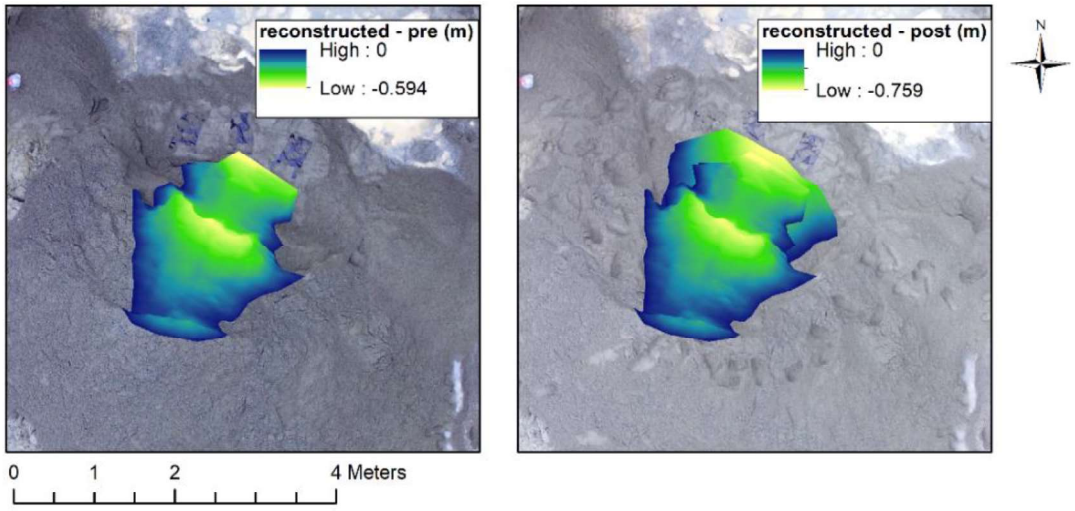

Figure 19: Elevation difference between the reconstructed rupture surface and the pre-, post- DEMs of the shallow landslide by vibration SV1

As mentioned in section 3.4, in total eight checkpoints were assigned to the undisturbed area around the landslide affected area through visual inspection (Figure 20). The mean difference and standard deviation between DEMs were shown in table 7. Then the volumes with their error range based on the checkpoints were presented in Figure 21. The volumes generated by empirical area-volume relationship by Larsen and Guzzetti were also shown in Figure 21 for comparison. The results of other landslides were presented in appendix 4.

The volumes by subtracting the measured rupture surface from post- and pre- DEMs were considered as references for the deposited volume and the initial volume of the landslide. As the structure of the material was disturbed during the failure, for a landslide, these two volumes are not necessarily identical. The initial volume was used to evaluate the errors of the depletion volume, as well as the volume by the difference between the reconstructed surface and the pre-DEM. The deposited volume was used to evaluate the evaluate the error of the accumulation volume, as well as the volume by the difference between the

reconstructed surface and the post-DEM. For the errors of the area-volume relationship, since the volumes that used in the statistical regression were basically from the field investigation after the slope failure, the errors of them were also estimated by comparing them with the deposited volume. The errors of all landslides were calculated and shown in Table 8 and Figure 22. In this case of SV1, the proposed method generated the most accurate results with errors 0.6% and 10.0% for the initial and deposited volume respectively. For landslide SV1, The Guzzetti's area-volume relationship generated a deposit volume with a -16.5% error which is close to the proposed method and performs better than Larsen which is overpredicting 36.2% in this case. The depletion and accumulation volume show significant underestimation.

For all these analogue experiments conducted, by checking Table 8 and Figure 10, both the proposed methods and the Guzzetti's area-volume relationship can produce a reliable result with the mean inaccuracy close to zero. Nevertheless, by looking at every experimental landslide individually, the proposed method always provided a more accurate result compared with Guzzetti's area-volume relationship. Larsen's area-volume relationship tend to overestimate the volumes in this case.

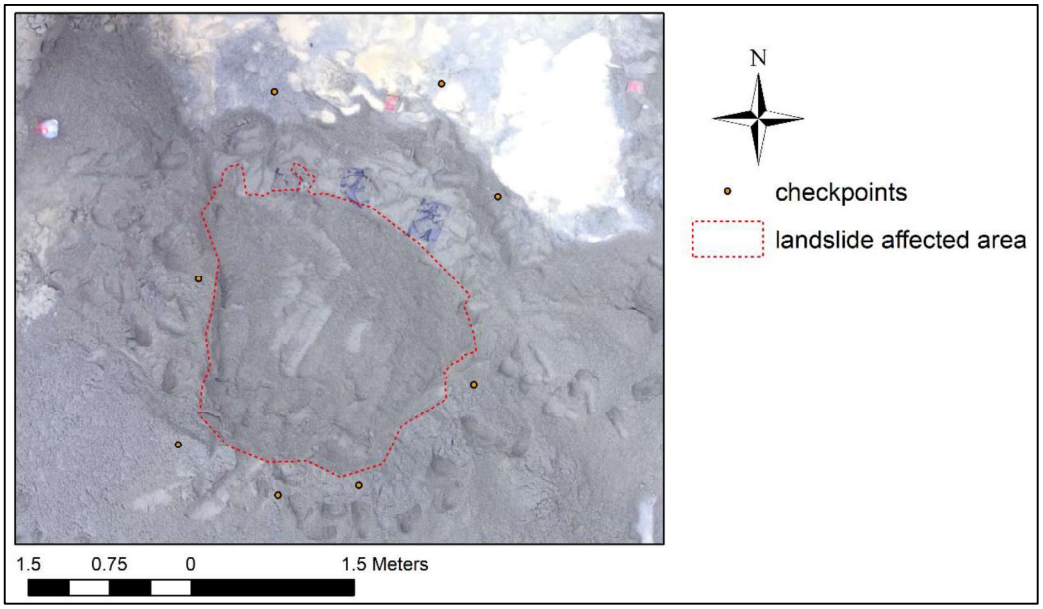

Figure 20: Checkpoints' locations used to evaluate the systematic difference between different DEMs for landslide shallow landslide triggered by vibration SV1.

Table 7: *The mean difference and the standard deviation between DEMs of SV1 based on the plotted checkpoints*

	Post - Pre	Rupture surface - Pre	Rupture surface - Post
Mean difference (m)	-0.032	0.035	0.067
Standard deviation (m)	0.039	0.014	0.038

4.4. Summary

The paraboloid was selected as the suitable geometric shape for the rupture surfaces of all the landslide types in the experiments. Comparing with the accumulation volumes, depletion volumes, and the volumes calculated and empirical area-volume relationships, the proposed methods provided more accurate results for the analogue landslides.

Table 8: Errors of the volume calculated by several pairs of DEM difference and the empirical area-volume relationship for SV1, as compared to the measured volume (pre-failure – rupture surface volume). Positive values indicate overestimation, while negative values indicate underestimation. The errors of the proposed method were highlighted with yellow.

Volume	SV1	SV2	SV3	SV4	SE1	SE2	SE3	SE4	D
Accumulation	-51.1%	/	/	/	-44.4%	-9.5%	-61.7%	-70.1%	-66.9%
Depletion	-51.7%	/	/	/	-61.6%	-37.9%	-69.8%	-69.6%	-70.9%
Reconstructed - post	10.0%	/	/	/	-22.5%	-4.4%	-1.8%	29.2%	15.2%
Reconstructed - pre	0.6%	/	/	/	-32.6%	-17.4%	-18.6%	12.3%	38.6%
Guzzetti's area-volume relationship	-16.5%	-16.3%	48.8%	13.7%	-7.6%	22.5%	34.7%	-24.7%	-55.4%
Larsen's area-volume relationship	35.7%	96.7%	155.7%	173.5%	85.4%	136.6%	140.3%	44.2%	-8.6%

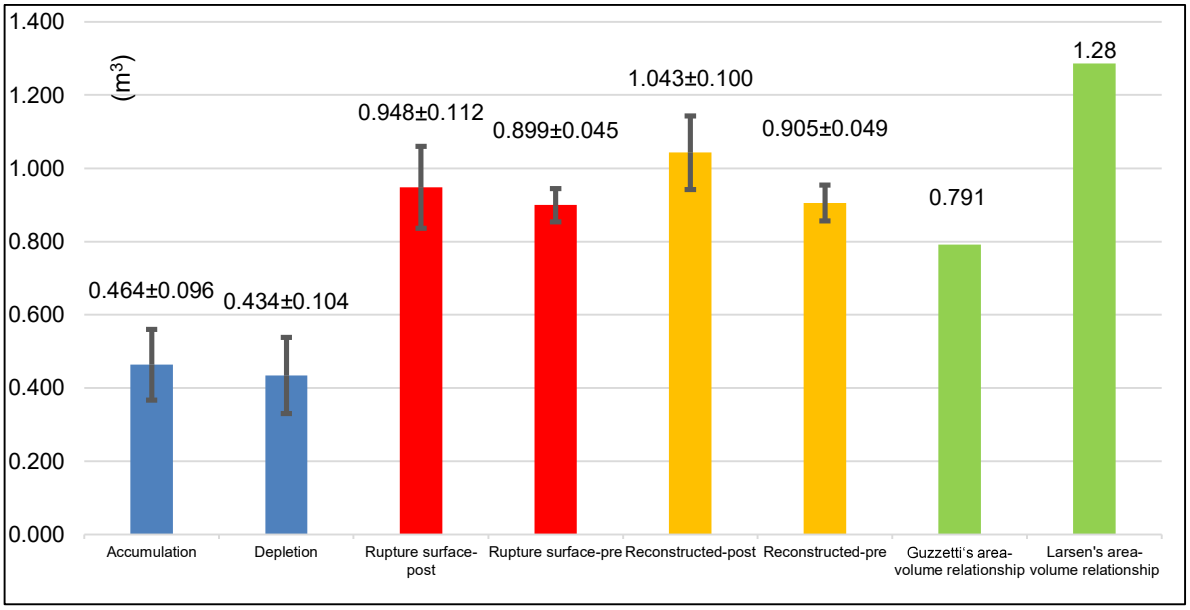

Figure 21: the volume figures for the shallow landslide triggered by vibration SV1 calculated by several pairs of DEM difference and the empirical area-volume relationships. The accumulation and depletion are the net gain and loss based on the pre- and post- failure DEM difference. The "rupture surface – post" and "rupture surface – pre" mean the volumes calculated by the difference between the DEM in which the displaced material was moved out, with the pre- and post- failure DEM difference. The "reconstructed – post" and "reconstructed – pre" mean the volumes calculated by the reconstructed rupture surface by the proposed method and the post- and pre- failure DEM difference. The error bars infer the uncertain range of the volume calculation from the DEMs' systematic difference. The green columns are the volume calculated by the area-volume relationships.

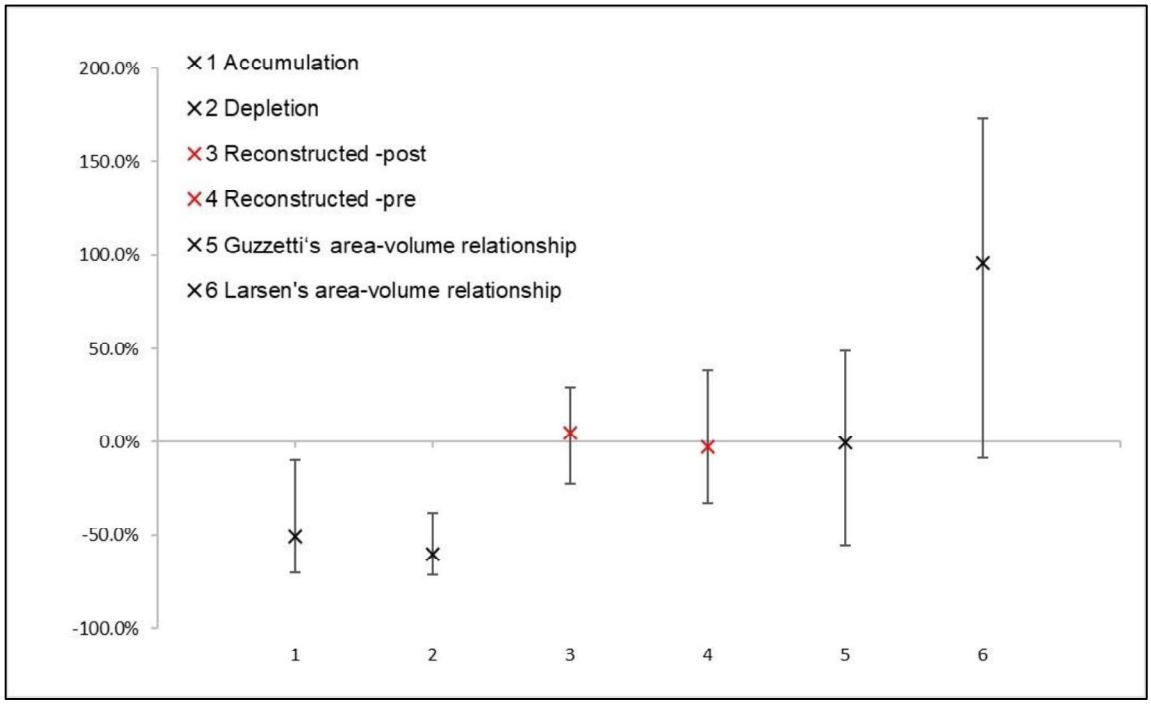

Figure 22: The inaccuracy of volume estimation for different methods based on the landslides on sand piles. Positive values indicate the percentage of overestimation, while negative values indicate underestimation. The cross shape indicates the mean inaccuracy of each method and the bar indicates the range from the maximum to the minimum of the inaccuracy among the landslides conducted. The accumulation and the depletion represent taking the net gain and lost in the pre- and post- failure DEM difference as the deposited and initial volume of the experimental landslides. The "reconstructed - post" and "reconstructed - pre" represents the volume calculated by the difference between the reconstructed rupture surface with the pre- and post- failure DEMs. The proposed method in this study is highlighted with red.

5. APPLICATION TO THE CASE STUDY OF VAJONT

5.1. Introduction

The Vajont landslide was selected as case study to test the method because the DEMs of the situation before and after the landslide occurred and of the rupture surface are available. Thus, it is a suitable case to test the applicability of the proposed method. The Vajont landslide occurred in the Dolomite region of the Alps (46°16'02"N, 12°19'44"E), the catastrophic landslide has been considered as one of the most destructive landslide events of the past century due to its large magnitude and its disastrous effect. The landslide took place on 9th October 1963 with a reported bulk slide volume of 270-300 million m^3 collapsing into a reservoir in the gorge and causing a flood wave over-topping the dam spanning at the gorge. Towns situating behind the dam were destroyed by the flood and more than 2000 people were killed (Barla & Paronuzzi, 2013). The commonly accepted explanation of the mechanism of the Vajont landslide is that the increasing water level in the reservoir led a rise of the pore water pressure in the weak layers, which decreased the effective normal stress and created a favorable condition for the slope failure (Kilburn & Petley, 2003). The panoramic views of the Vajont landslide are shown in Figure 23.

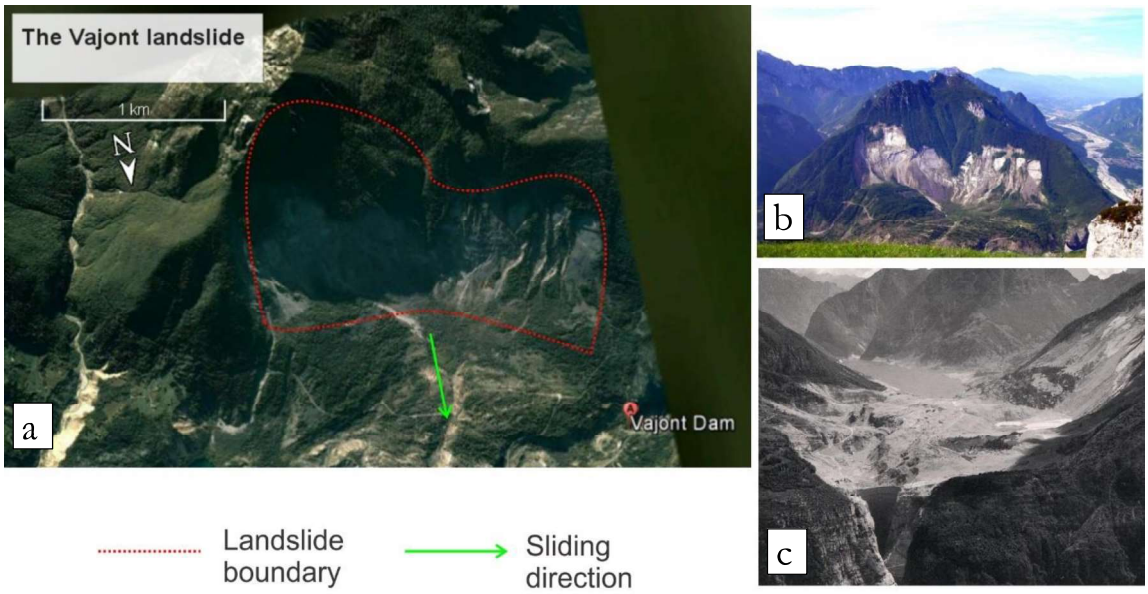

Figure 23: The panoramic view of the Vajont landslide. (a) is the google earth image taken in 2015. (b) is a panoramic photo taken in 2003. (c) is the photo taken immediately after the landslide.

5.2. Data description

The available DEMs are listed in Table 9. The pre- and post-event DEMs were both interpolated by contours with a contour interval of 10m and the rupture surface was interpreted by van Westen from outcropping failure surface indications, side scaprs an upper scarps, and the contour was drawn with a contour interval of 10m in the flatter area in the slope toe part, and contour lines spacing of 50m in the steeper upper part.

Several possible methodological problems exist in contour-based DEMs, such as under- or over-sampling of the terrain between contour lines, errors in digitizing, interpolation methods, vegetation correction. However, in this case, the approaches were used to generate the contours are not known. The only

information about the contour creation is that the rupture surface was interpreted by boreholes and field investigation. Due to this gap, the quality of these contours was not discussed in this study.

Table 9: Available DEMs for the Vajont landslide

DEM types	Description
Pre-event DEM	Pre-event DEMs derived from contour lines with 10m-interval.
Post-event	Pre-event DEMs derived from contour lines with 10m-interval
Rupture surface	DEM of rupture surface derived from 10m-interval in the flat part, 50m-interval in the steep part

5.3. Data processing

For the proposed method, a set of points with known coordinates x, y, z on the scarp and several points with known depths to the sliding layer are required to reconstruct the rupture surface. To acquire the points on the scarp, first the scarp area was digitalized on the post-landslide terrain by visually comparing the post- and pre- topography, the Fishnet function in ArcMap was used to create a set of elevation points with spacing of 30m on the scarp and their elevations were extracted from the post-DEM. For simulating boreholes, four points were selected on the DEM of the rupture surface, their location was shown in Figure 24.

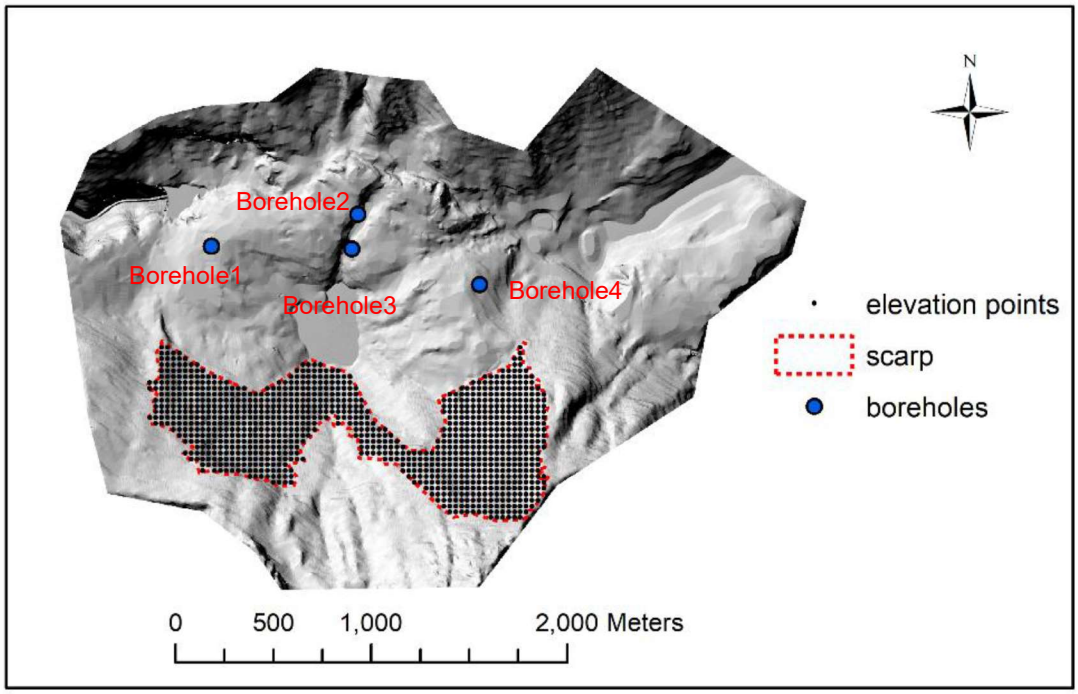

Figure 24: The locations of the elevation points on the scarp and the simulated boreholes. The basemap is the hillshade map of the topography after the landslide.

Then these elevation points and the simulated boreholes were used as the input in the MATLAB script to reconstruct the rupture surface. After that, the volumes were computed by the difference between the reconstructed failure surface and the pre- and post- DEMs. For comparison, the volume of depletion, accumulation and the empirical area-volume relationship were also calculated. Also, to test how the method would perform when no boreholes are available, the fitted surface and volumes were also generated from only the elevation points on the scarp.

5.4. Results

Using the proposed methods, the rupture surface was reconstructed as shown in Figure 25 and the volume based on different pairs of elevation models is presented in Figure 26. The initial volume of the displaced mass (the first red column in Figure 26) was calculated by the difference between the pre-DEM and the rupture surface and was set as the reference to evaluate the accuracies of the depletion volume and the volume calculated by the difference between the reconstructed rupture surface and the pre-DEM. Similarly, the deposited volume (the second red column in Figure 26) of the displaced mass was calculated by the difference between the reconstructed rupture surface and the post-DEM and was set as the reference for the accumulation volume and the volume calculated by the difference between the reconstructed rupture surface and the pre-DEM. The errors were shown in table 10.

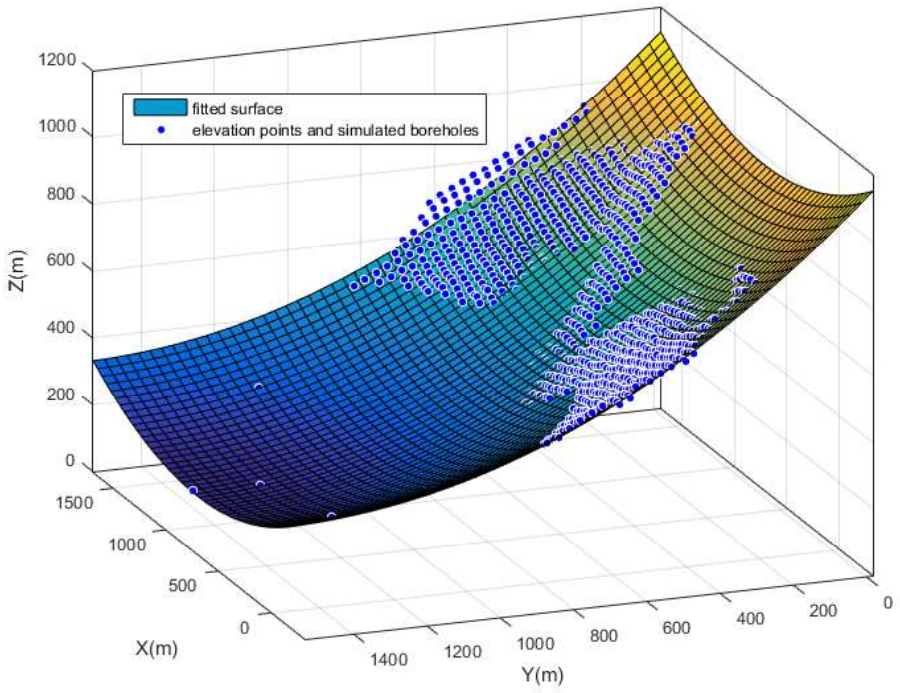

Figure 25: The reconstructed rupture surface of the Vajont landslide based on both the scarp information as well as four simulated boreholes. The blue points on the upper part are the elevation points extracted on the scarp from the post-failure DEM, while the four points on the lower part are the simulated boreholes.

As Table 10 shows, the volumes calculated by the proposed method with boreholes (the yellow columns in Figure 26) are evidently more accurate than other approaches. However, it is noticeable that when there are

no boreholes, the proposed method would cause a large overestimation (the row with dark green in Table 10). Three profiles were made for checking the reconstructed rupture surfaces (Figure 27-28). The profiles show that, when there is no borehole, the reconstructed surface tends to go deeper than the true rupture surface. This is because the scarp has relatively steeper slope angles which are more vertical compared with the slope angles at the toe of the rupture surface. It means that the boreholes play a crucial role in controlling the geometry of the reconstruction. It also can be seen from the profiles that in the Vajont landslides, the slope in the opposite bank blocked the movement of the landslide. Thus, the base of the deposited mass is relatively higher than the reconstructed surface and was not addressed in the proposed method. It could cause a potential overestimation because the covered opposite slope was wrongly considered as a part of the mobilized mass. In this case, as this part of the volume is not significant compared with the landslide body, the error was not reflected in the result.

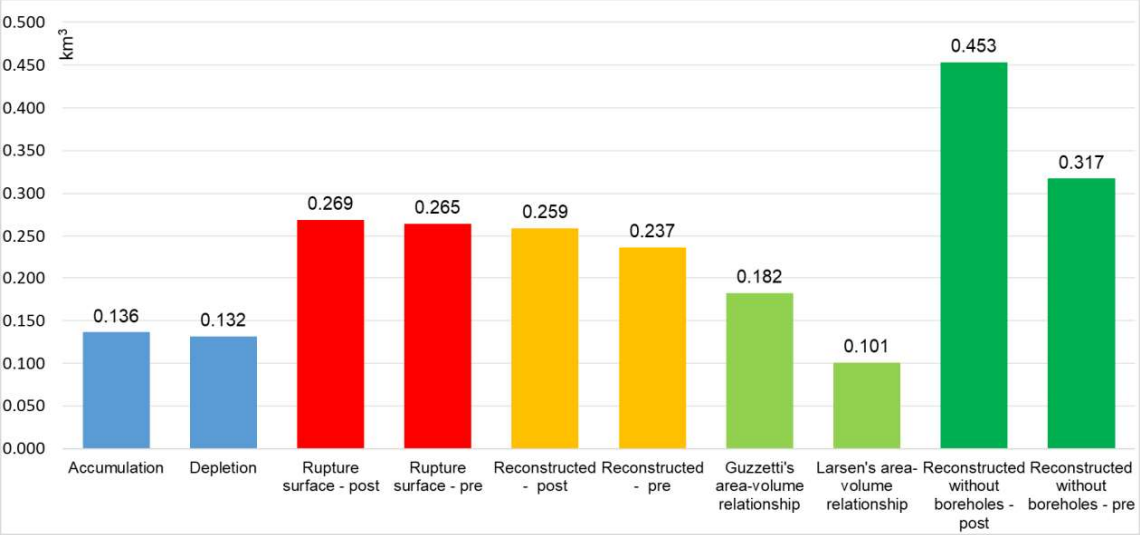

Figure 26: the volume figures of the Vajont landslide. The accumulation and depletion are the net gain and loss based on the pre- and post- failure DEM difference. The "rupture surface – post" and "rupture surface – pre" mean the volumes calculated by the difference comparing the rupture surface with the post-DEM and the pre-DEM respectively. The "reconstructed – post" and "reconstructed – pre" mean the volumes calculated by comparing the reconstructed rupture surface by the method proposed using both the boreholes and scarp information with the post- and the pre- DEM. The light green columns are the volumes calculated by the empirical area-volume relationships. The dark green columns are the volumes calculated by the reconstructed rupture surface by the scarp alone.

Table 10: Errors of volumes calculated for the Vajont landslide. Positive values indicate overestimation, while negative values indicate underestimation. The color is responding to Figure 26.

Volume	Error (%)
Accumulation	-47.5%
Depletion	-44.4%
Reconstructed - post	3.8%
Reconstructed - pre	11.8%
Guzzetti's area-volume relationship	-29.8%
Larsen's area-volume relationship	-61.2%
Reconstructed without boreholes - post	74.7%
Reconstructed without boreholes - pre	19.9%

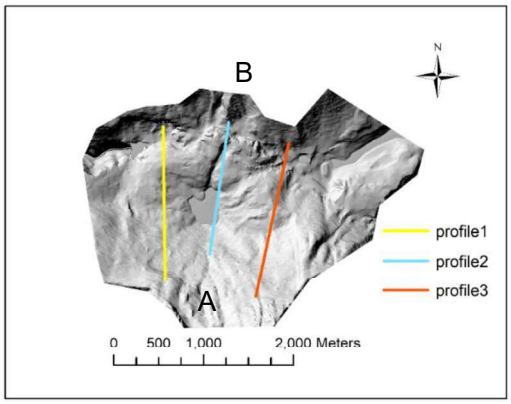

Figure 27: The locations of the three profiles of the Vajont landslides. (A) and (B) indicates the start and the end of the profiles.

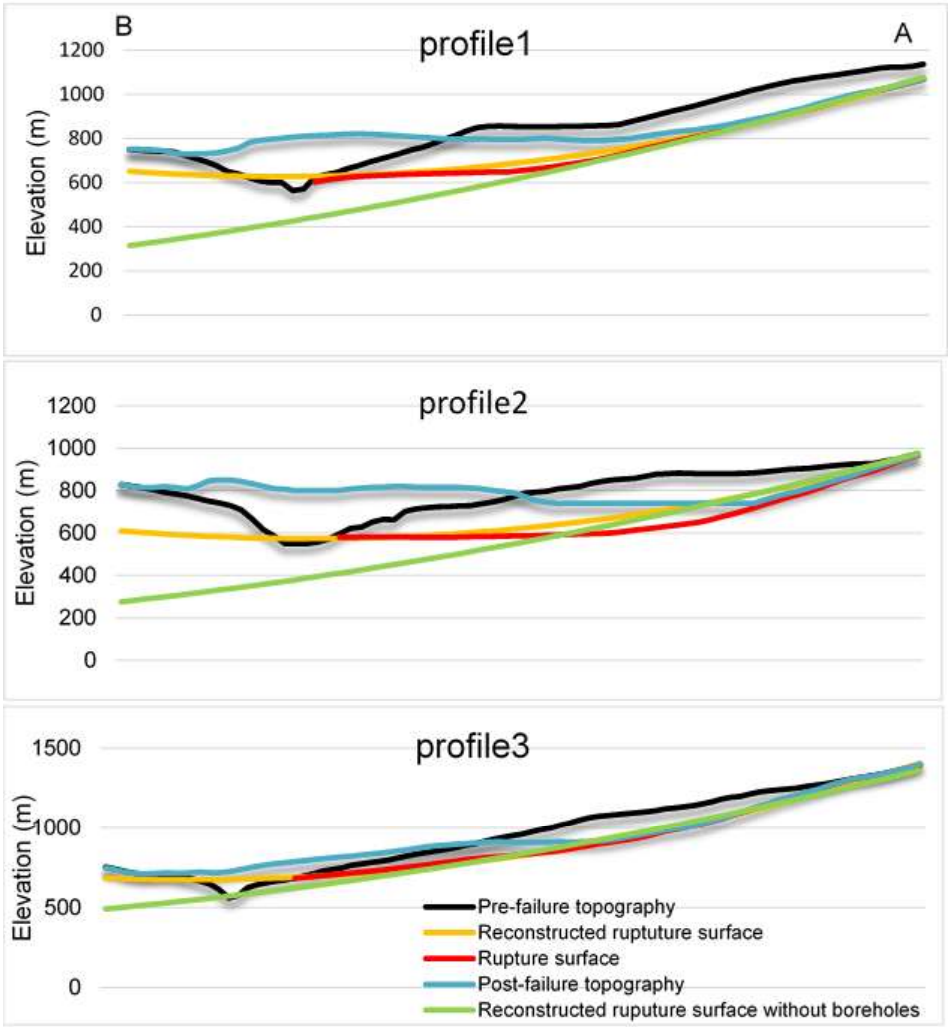

Figure 28 The profiles of the Vajont landslides. The location of these profiles are shown in Figure 27.

5.5. Sensitivity analysis

In the proposed method, the rupture surface reconstruction is associated with two input data, boreholes and elevation points on the scarp. Therefore, it necessary to analyze the sensitivity of them with respect to the variance in volume calculation. For this purpose, two tests were designed to assess the sensitivity of the elevation points on the scarp and the location of the boreholes respectively. In the first test, the all the four simulated boreholes were incorporated in the rupture surface reconstruction, while the number of the points used to extract the elevation information on the scarp was decreased by changing the spacing of them. In the second test, the spacing of the points on the scarp retains as 30m and the four boreholes were used respectively in the fitting. The results are shown in the subsections 5.5.1 and 5.5.2.

5.5.1. Number of points on the scarp

In order to test the sensitivity of the proposed method to the elevation points on the scarp, the 30m spacing of the points for extracting the elevation information from the scarp was adjusted to 60m, 100m, 200m, and 300m. Correspondingly, the number of points decreased from 1001 to 252, 91, 23 and 11 respectively. Incorporating these point sets respectively with the four boreholes in the proposed MATLAB script and subtracting the fitted surface from the pre- and post- failure DEMs, the initial and deposited volume were estimated. It can be clearly seen in Figure 29, with the increase in the spacing of the elevation points, the proposed method was offering robust volume figures (with the maximal variation of 1% from using 1001 elevation points on the scarp with 30m point spacing). It indicates that the proposed method is insensitive to the number of points on the scarp.

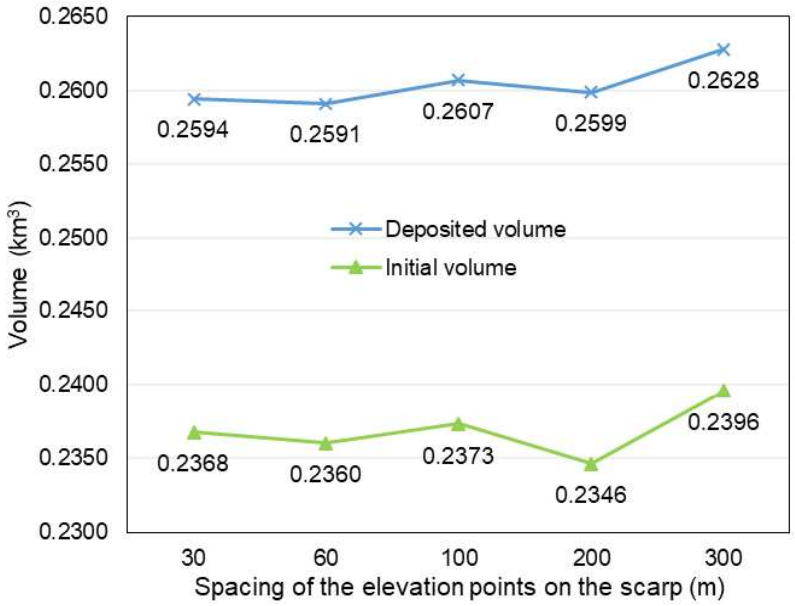

Figure 29: The initial and deposited volume estimated by the proposed methods with different spacing of the elevation points on the scarp.

5.5.2. Boreholes

To analyze the effect of boreholes, each borehole (the locations of them were shown in Figure 24) was respectively input in the surface fitting with the same set of the elevation points on scarp which has a point spacing of 30m. After intercepting the fitted rupture surfaces with the pre- and the post- DEMs, the initial and the deposited volumes was estimated (Figure 30). By looking at Figure 30, when a single borehole is used alone, the location of the borehole affects the result more significantly (with the maximal variation of

37% and 14% for evaluating the deposited and the initial volume from using 4 boreholes). It indicates that the proposed method is more sensitive to the borehole. This finding emphasizes that the borehole data should be considered as a relatively crucial factor in the proposed method.

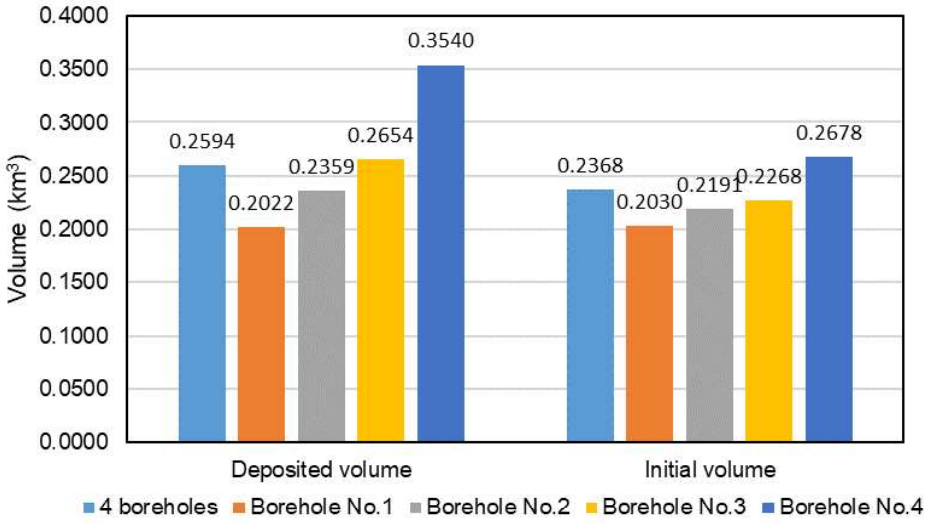

Figure 30: Deposited volume and the initial volume estimated.

5.6. Summary

As well as the analogue models, in the Vajont landslide, it can be clearly seen that the proposed method still performs significantly better than others. In this real case, it overcame the underestimation when taking the depletion volume or the accumulation volume as the actual landslide volume and provided also a more accurate result than the empirical area-volume relationships.

But as mentioned in section 5.4, when the landslide happens in a complex topography like the Vajont case, the pre-failure topography at the slope toe may not coincide with the extension of the reconstructed rupture surface. The pre-event topography is still important in terms of getting an accurate result.

It is worth noting that the availability of boreholes is a key concern in the proposed methods. As shown in section 5.4, the boreholes are still an indispensable input, since they control how the rupture surface continue in the under the sliding mass. If they are not available it can lead to a significant overestimation of the volume. Also, concerning the result of the sensitivity analysis in section 5.5, insufficient boreholes or the errors in interpreting the rupture surface may cause an inaccuracy in the final results. So, when applying the proposed method, it requires to be more cautious with the input borehole data.

6. DISCUSSIONS AND SUGGESTIONS

In this chapter, based on the sand experiments and the case study of the Vajont landslide, an overall workflow of the volume calculation using the proposed method was made and the research questions are answered in section 6.1, and suggestions for future research directions are made in section 6.2.

6.1. Discussions

In this study, a new method was designed for landslide volume calculation based on a reconstructed rupture surface and tested in analog experiments and a real case.

In the analogue experiments, three types of landslides were simulated, the deep-seated landslide triggered by water infiltration, the shallow landslide triggered by toe excavation and the shallow landslide triggered by vibration. Then, based on the rupture surfaces of these three types of landslide, the geometric shape of the rupture surface reconstruction was determined. Then by fitting the geometric shape to the scarp and a point on the rupture surface, the rupture surface was reconstructed. By subtracting rupture surfaces from the pre- and post- topography, the initial and deposited volumes of the analogue landslides were estimated.

After validating the proposed with the volume figures calculated by digging out the displaced material. The method was then applied in the Vajont landslide. To calculate the initial and deposited volumes of landslides. The input data of the proposed method consists of points with known depths of the rupture surface and multi-temporal DEMs with a legible scarp. The sensitivity of the proposed method was assessed based on the Vajont landslide.

Based on the result, the research questions were answered as follows.

- What are the best fitted geometric shapes of the surfaces of rupture for different landslide types?

In this study, two types of geometric shapes, the paraboloid and plane, were tested to fit the rupture surface in the analogue experiments conducted in sand piles. The RMSE and R^2 of the fitting show that in all the three types of landslides simulated in this study, the paraboloid always performs better fitting results.

- In the experimental landslides, what are the volumes calculated by the fitted surface of ruptures and how are the calculated figures compared with the volume figures calculated by the previous methods?

- In the real landslide, what are the volumes calculated by the proposed method and how do the results compare with those from previous methods?

In both analogue experiments and the Vajont landslide, the proposed method shows good capability in the initial and deposited landslide volume estimation. According to the accuracy analysis of the analogue landslides, on average, the Guzzetti's empirical area-volume relationship also presents good capability in estimating the deposited volume. But, the volumes calculated by Guzzetti's empirical area-volume relationship come with a wider range of error which indicates that it may not be as suitable as the proposed method for the volume estimation of a single landslide. Similarly, for another empirical area-volume relationship proposed by Larsen, the deposited volumes tend to be underestimated in the analogue landslides, while in the case of Vajont, a significant underestimation is found. As for the multi-DEM

difference, the underestimation can always be found when taking the depletion and accumulation volume as the initial and deposited volume.

- What are the pros and cons of each method?

Two criteria were set to evaluate the three methods: data requirement and accuracy.

From the perspective of the data requirement, the area-volume relationship relies less on the input data since it only requires the extent of the landslide affected area while the multi-temporal DEM difference requires both the pre- and post- failure DEMs. For the proposed method, when the landslides happen in relatively simple terrains like the experimental landslides in the sand piles in which the pre-topography coincide with the extension of the reconstructed failure surface, the deposited volume can be derived from post-DEM and the points with known depths of the rupture surface. But for the landslide occurring in the complex topography like the Vajont landslide, after the failure, the sliding mass were blocked by the slope on the opposite bank and deposited on it, the reconstructed sliding surface cannot address the baseline of this deposition. Thus, in these cases, subtracting the reconstructed rupture surface with pre-DEM to get the initial volume of the landslide is more reasonable.

With respect to the accuracy, the proposed method is robustly providing the highest accuracy when the points with known depths of failures surface are available. However, a main uncertainty lies on the input data of the points with known depths of the failure surface due to the high sensitivity. So, when applying the proposed method, the quality of borehole data should always be viewed with caution. For the area-volume relationship, according to the results in chapter 4 and chapter 5, it may provide an overall correct volume at a regional scale averagely, but the accuracy depends a lot on the equation selection. The performance of area-volume relationships varies a lot when the equations from the different literature were applied (Larsen's and Guzzetti's), to avoid this uncertainty, for every area, it is recommended to use the empirical relationship which has been localized. And when looking for multi-temporal DEM difference, an obvious underestimation exists when taking the depletion and accumulation volumes as the initial and the deposited landslide volume. Therefore, for generating an accurate volume of the mobilized mass, this underestimation must be corrected. Besides the underestimation problem, another issue to be addressed when applying multi-temporal DEM difference is the quality of the DEMs. For the multi-temporal DEM selection, the priority should be given to the DEMs with high resolution, less vegetation cover and from same sources.

These difference between the three methods should be considered when implementing landslide volume estimation. For precisely measuring individual landslides, the proposed method should be considered first. However, when applying the volume analysis in a regional area for multiple landslides, the proposed method will not be appropriate, since acquiring borehole data for each landslide is difficult due to time and labor consuming. In that situation, the area-volume relationship and multi-temporal DEM difference are preferable.

The overall workflow of the proposed method is illustrated in Figure 31.

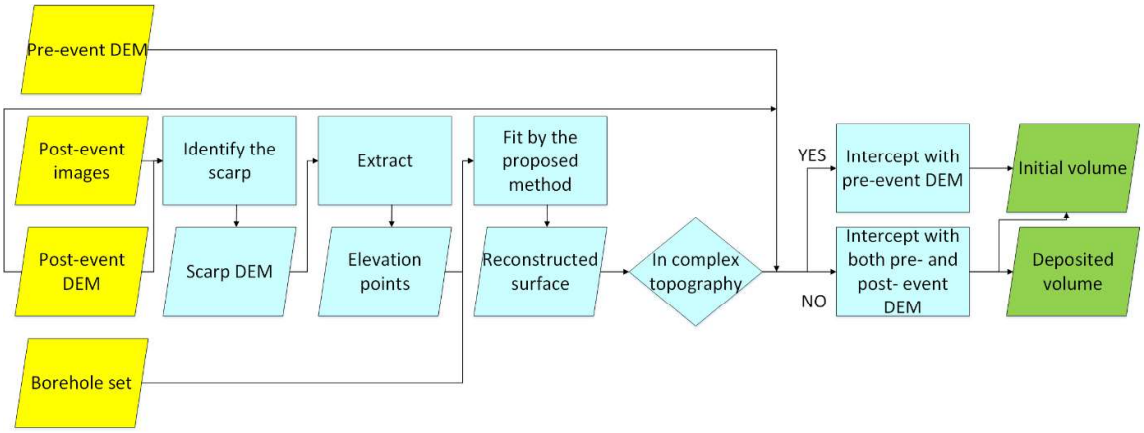

Figure 31: The overall workflow of the proposed method. The yellow boxes are the input data, the green boxes are the output result, the blue boxes are the intermediate procedures.

6.2. suggestions

The scientific significance of this research could be summarized as follows:

- Providing a volume estimation method which could be applied in landslides with a small amount of borehole data.
- Overcoming the uncertainty of the landslide volumes by the conventional multi-temporal DEM difference and the area-volume relationships.
- Offering a relatively accurate volume estimation which is useful in further studies like risk and hazard assessment or landslide mechanism.

Since at the current stage, the MATLAB script is still designed for fitting the rupture surface for single landslides, and the volume calculation is still based on manual operation in ArcMap, so a possible direction is to develop an automatic GIS-based plug-in in which the landslide volume can be generated automatically from input data of the pre- and post- failure terrains, sets of boreholes as well as the scarp boundaries of the landslides to be measured. The expected product could be an efficient tool in quantitive risk and hazard analysis. In this context, this work could be anticipated as a starting point.

LIST OF REFERENCES

Adegbe, M., Ako, T. A., Onoduku, U. S., Asema, A. I., Unubi, A. S., & Inyang, E. B. (2014). Determination of the Volume of Debrisfrom Yingxiu Landslides, Southwest China: Geomorphological and Field Observation Approaches. *Journal of Natural Sciences*, *2*(1), 95–105.

Awal, R., Nakagawa, H., Baba, Y., & Sharma, R. H. (2007). Numerical and Experimental Study on Landslide Dam Failure By Sliding. *Proceedings of Hydraulic Engineering*, *51*(50), 7–12. https://doi.org/10.2208/prohe.51.7

Barla, G., & Paronuzzi, P. (2013). The 1963 Vajont Landslide: 50th Anniversary. *Rock Mechanics and Rock Engineering*, *46*(6), 1267–1270. https://doi.org/10.1007/s00603-013-0483-7

Bosa, S., & Petti, M. (2011). Shallow water numerical model of the wave generated by the Vajont landslide. *Environmental Modelling & Software*, *26*(4), 406–418. https://doi.org/10.1016/j.envsoft.2010.10.001

Bozzano, F., Bretschneider, A., Esposito, C., Martino, S., Prestininzi, A., & Scarascia Mugnozza, G. (2013). Lateral spreading processes in mountain ranges: Insights from an analogue modelling experiment. *Tectonophysics*, *605*, 88–95. https://doi.org/10.1016/j.tecto.2013.05.006

Brardinoni, F., & Church, M. (2004). Representing the landslide magnitude-frequency relation: Capilano River basin, British Columbia. *Earth Surface Processes and Landforms*, *29*(1), 115–124. https://doi.org/10.1002/esp.1029

Catani, F., Tofani, V., & Lagomarsino, D. (2016). Spatial patterns of landslide dimension: A tool for magnitude mapping. *Geomorphology*, *273*, 361–373. https://doi.org/10.1016/j.geomorph.2016.08.032

Centre for Research on the Epidemiology of Natural Disasters. (2017). Database | EM-DAT. Retrieved July 26, 2017, from http://www.emdat.be/database

Chen, R. F., Chang, K. J., Angelier, J., Chan, Y. C., Deffontaines, B., Lee, C. T., & Lin, M. L. (2006). Topographical changes revealed by high-resolution airborne LiDAR data: The 1999 Tsaoling landslide induced by the Chi-Chi earthquake. *Engineering Geology*, *88*(3–4), 160–172. https://doi.org/10.1016/j.enggeo.2006.09.008

Chen, Z., Zhang, B., Han, Y., Zuo, Z., & Zhang, X. (2014). Modeling accumulated volume of landslides using remote sensing and DTM data. *Remote Sensing*, *6*(2), 1514–1537. https://doi.org/10.3390/rs6021514

Clague, J. J. (2013). Landslide. *Encyclopedia of Natural Hazards*, 594–602. https://doi.org/10.1007/978-1-4020-4399-4_212

Cruden, D. M., & Varnes, D. J. (1996). Landslides: investigation and mitigation. Chapter 3-Landslide types and processes. *Transportation Research Board Special Report*, *247*.

Dade, W., & Huppert, H. (1998). Long-runout rockfalls. *Geology*, *26*(9), 803–806. https://doi.org/10.1130/0091-7613(1998)026<0803:LRR>2.3.CO

Dai, F. C., & Lee, C. F. (2001). Frequency-volume relation and prediction of rainfall-induced landslides. *Engineering Geology*, *59*(3–4), 253–266. https://doi.org/10.1016/S0013-7952(00)00077-6

Dai, F. C., Xu, C., Yao, X., Xu, L., Tu, X. B., & Gong, Q. M. (2011). Spatial distribution of landslides triggered by the 2008 Ms 8.0 Wenchuan earthquake, China. *Journal of Asian Earth Sciences*, *40*(4), 883–895. https://doi.org/10.1016/j.jseaes.2010.04.010

Del Ventisette, C., Gigli, G., Bonini, M., Corti, G., Montanari, D., Santoro, S., … Casagli, N. (2015). Insights from analogue modelling into the deformation mechanism of the Vaiont landslide. *Geomorphology*, *228*, 52–59. https://doi.org/10.1016/j.geomorph.2014.08.024

Dewitte, O., & Demoulin, A. (2005). Morphometry and kinematics of landslides inferred from precise DTMs in West Belgium. *Natural Hazards and Earth System Science*, *5*(2), 259–265. https://doi.org/10.5194/nhess-5-259-2005

Dewitte, O., Jasselette, J. C., Cornet, Y., Van Den Eeckhaut, M., Collignon, A., Poesen, J., & Demoulin, A. (2008). Tracking landslide displacements by multi-temporal DTMs: A combined aerial stereophotogrammetric and LIDAR approach in western Belgium. *Engineering Geology*, *99*(1–2), 11–22. https://doi.org/10.1016/j.enggeo.2008.02.006

Eckersley, J. D. (1991). Discussion: Instrumented laboratory flowslides. *Géotechnique*, *41*(2), 277–279. https://doi.org/10.1680/geot.1991.41.2.277

Emery, N., Carrea, D., Abellán, A., Oppikofer, T., & Jaboyedoff, M. (2014). Modelling of landslide failure surface using SLBL: from analogue modelling to real scale rotational landslides. *Geophysical Research Abstracts*, *16*, 14031.

Fan, X., Van Westen, C. J., Korup, O., Gorum, T., Xu, Q., Dai, F., … Wang, G. (2012). Transient water

and sediment storage of the decaying landslide dams induced by the 2008 Wenchuan earthquake, China. *Geomorphology*, *171–172*, 58–68. https://doi.org/10.1016/j.geomorph.2012.05.003

Grohmann, C. H., Sawakuchi, A., & Mendes, V. (2011). Cell size influence on DEM volume calculation. In *Changes* (Vol. c, pp. 63–66).

Grohmann, C. H., & Sawakuchi, A. O. (2013). Influence of cell size on volume calculation using digital terrain models: A case of coastal dune fields. *Geomorphology*, *180–181*, 130–136. https://doi.org/10.1016/j.geomorph.2012.09.012

Guzzetti, F., Ardizzone, F., Cardinali, M., Galli, M., Reichenbach, P., & Rossi, M. (2008). Distribution of landslides in the Upper Tiber River basin, central Italy. *Geomorphology*, *96*(1–2), 105–122. https://doi.org/10.1016/j.geomorph.2007.07.015

Guzzetti, F., Ardizzone, F., Cardinali, M., Rossi, M., & Valigi, D. (2009a). Landslide volumes and landslide mobilization rates in Umbria, central Italy. *Earth and Planetary Science Letters*, *279*(3–4), 222–229. https://doi.org/10.1016/j.epsl.2009.01.005

Guzzetti, F., Ardizzone, F., Cardinali, M., Rossi, M., & Valigi, D. (2009b). Landslide volumes and landslide mobilization rates in Umbria, central Italy. *Earth and Planetary Science Letters*, *279*(3–4), 222–229. https://doi.org/10.1016/j.epsl.2009.01.005

Hungr, O., Leroueil, S., & Picarelli, L. (2014, April 30). The Varnes classification of landslide types, an update. *Landslides*. Springer Berlin Heidelberg. https://doi.org/10.1007/s10346-013-0436-y

IAEG. (1990). Suggested nomenclature for landslides. *Bulletin of the International Association of Engineering Geology - Bulletin de l'Association Internationale de Géologie de l'Ingénieur*, *41*(1), 13–16. https://doi.org/10.1007/BF02590202

Iverson, R. M. (1997). The physics of debris flows. *Reviews of Geophysics*, *35*(3), 245–296. https://doi.org/10.1029/97RG00426

Iverson, R. M. (2015). Scaling and design of landslide and debris-flow experiments. *Geomorphology*, *244*, 9–20. https://doi.org/10.1016/j.geomorph.2015.02.033

Jongmans, D., & Garambois, S. (2007). Geophysical investigation of landslides : a review. *Bulletin de La Societe Geologique de France*, *178*(2), 101–112. https://doi.org/10.2113/gssgfbull.178.2.101

Kerle, N. (2002). Volume estimation of the 1998 flank collapse at Casita volcano, Nicaragua: A comparison of photogrammetric and conventional techniques. *Earth Surface Processes and Landforms*, *27*(7), 759–772. https://doi.org/10.1002/esp.351

Kilburn, C. R. ., & Petley, D. N. (2003). Forecasting giant, catastrophic slope collapse: lessons from Vajont, Northern Italy. *Geomorphology*, *54*(1–2), 21–32. https://doi.org/10.1016/S0169-555X(03)00052-7

Konecny, G. (2014). *Geoinformation : remote sensing, photogrammetry, and geographic information systems*. CRC Press.

Küng, O., Strecha, C., Beyeler, A., Zufferey, J., Floreano, D., Fua, P., & Gervaix, F. (2012). THE ACCURACY OF AUTOMATIC PHOTOGRAMMETRIC TECHNIQUES ON ULTRA-LIGHT UAV IMAGERY. *ISPRS - International Archives of the Photogrammetry, Remote Sensing and Spatial Information Sciences*, *XXXVIII-1/*, 125–130. https://doi.org/10.5194/isprsarchives-XXXVIII-1-C22-125-2011

Larsen, I. J., Montgomery, D. R., & Korup, O. (2010). Landslide erosion controlled by hillslope material. *Nature Geoscience*, *3*(4), 247–251. https://doi.org/10.1038/ngeo776

Le Roux, O., Jongmans, D., Kasperski, J., Schwartz, S., Potherat, P., Lebrouc, V., … Meric, O. (2011). Deep geophysical investigation of the large Séchilienne landslide (Western Alps, France) and calibration with geological data. *Engineering Geology*, *120*(1), 18–31. https://doi.org/10.1016/j.enggeo.2011.03.004

Lo, C.-M., Lin, M.-L., Tang, C.-L., & Hu, J.-C. (2011). A kinematic model of the Hsiaolin landslide calibrated to the morphology of the landslide deposit. *Engineering Geology*, *123*, 22–39. https://doi.org/10.1016/j.enggeo.2011.07.002

Lourenço, S. D. N., Sassa, K., & Fukuoka, H. (2006). Failure process and hydrologic response of a two layer physical model: Implications for rainfall-induced landslides. *Geomorphology*, *73*(1–2), 115–130. https://doi.org/10.1016/j.geomorph.2005.06.004

Lugaizi, I. (2008). *Landslide volume monitoring using geophysics and multi - temporal digital elevation models : a case study of Trieves area, France*. ITC, Enschede.

Manzella, I., & Labiouse, V. (2009). Flow experiments with gravel and blocks at small scale to investigate parameters and mechanisms involved in rock avalanches. *Engineering Geology*, *109*(1–2), 146–158. https://doi.org/10.1016/j.enggeo.2008.11.006

Marchesini, I., Cencetti, C., & De Rosa, P. (2009). A preliminary method for the evaluation of the landslides volume at a regional scale. *GeoInformatica*, *13*(3), 277–289. https://doi.org/10.1007/s10707-008-0060-5

Martha, T. R., Kerle, N., Jetten, V., Van Westen, C. J., & Vinod Kumar, K. (2010). Landslide volumetric analysis using cartosat-1-derived DEMs. *IEEE Geoscience and Remote Sensing Letters*, *7*(3), 582–586. https://doi.org/10.1109/LGRS.2010.2041895

Mergili, M. (2012). *Model outline and manual.*

Murty, T. S. (2003). Tsunami Wave Height Dependence on Landslide Volume. *Pure and Applied Geophysics*, *160*(10–11), 2147–2153. https://doi.org/10.1007/s00024-003-2423-z

Niethammer, U., James, M. R., Rothmund, S., Travelletti, J., & Joswig, M. (2012). UAV-based remote sensing of the Super-Sauze landslide: Evaluation and results. *Engineering Geology*, *128*, 2–11. https://doi.org/10.1016/j.enggeo.2011.03.012

Nikolaeva, E., Walter, T. R., Shirzaei, M., & Zschau, J. (2014). Landslide observation and volume estimation in central Georgia based on L-band InSAR. *Natural Hazards and Earth System Sciences*, *14*(3), 675–688. https://doi.org/10.5194/nhess-14-675-2014

Okura, Y., Kitahara, H., Ochiai, H., Sammori, T., & Kawanami, A. (2002). Landslide fluidization process by flume experiments. *Engineering Geology*, *66*(1–2), 65–78. https://doi.org/10.1016/S0013-7952(02)00032-7

Olivares, L., & Damiano, E. (2007). Postfailure Mechanics of Landslides: Laboratory Investigation of Flowslides in Pyroclastic Soils. *Journal of Geotechnical and Geoenvironmental Engineering*, *133*(1), 51–62. https://doi.org/10.1061/(ASCE)1090-0241(2007)133:1(51)

Parsons, J. D., Whipple, K. X., & Simoni, A. (2001). Experimental Study of the Grain-Flow, Fluid-Mud Transition in Debris Flows. *The Journal of Geology*, *109*(4), 427–447. https://doi.org/10.1086/320798

Reid, M. E., Brien, D. L., & Waythomas, C. F. (2010). Preliminary slope-stability analysis of Augustine Volcano. In *The 2006 Eruption of Augustine Volcano, Alaska* (pp. 321–332).

Reid, Christian, S. B., Brien, D. L., & Henderson, S. . (2015). *Scoops3D — Software to Analyze Three-Dimensional Slope Stability Throughout a Digital Landscape. U.S. Geological Survey Techniques and Methods, book 14*. https://doi.org/10.3133/tm14A1

Samia, J., Temme, A., Bregt, A., Wallinga, J., Guzzetti, F., Ardizzone, F., & Rossi, M. (2017). Characterization and quantification of path dependency in landslide susceptibility. *Geomorphology*, *292*, 16–24. https://doi.org/10.1016/j.geomorph.2017.04.039

Samyn, K., Travelletti, J., Bitri, A., Grandjean, G., & Malet, J.-P. (2012). Characterization of a landslide geometry using 3D seismic refraction traveltime tomography: The La Valette landslide case history. *Journal of Applied Geophysics*, *86*, 120–132. https://doi.org/10.1016/j.jappgeo.2012.07.014

Scheidegger, A. E. (1973). On the prediction of the reach and velocity of catastrophic landslides. *Rock Mechanics Felsmechanik Mécanique Des Roches*, *5*(4), 231–236. https://doi.org/10.1007/BF01301796

Shuxin, C., Yongsheng, W., & Fei, C. (2002). A study of differential GPS positioning accuracy. *Microwave and Millimeter Wave Technology, 2002. Proceedings. ICMMT 2002. 2002 3rd International Conference on*, 361–364. https://doi.org/10.1109/ICMMT.2002.1187711

Tang, C., Van Westen, C. J., Tanyas, H., & Jetten, V. G. (2016). Analysing post-earthquake landslide activity using multi-temporal landslide inventories near the epicentral area of the 2008 Wenchuan earthquake. *Natural Hazards and Earth System Sciences*, *16*(12), 2641–2655. https://doi.org/10.5194/nhess-16-2641-2016

Tanyaş, H., van Westen, C. J., Allstadt, K. E., Anna Nowicki Jessee, M., Görüm, T., Jibson, R. W., … Hovius, N. (2017). Presentation and Analysis of a Worldwide Database of Earthquake-Induced Landslide Inventories. *Journal of Geophysical Research: Earth Surface*, *122*(10), 1991–2015. https://doi.org/10.1002/2017JF004236

Tseng, C. M., Lin, C. W., Stark, C. P., Liu, J. K., Fei, L. Y., & Hsieh, Y. C. (2013). Application of a multi-temporal, LiDAR-derived, digital terrain model in a landslide-volume estimation. *Earth Surface Processes and Landforms*, *38*(13), 1587–1601. https://doi.org/10.1002/esp.3454

Uysal, M., Toprak, A. S., & Polat, N. (2015). DEM generation with UAV Photogrammetry and accuracy analysis in Sahitler hill. https://doi.org/10.1016/j.measurement.2015.06.010

Van Niel, T. G., McVicar, T. R., Li, L., Gallant, J. C., & Yang, Q. (2008). The impact of misregistration on SRTM and DEM image differences. *Remote Sensing of Environment*, *112*(5), 2430–2442. https://doi.org/10.1016/j.rse.2007.11.003

van Westen, C. J., Castellanos, E., & Kuriakose, S. L. (2008). Spatial data for landslide susceptibility, hazard, and vulnerability assessment: An overview. *Engineering Geology*, *102*(3–4), 112–131.

https://doi.org/10.1016/j.enggeo.2008.03.010
Varnes, D. J. (1978). Slope Movement Types and Processes. *Transportation Research Board Special Report*, (176), 11–33. https://doi.org/In Special report 176: Landslides: Analysis and Control, Transportation Research Board, Washington, D.C.
Wang, G., & Sassa, K. (2001). Factors affecting rainfall-induced flowslides in laboratory flume tests. *Géotechnique*, *51*(7), 587–599. https://doi.org/10.1680/geot.2001.51.7.587
Zhanpeng, C., Tingwu, L., & Qinghong, Y. (2013). Measuring and calculation methods for landslide volume with 3-D laser scanner inWenchuan earthquake area. *Transactions of the Chinese Society of Agricultural Engineering*, *29*, 135–144. https://doi.org/10.3969/j.issn.1002-6819.2013.08.016

APPENDIX

Appendix 1: The MATLAB script of the reconstruction and rasterization of the rupture surface in the proposed method

```
% read the slip surface point cloud file, in txt format
% the first 3 colunms are x,y,z
% change the filename into your filename
scarp = dlmread('scarp');
borehole = dlmread('borehole');

% extract X,Y,Z, and assign the same weight to the scarp and the bore holes
X_s = scarp(:,1);
Y_s = scarp(:,2);
Z_s = scarp(:,3);

%bore hole 1,2,3. The numbers of boreholes can be adjusted here.
X_bh1([1:length(X_s)],1) = borehole(1,1);
Y_bh1([1:length(Y_s)],1) = borehole(1,2);
Z_bh1([1:length(Z_s)],1) = borehole(1,3);

X_bh2([1:length(X_s)],1) = borehole(2,1);
Y_bh2([1:length(Y_s)],1) = borehole(2,2);
Z_bh2([1:length(Z_s)],1) = borehole(2,3);

X_bh3([1:length(X_s)],1) = borehole(3,1);
Y_bh3([1:length(Y_s)],1) = borehole(3,2);
Z_bh3([1:length(Z_s)],1) = borehole(3,3);

X_bh4([1:length(X_s)],1) = borehole(4,1);
Y_bh4([1:length(Y_s)],1) = borehole(4,2);
Z_bh4([1:length(Z_s)],1) = borehole(4,3);

X = [ X_s X_bh1 X_bh2 X_bh3 X_bh4 ];
Y = [ Y_s Y_bh1 Y_bh2 Y_bh3 Y_bh4 ];
Z = [ Z_s Z_bh1 Z_bh2 Z_bh3 Z_bh4 ];

% fit the quadric surface
% input preparation
[xData, yData, zData] = prepareSurfaceData( X, Y, Z );

% Set up fittype and options.
ft = fittype( 'poly22' );

% Fit model to data, gof = godness of fitting
[fitresult, gof] = fit( [xData, yData], zData, ft );
```

```
% Plot fit with data. use your specific name instead of 'fitting'.
figure( 'Name', 'fitted surface' );
h = plot( fitresult, [xData, yData], zData );
legend( h, 'fitted surface', 'point cloud', 'Location', 'NorthEast' );

% Label axes, adjust the view.
xlabel X
ylabel Y
zlabel Z
grid on
view( -110.5, 24.0 );

%show the fit formula and coefficients
fitformula = formula(fitresult);
coeffs = coeffvalues(fitresult);

%rasterize the fitted surface
%read the post-DEM GeoTIFF that you want to perform the calculation on
[meshgrid_extent, R] = geotiffread('extent4matlab.tif');

%creat wolrdfile matrix and return the X ,Y coordinate at lift top and the cell sizes
W = worldFileMatrix(R);
X_lt = W(1,3) ;
Y_lt = W(2,3) ;
csX = W(1,1)  ;
csY = W(2,2)  ;

%extrat X,Y coordinate into two matrix
[X_mesh,Y_mesh] = meshgrid( X_lt : csX : X_lt + ( length( meshgrid_extent ) - 1) * csX ,...
Y_lt : csY : (length(meshgrid_extent) - 1 ) * csY + Y_lt);

%generate the elevation model
Z_mesh = coeffs(1,1) + ...
coeffs(1,2) .* X_mesh + ...
coeffs(1,3) .* Y_mesh + ...
coeffs(1,4) .* X_mesh .^2 + ...
coeffs(1,5) .* X_mesh .* Y_mesh +...
coeffs(1,6) .* Y_mesh .^2;
%write the elevation model into geotiff format
info = geotiffinfo('extent4matlab.tif');
geotiffwrite('Reconstructed_borehole_4_1.tif', Z_mesh, R, 'GeoKeyDirectoryTag',
info.GeoTIFFTags.GeoKeyDirectoryTag);
```

Appendix 2: Point cloud density of the experimental landslides. The colors on points represent the number of the neighboring points in its 5cm radium sphere. (a) is the point cloud of pre-failure topography, (b) is the point cloud of post-failure topography, (c) is the point cloud of the rupture surface.

Appendix 2-1: Point cloud density of the experimental deep-seated landslide D

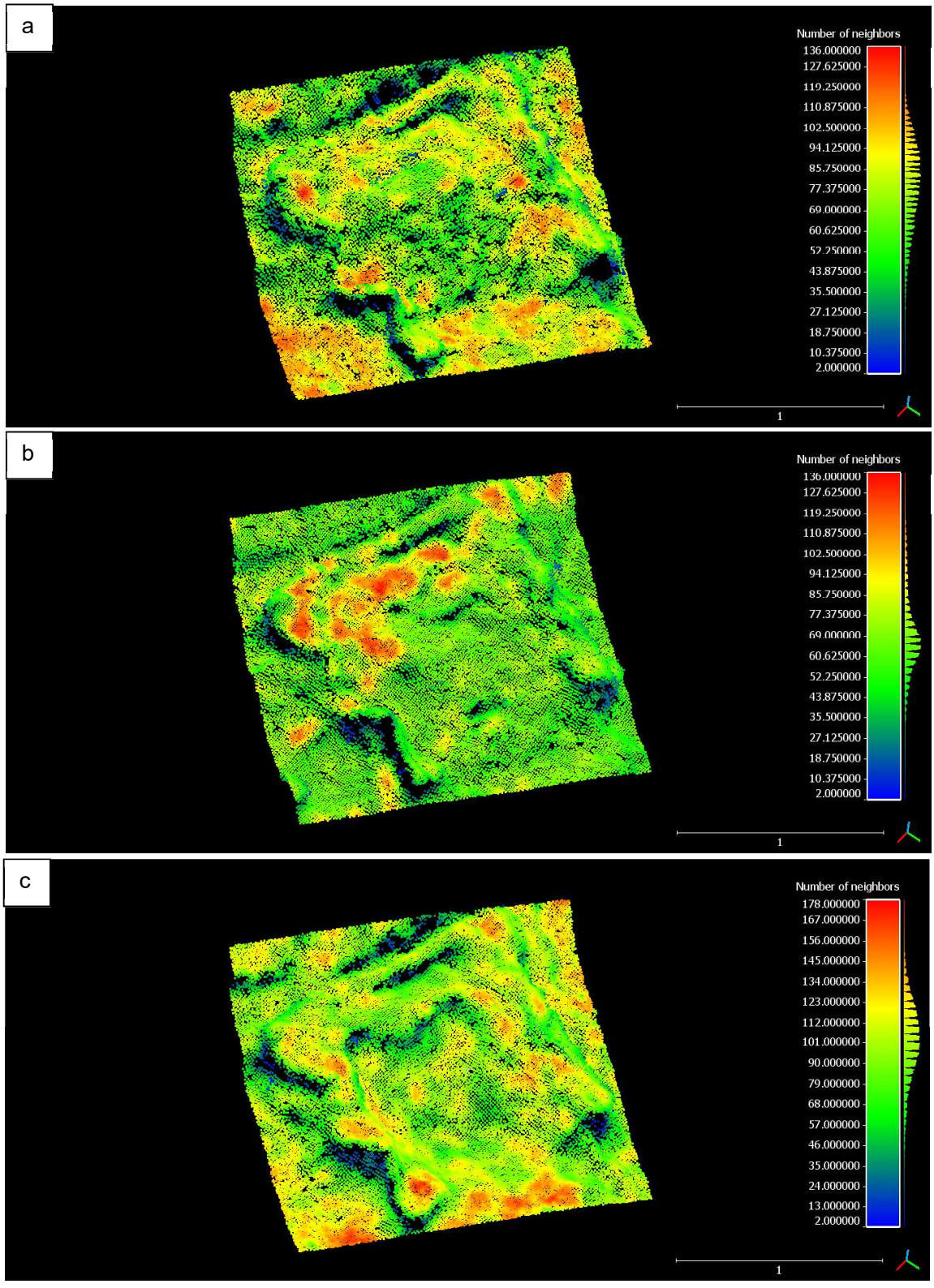

Appendix 2-2: Point cloud density of the experimental shallow landslide triggered by toe excavation SE1

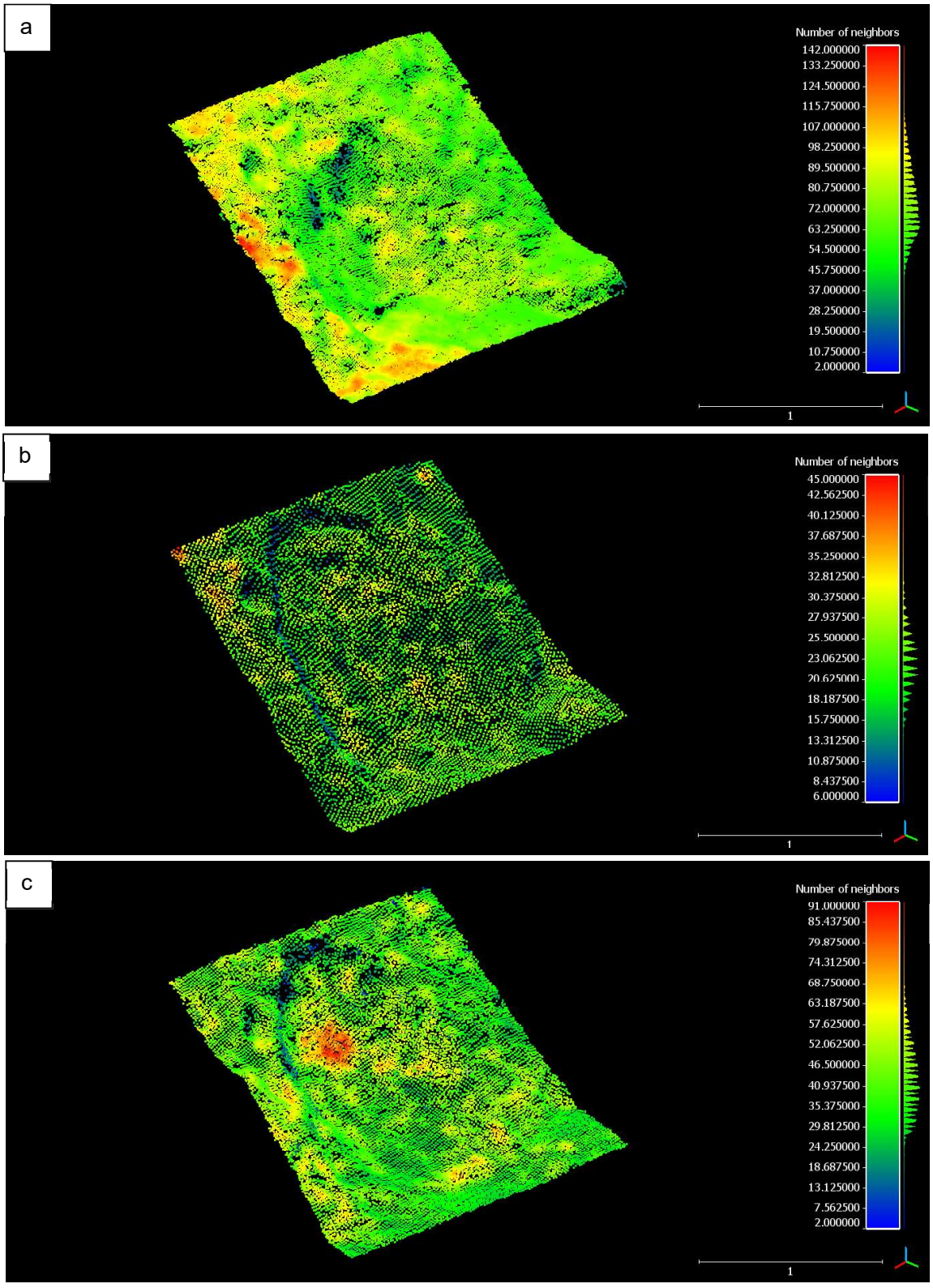

Appendix 2-3: Point cloud density of the experimental shallow landslide triggered by toe excavation SE2

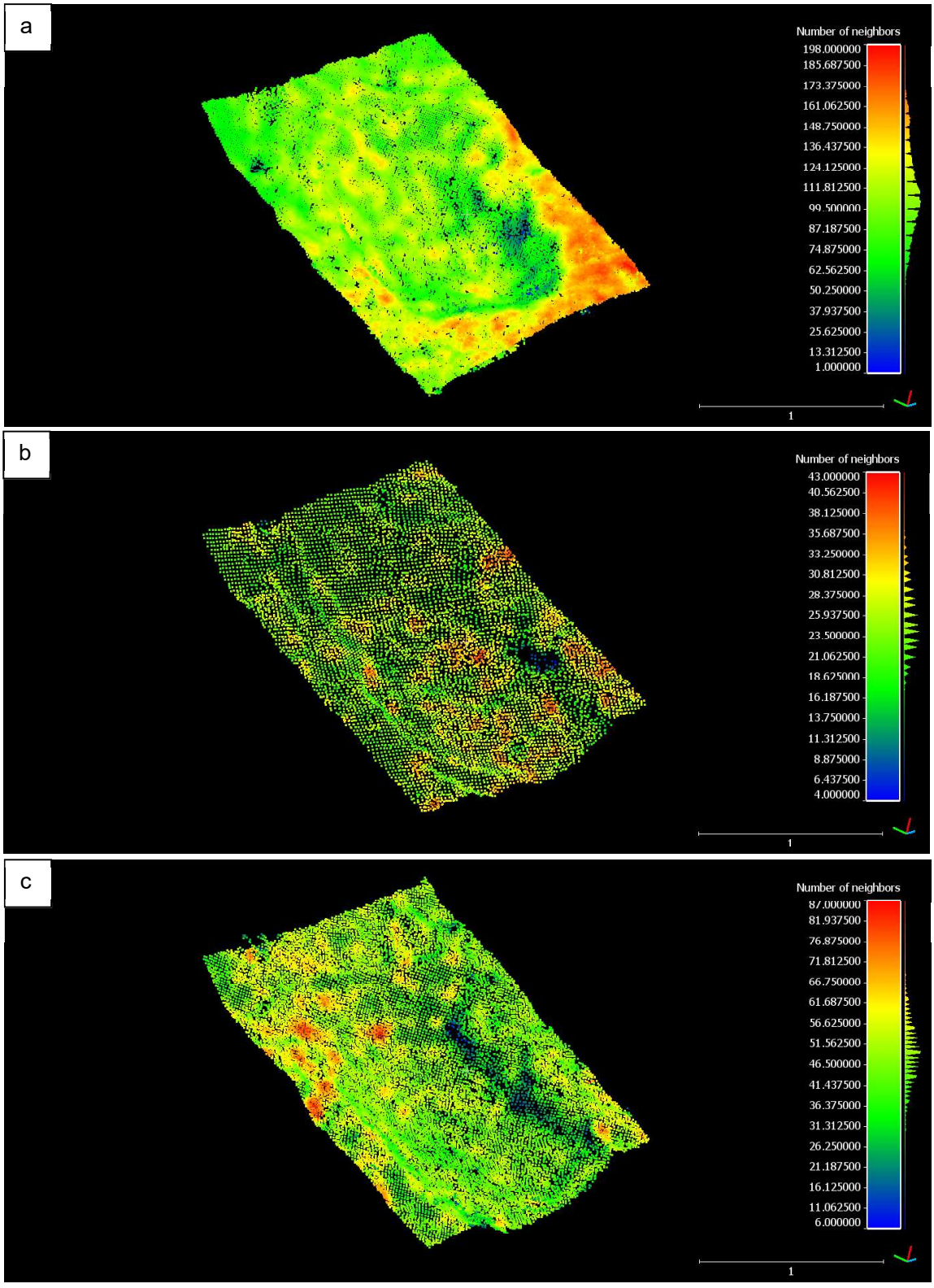

Appendix 2-4: Point cloud density of the experimental shallow landslide triggered by toe excavation SE3

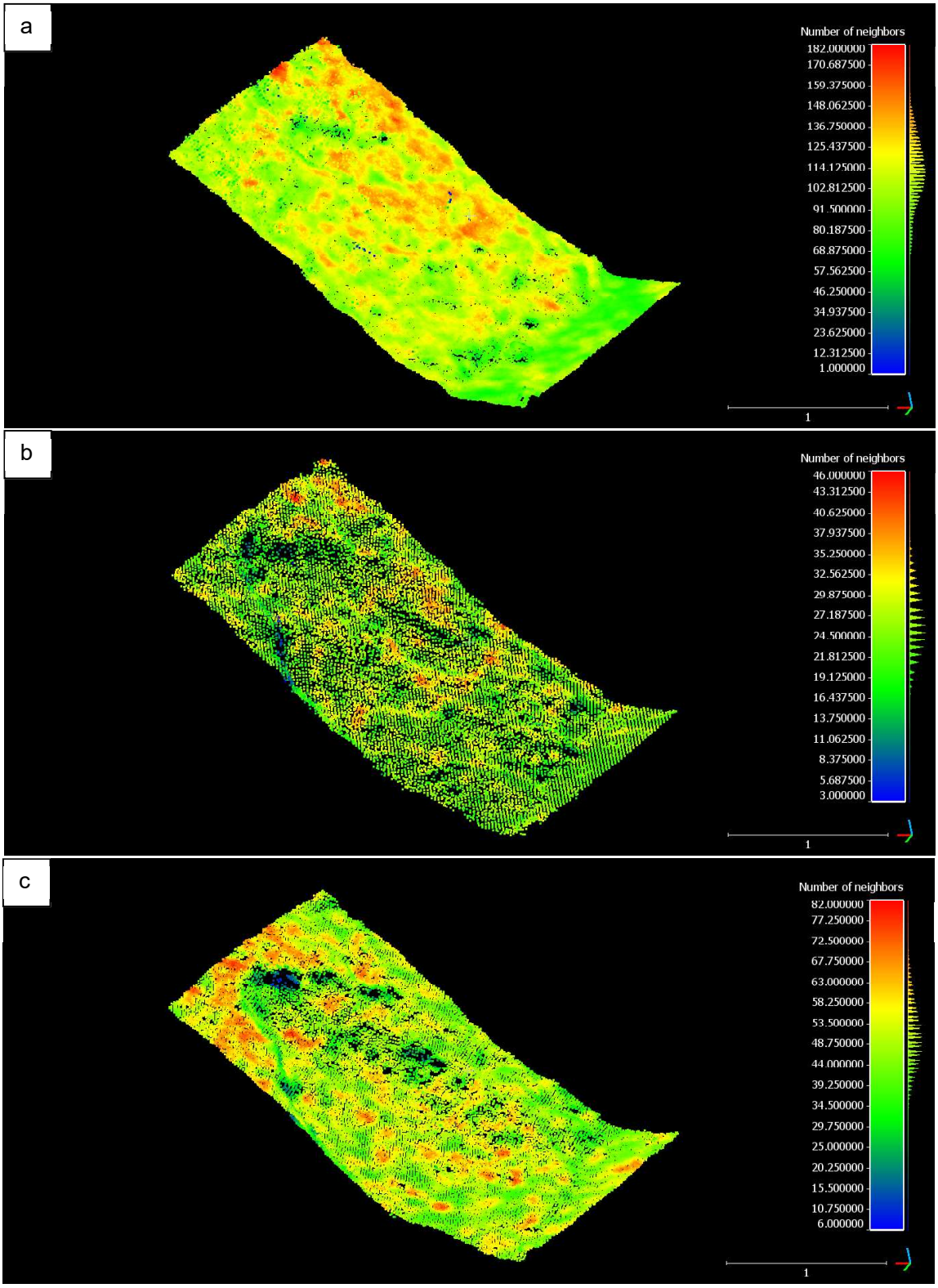

Appendix 2-5: Point cloud density of the experimental shallow landslide triggered by toe excavation SE4

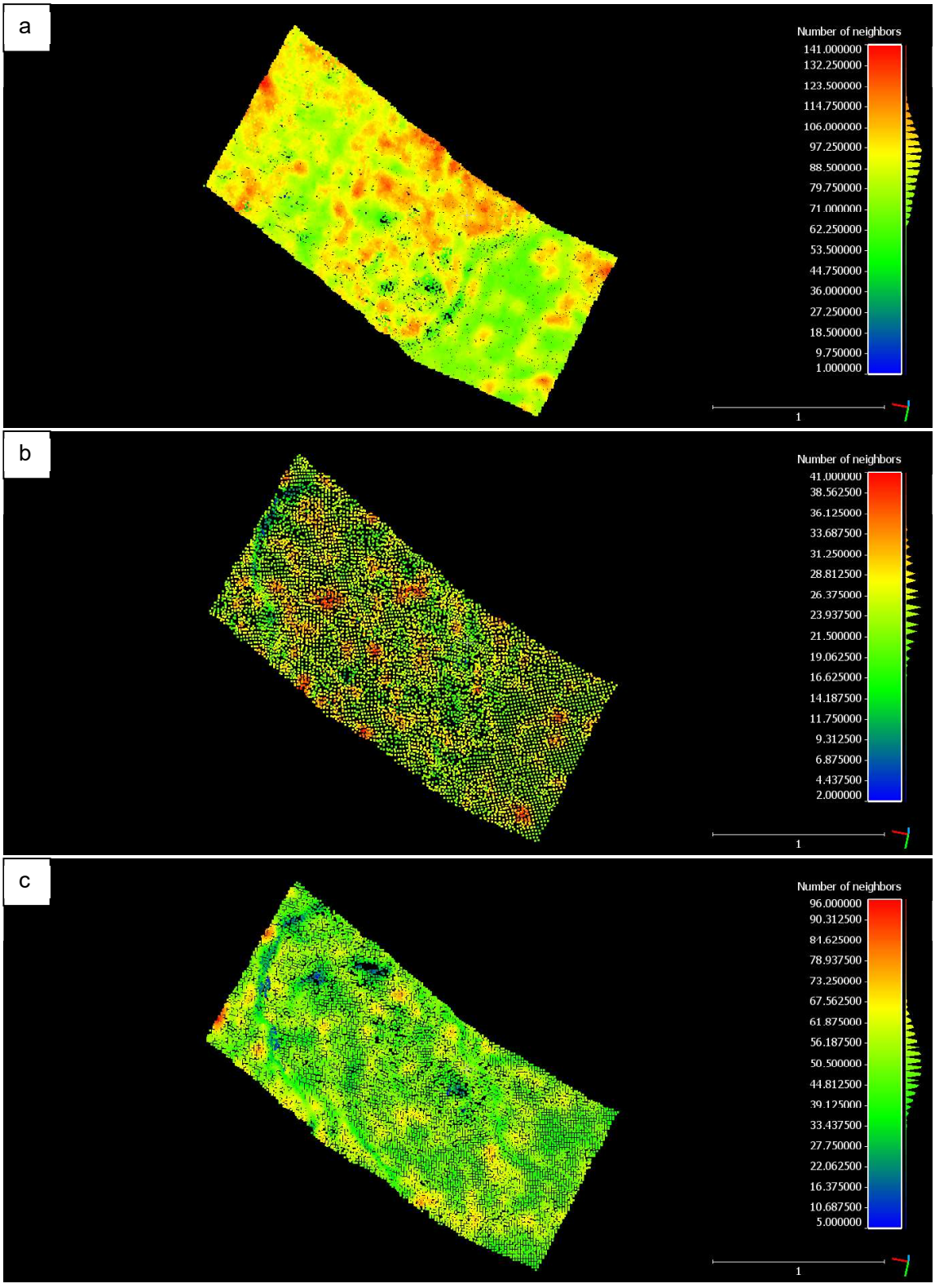

Appendix 2-6: Point cloud density of the experimental shallow landslide triggered by vibration SV2

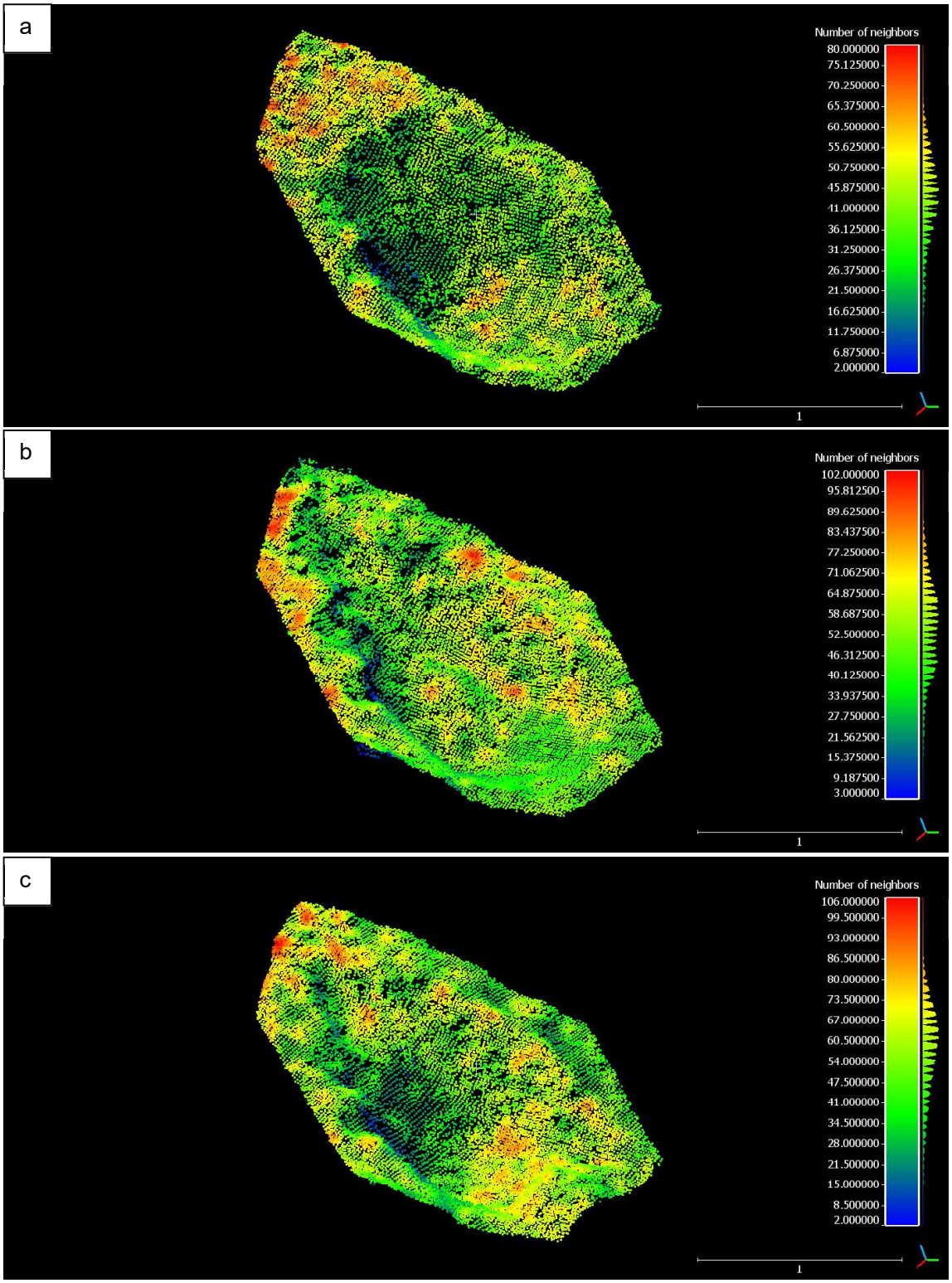

Appendix 2-7: Point cloud density of the experimental shallow landslide triggered by vibration SV3

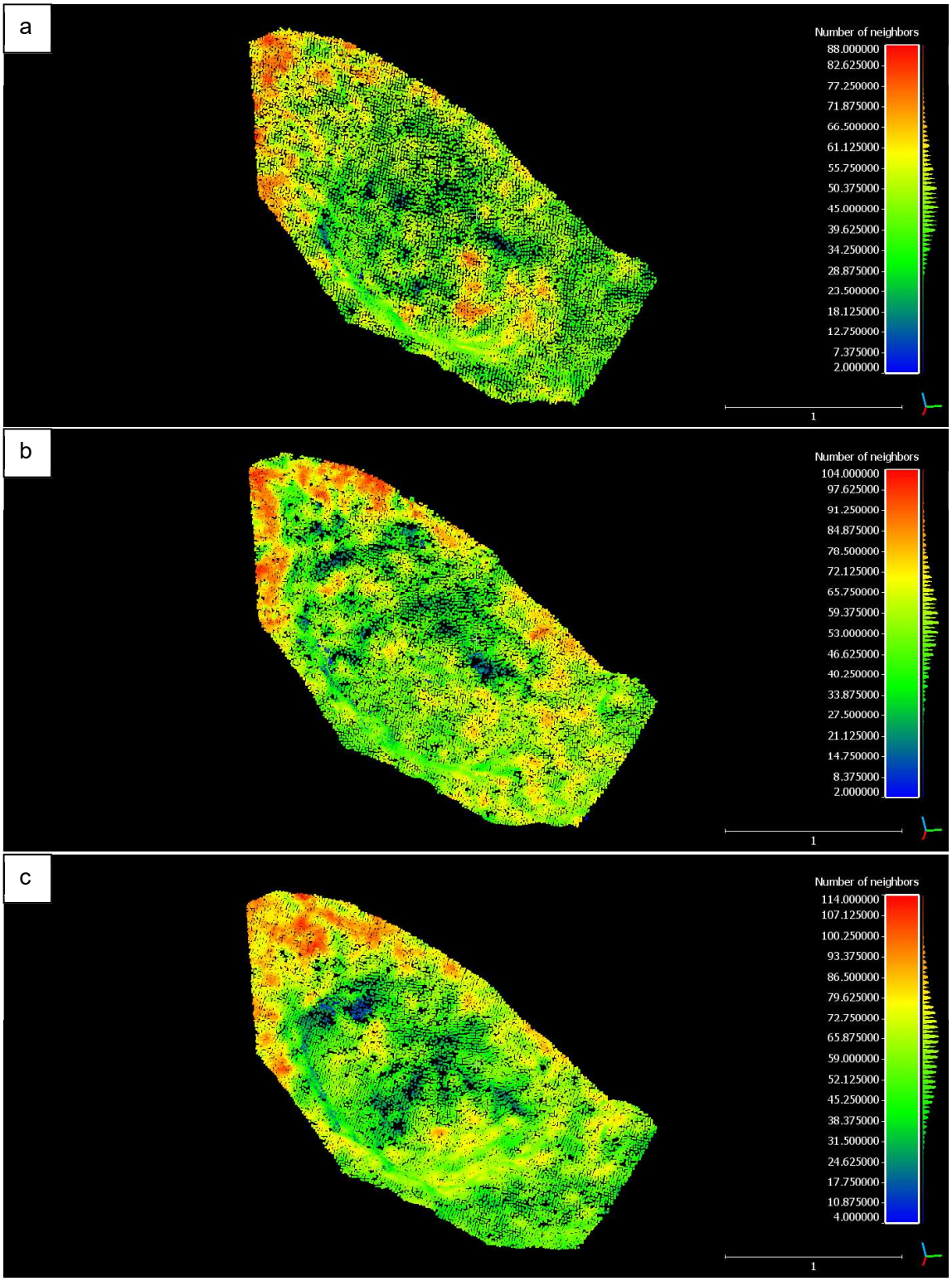

Appendix 2-8: Point cloud density of the experimental shallow landslide triggered by vibration SV4

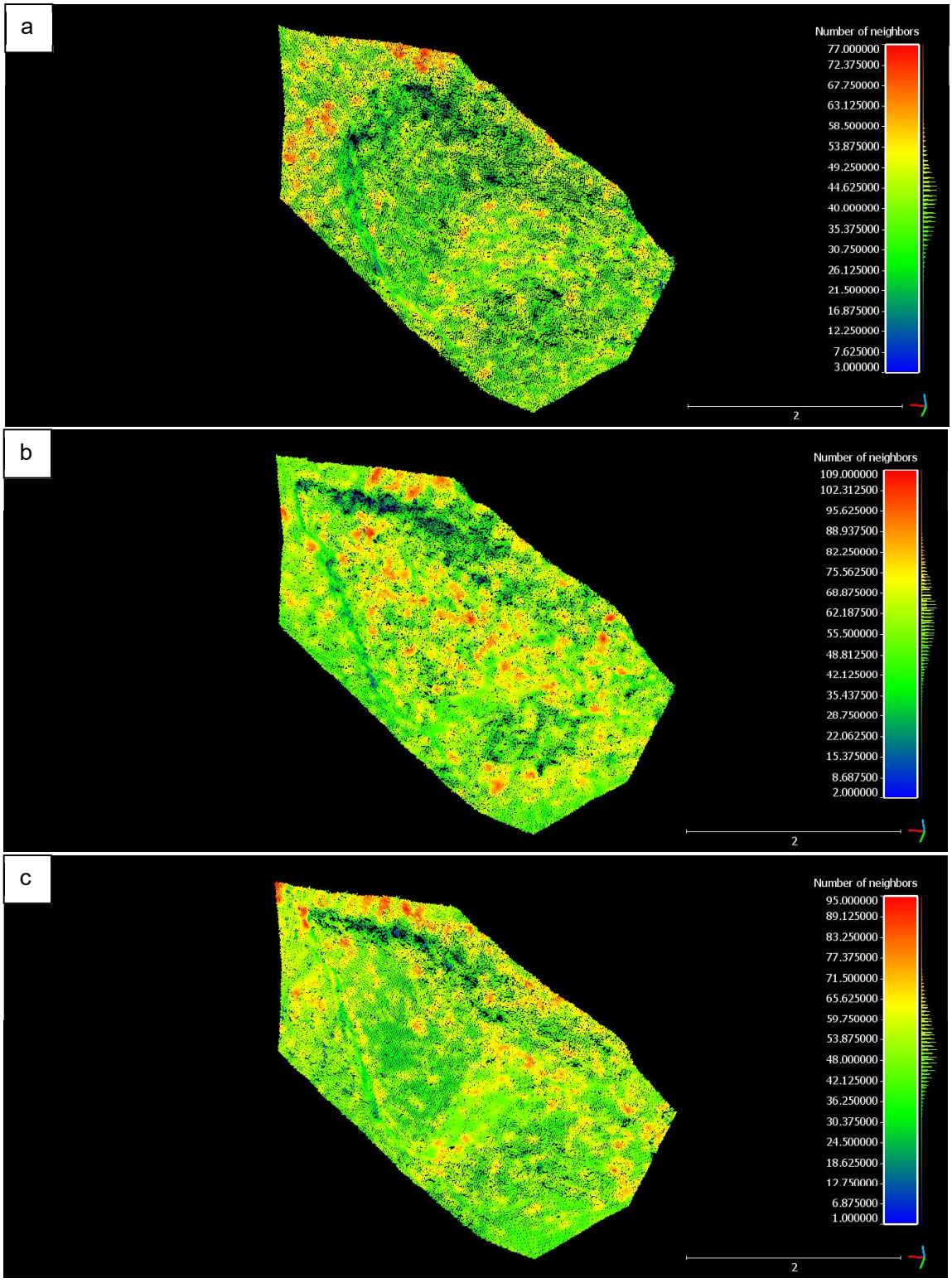

Appendix 3: Fitting of the paraboloid and plane from the rupture surface point cloud of the experimental landslides. The blue points are the initial point cloud of the rupture surface and the surfaces are the fitted plane and paraboloid.

Appendix 3-1: The Deep-seated landslide D

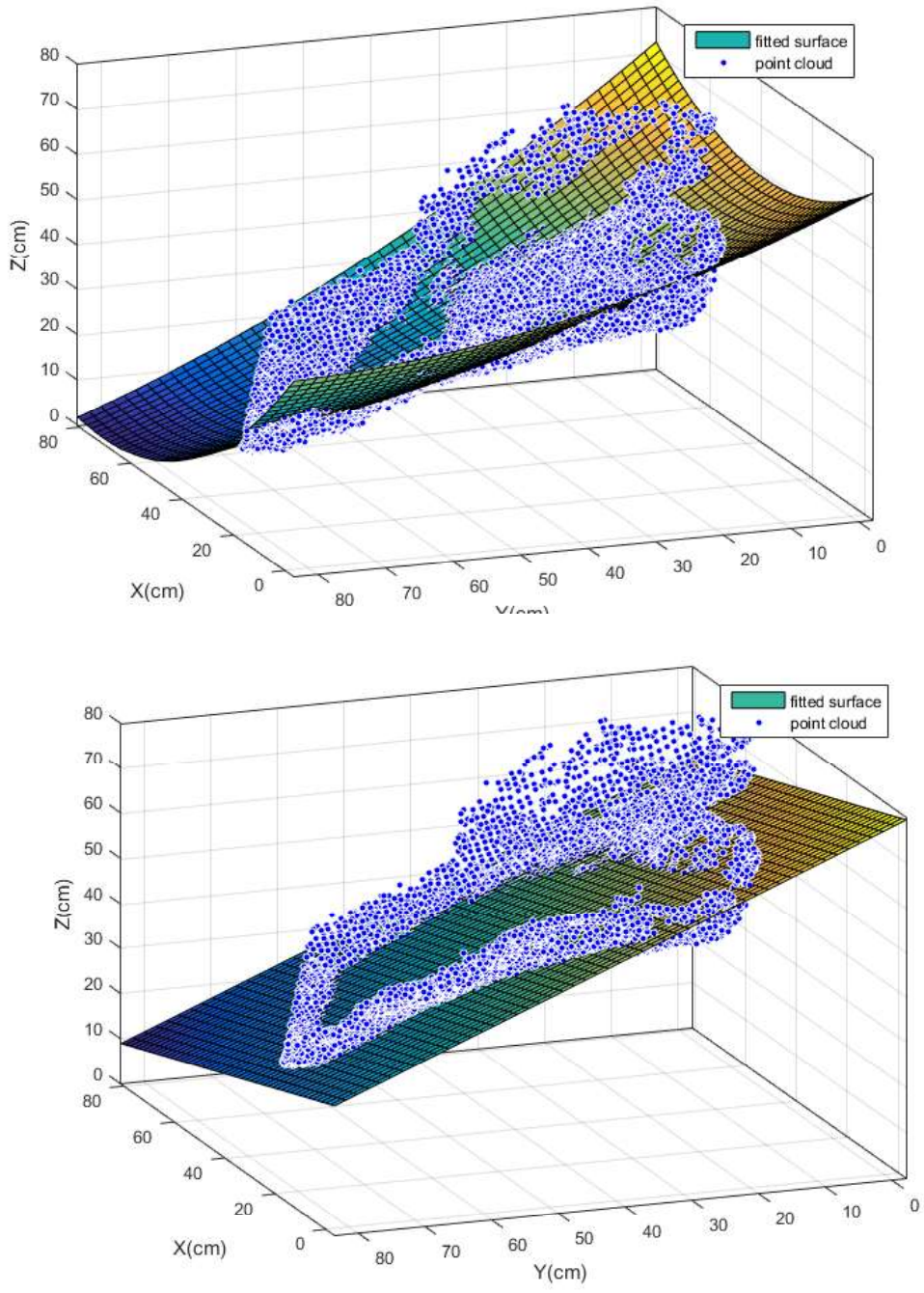

Appendix 3-2: The shallow landslide by toe excavation SE1

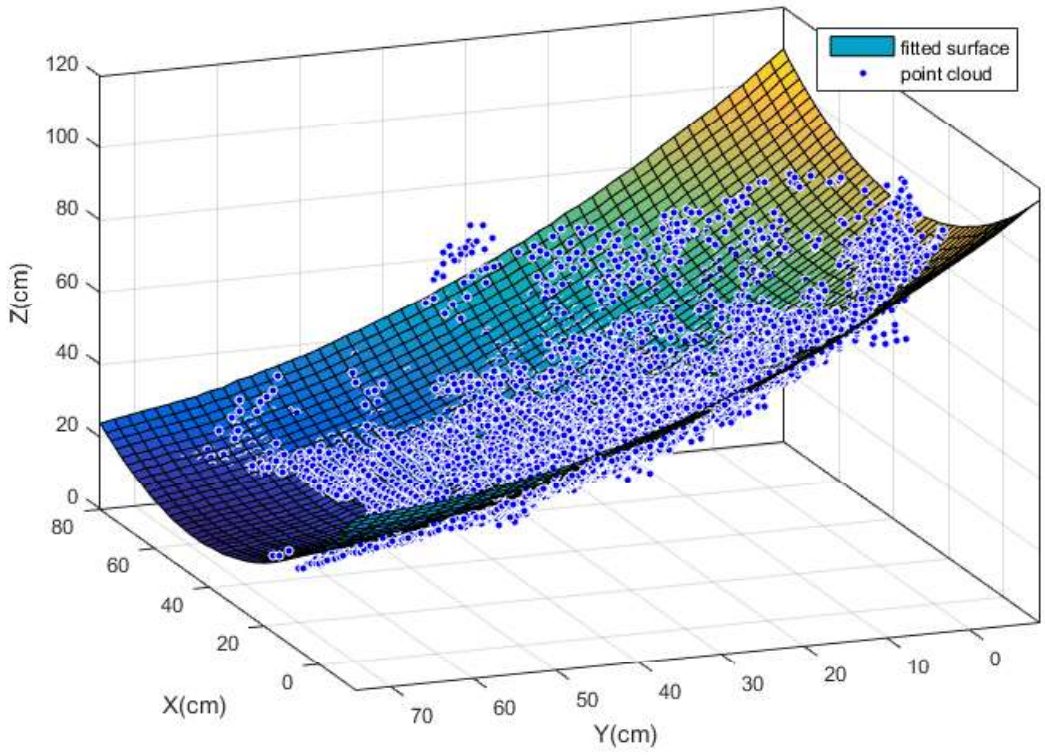

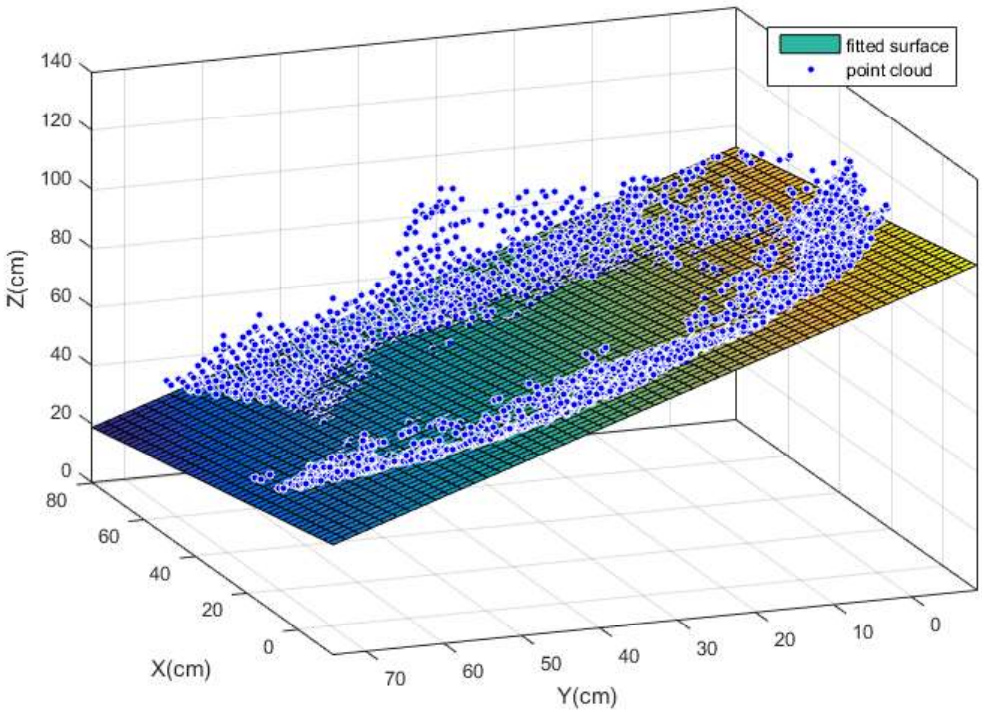

Appendix 3-3: The shallow landslide by toe excavation SE2

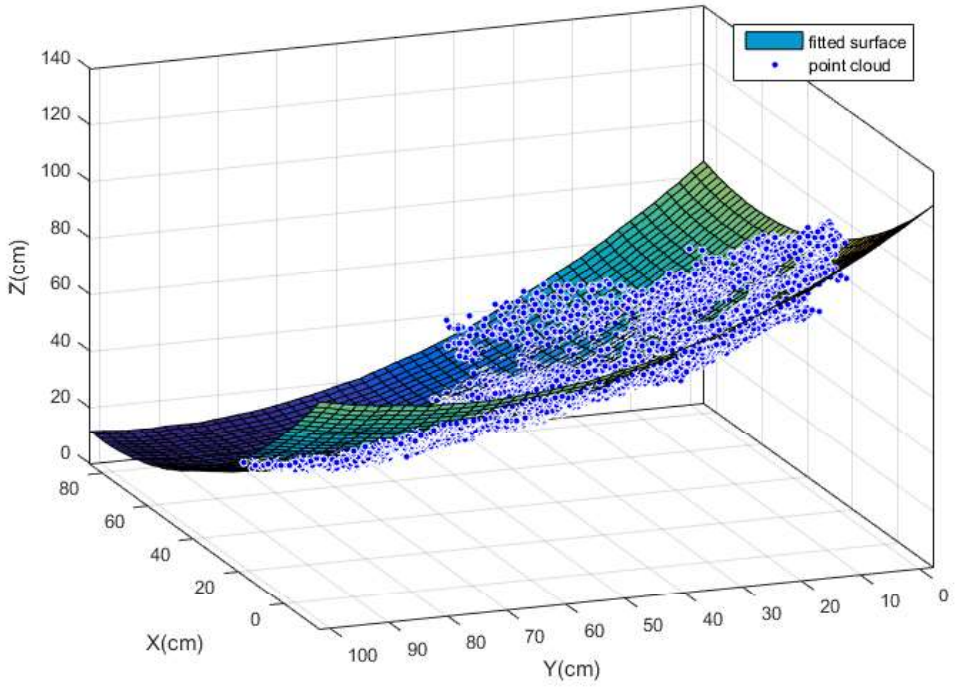

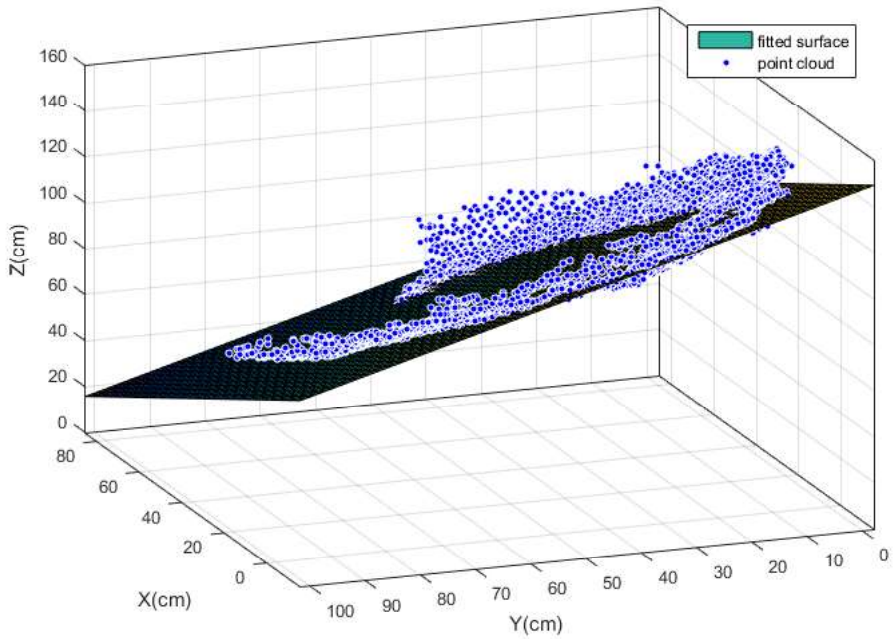

Appendix 3-4: The shallow landslide by toe excavation SE3

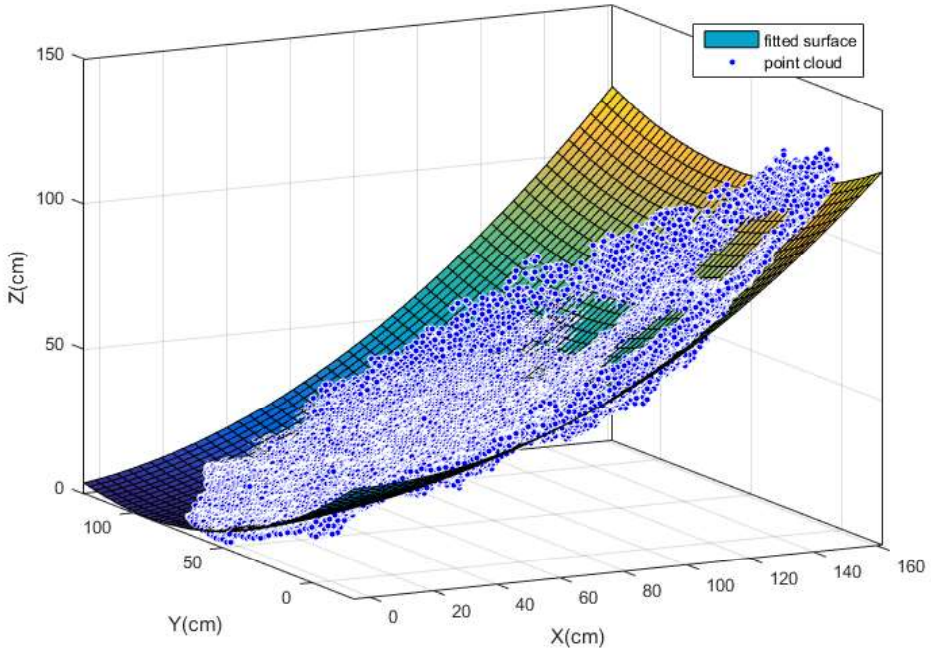

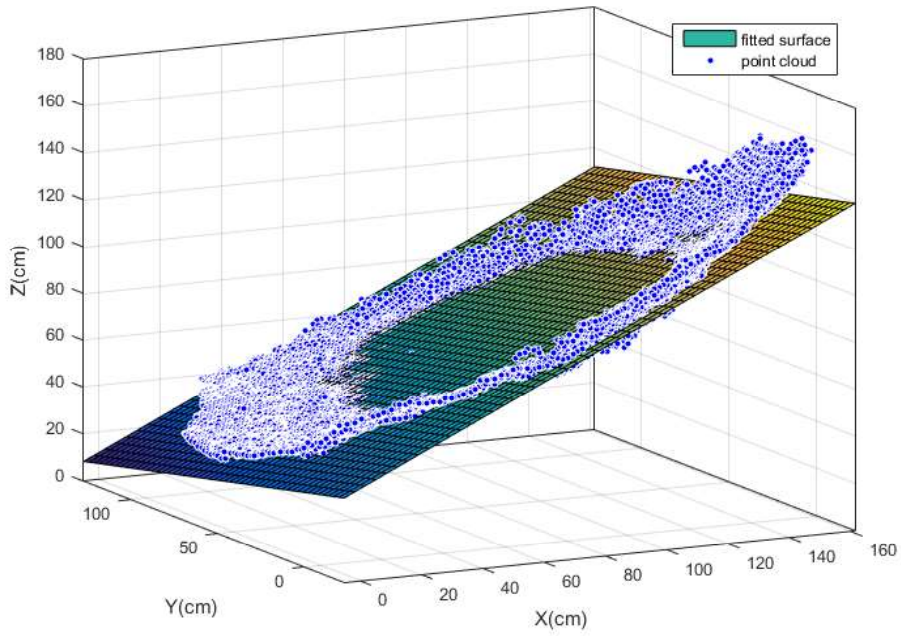

Appendix 3-5: The shallow landslide by toe excavation SE4.

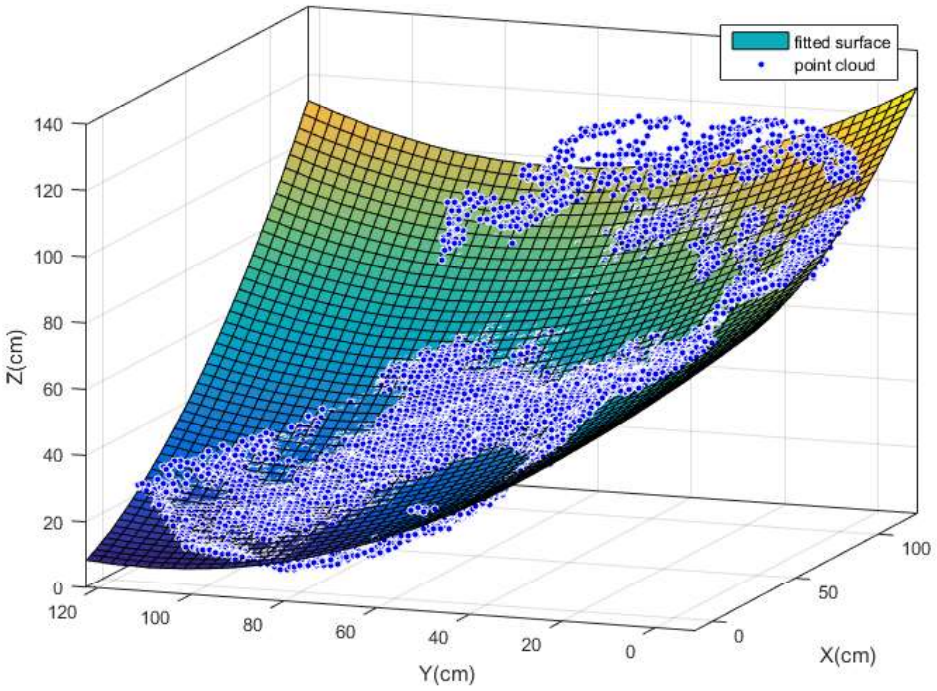

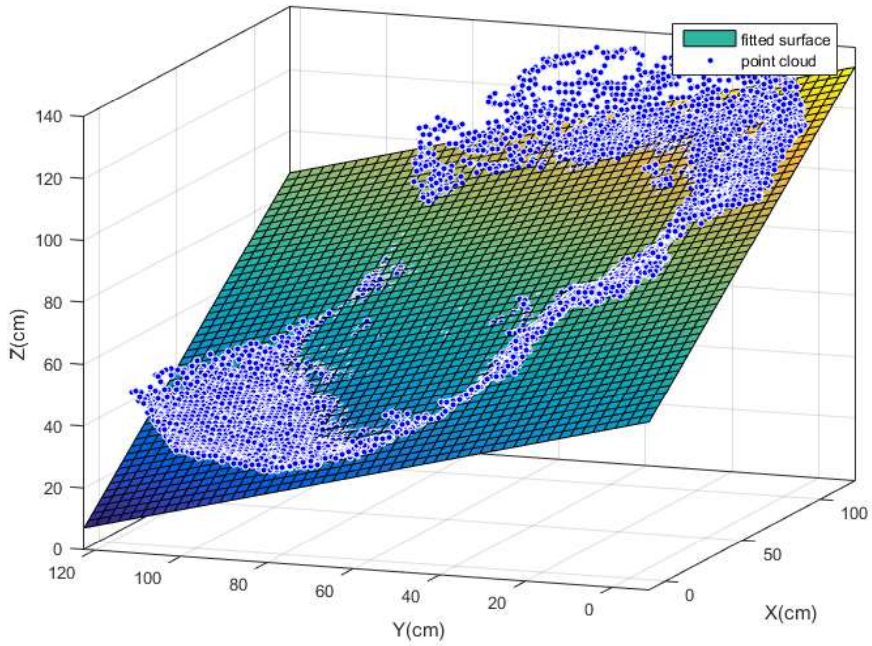

Appendix 4: The volume figures for the deep-seated landslide D and the landslides triggered by toe excavation SE1-SE4 calculated by several pairs of DEM difference and the empirical area-volume relationship. The accumulation and depletion are the net gain and loss based on the pre- and post- failure DEM difference. The "rupture surface – post" and "rupture surface – pre" mean the volumes calculated by the difference between the DEM in which the displaced material was moved out, with the pre- and post- failure DEM difference. The "reconstructed – post" and "reconstructed – pre" mean the volumes calculated by the reconstructed rupture surface by the proposed method and the post- and pre- failure DEM difference. The error bars infer the uncertain range of the volume calculation from the DEMs' systematic difference. The green columns are the volume calculated by the area-volume relationships.

Appendix 4-1: Volumes of the Deep-seated landslide D

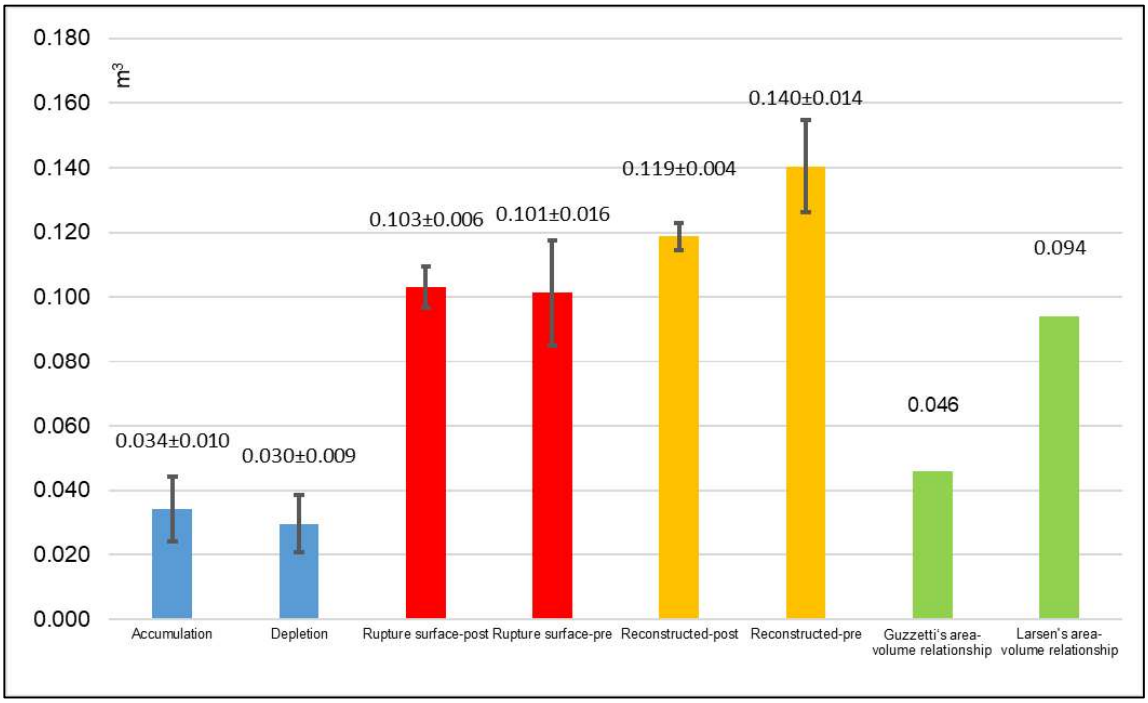

Appendix 4-2: Volumes of the shallow landslide triggered by toe excavation SE1

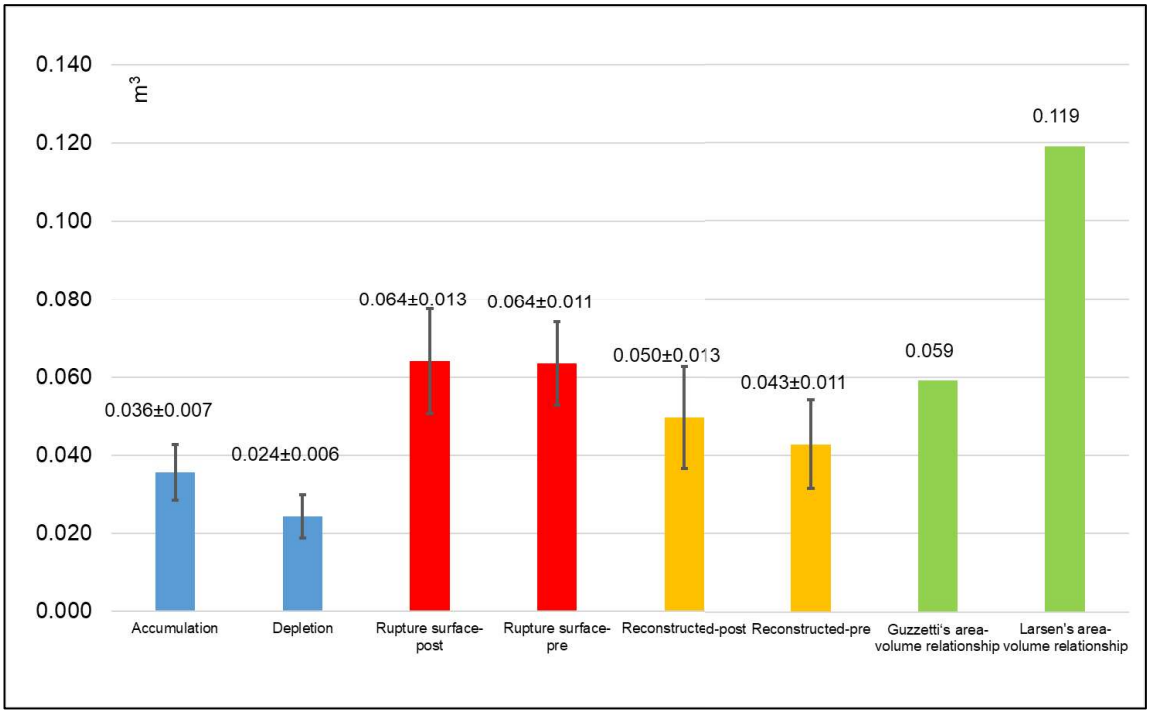

Appendix 4-2: Volumes of the shallow landslide triggered by toe excavation SE2

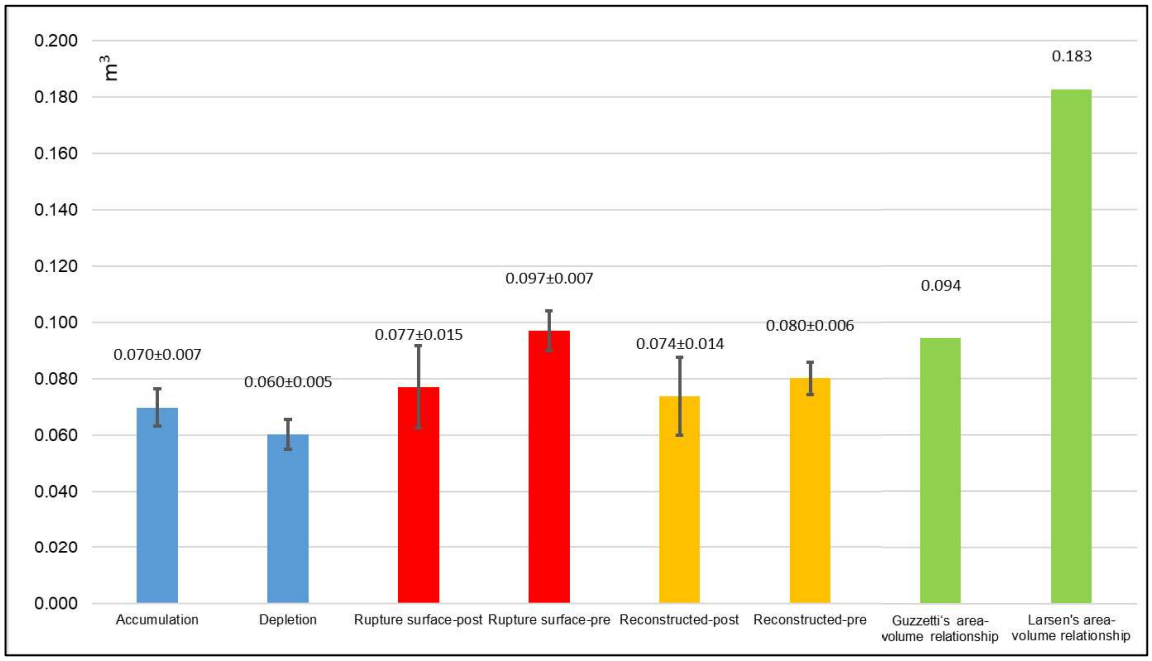

Appendix 4-3: Volumes of the shallow landslide triggered by toe excavation SE3

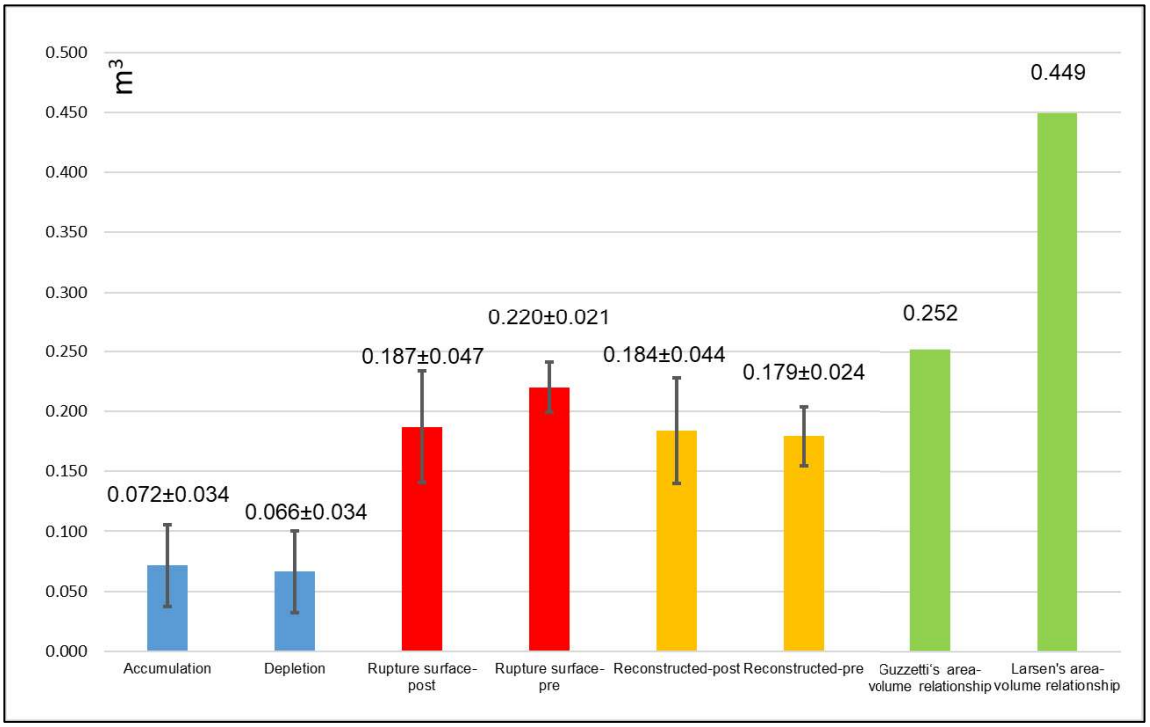

Appendix 4-3: Volumes of the shallow landslide triggered by toe excavation SE4

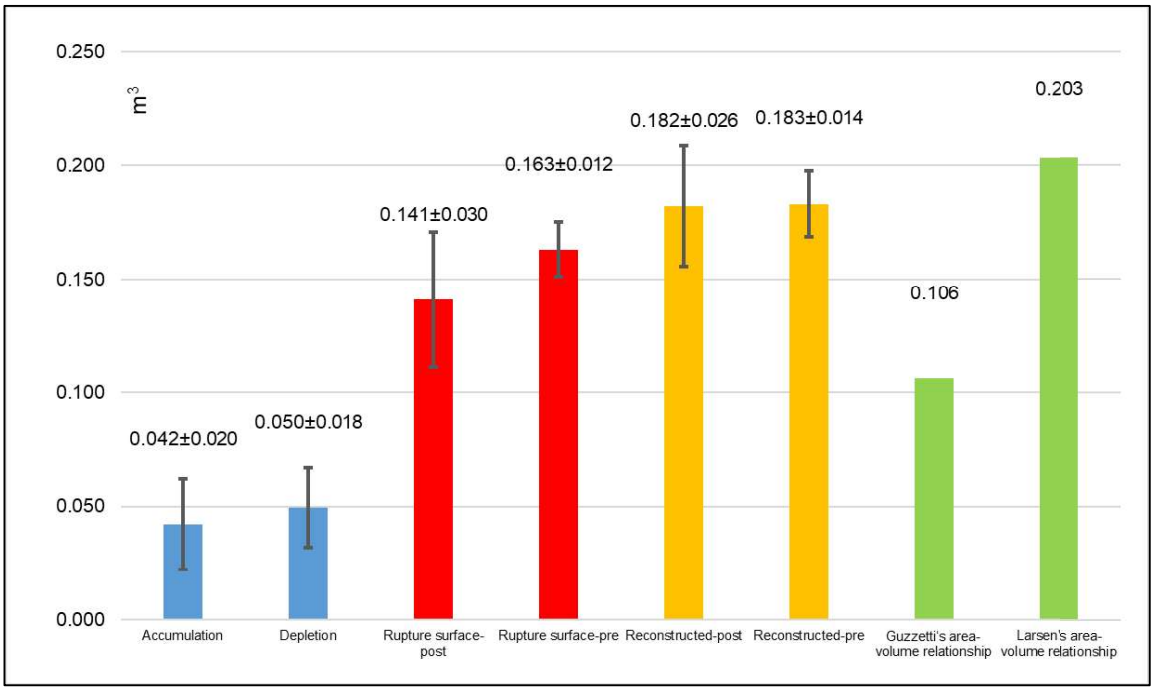

Appendix 5: Volumes figures for Landslides SV2, SV3, SV4 calculated by multi-temporal DEMs and area-volume relationships. The accumulation and depletion are the net gain and loss based on the pre- and post- failure DEM difference.